Yearbook

2008

Research Institute for Technical Physics and Materials Science

Hungarian Academy of Sciences

http://www.mfa.kfki.hu

Research Institute for Technical Physics and Materials Science
Hungarian Academy of Sciences

Director: Prof. István Bársony

Address: Konkoly Thege Miklós út 29-33,
H-1121 Budapest, Hungary
Postal: P.O.Box 49, H-1525 Budapest, Hungary
Phone: +36-1-392 2225
Fax: +36-1-392 2226
e-mail: info@mfa.kfki.hu
URL: http://www.mfa.kfki.hu

MTA MFA Yearbook 2008

Editors: Miklós Menyhárd, György Zoltán Radnóczi, Zsolt Zolnai
Published by: MTA MFA, Budapest, Hungary, 2008

CONTENTS

DIRECTOR'S FOREWORD

Do it yourself…when the ones - who's duty it was - don't! In view of the disarray and confusion in the research financing of 2008 this was the only feasible conclusion. Regardless the lack of vision and clear priorities in the national innovation policy, the management of our research institute decided to consequently follow the main line set out four years ago. *This collective effort bore fruits, MFA was able to achieve the highest turnover since its foundation of over 6M€!*

The scientific profile was crystallised out during the last years. It is directed towards the exploitation of the fundamental scientific results obtained in the fields of thin films, nanotechnology, photonics and microtechnology in integrated micro-and nanosystems primarily for sensorics and photovoltaics. The organisation chart of the institute was redrawn for better supporting the inter-departmental cooperation and the multidisciplinary approach being characteristic for MFA. The new organisation scheme renders the research activities to be carried out in six scientific departments supported by the financial and the technical department. Particular emphasis is put on nanoscience and –technology-type research in the Department of Nanostructures and the newly formed Department of Ceramics and Nanocomposites. Latter is mainly focussing on nanopreparation. The photonics department is dealing with non-destructive testing and (bio)sensing by integrated optical systems. Structural research is concentrated in the Thin films department. The department of Complex systems combines the computer simulation and image processing. The largest activity at MFA is the integration in form of MEMS/NEMS and PV devices carried out in the Microsystems department. The restructuring offered a good opportunity to offer young talents also the chance to acquire management experience in the position of deputy head of department. The average age of the management dropped to below 50 years from last years close to 60.

The inadequate education-policy of the government over the last years yielded a rapidly fading attractivity of studies in technical and natural scientific studies in Hungary. The consequence is meanwhile a serious lack of specialists, obviously, hiring of motivated PhD students, potential researchers is jeopardised, as well. What could we do about it ourselves?

A pioneering initiative, *the organisation of the first ever summer camp for senior-high school students with the motto: "Let's learn from each other" became the biggest success of the year at MFA.* The over 50 internet applications of youngsters interested in physics-chemistry and biology for participation in the event allowed the selection of 16 talents (among them four girls) from all over the country. They enjoyed the hospitality of MFA for a whole week. The students were assigned to mentors guiding them during the solution of self chosen tasks in different research laboratories, using the whole preparatory and analytic infrastructure of MFA. By the end of the week, in front of their invited teachers and the research collective of the institute they reported in "professionally" edited presentations, what they achieved.

This initiative was very much supported by the President and Vice President of the Academy, and thereby obtained a rather extensive media coverage. In a ceremony at the central building of the Academy all participants received a valuable book present from József Pálinkás, the president of HAS. The submitted written reports were evaluated by a jury later, and the best works were awarded a prize. Moreover, the decorated students obtained a chance to present their findings to the audience of a Nanotechnology Conference in Veszprém.

The echo of this initiative from the children, parents, and the teachers alike was overwhelming. Moreover, equally enthusiastic about the activity and the results were our colleagues. *The target of motivating children for selecting a study in natural and technical sciences for possibly becoming researcher later, was more than achieved.* This was reflected a. o. by the Certificate of Merit given by the National Federation of Teachers in Research (KUTOSZ), and by the Theodor Kármán Prize awarded to MFA by the Minister of Education and Culture in appreciation of the efficient support of education by the research institute. The good start asks for continuation!

In 2008 MFA obtained support for the establishment of a *National Technology Platform for Integrated Micro/Nanosystems. IMNTP* combines the precompetitive innovation effort of universities, research institutes and industry by elaboration of a domestic strategy based on the Strategic Research Agenda of the *European technology platforms for nanoelectronics (ENIAC) and photovoltaics (PV)*. Intensification of collaboration within the innovation-triangle is organised by the IMNTP platform office. By securing a Hungarian national commitment of 1.34 M€, in the first call of the ENIAC Joint Technology Initiative an IMNTP generated Hungarian consortium could win financing in the project *SE2A - Nanoelectronics for Safe, Fuel Efficient and Environment Friendly Automotive Solutions*.

The year also was important in expanding scientific co-operation with other institutions: Formal agreements were signed with the National Institute of Materials Science, Tsukuba and University of Technology and Economics, BME in establishing a joint graduate school, with BME TTK pver a joint Laboratory for E-Beam Lithography, with BMF KKVK over the joint Laboratory for Molecular Beam Epitaxy both at MFA. A strategic research agreement was signed with the State Printing Co. Inc., and with ITRI, Shinh-Chu.

A further standard element of our management's policy is the permanent *strive for renewal of the research infrastructure by new equipment purchase and improvement of laboratories and offices.* In 2008 the complete overhaul of a chemical and a bio-lab, the renovation of two offices and the whole corridor at the central building, as well as the construction of a new archive was accomplished. In spite of inadequate governmental funding, and the inaccessibility of the European Structural Funds for the development of research infrastructure, the conditions of MFA could substantially been improved last year, too. By investing ca. 1M€ from own means for new equipment, we compensated at least partially for the uncompetitive salaries. Among others a Süss MicroTech MA6/BA6 mask-aligner, wafer bonder and nano-imprinting tool, a fotoresist processing line, a Malvern Zetasizer, two new manipulators for the LEO FESEM, a Woollam M2000DI spectroscopic ellipsometer, a Tribologic Tester for thin films, and a closed-loop cooling for the JEOL TEM were purchased.

Four of our young colleagues obtained PhDs, all summa cum laude. The scientific advisor of MFA, Laszló P. Biró became titular professor of the Science University of Szeged. Levente Tapasztó is the second MFA scientist to win the Junior Prima Prize in physics for his pioneering work on graphene. The title page of the June issue of Nature Nanotechnology, featured his original illustration on "Tailor-made graphene nanoribbons". Géza Ódor's theoretical book on "Universality in Nonequilibrium Lattice Systems" was published by World Scientific.

In 2008 MFA colleagues obtained a number of distinctions: the 75 years old József Gyulai the Memorial Medal of the Széchenyi Society, Péter Barna the award "A life for Thin Films" of the European Surface Coaters, István Bársony the Officer's Cross of the Orden of Merit of the Republic of Hungary and the Dennis Gábor Prize for innovation. The MFA prize was awarded to Gábor Battistig and Zsolt E. Horváth, the Junior Prize to Anita Pongrácz.

Facing the difficulties at times of world economy crisis we are confident in the selected research strategy, which led to an improved reputation of MFA, giving some ammunition for surviving the austerity period to come.

Budapest, January 2009.

István Bársony

GENERAL INFORMATION

Organisation

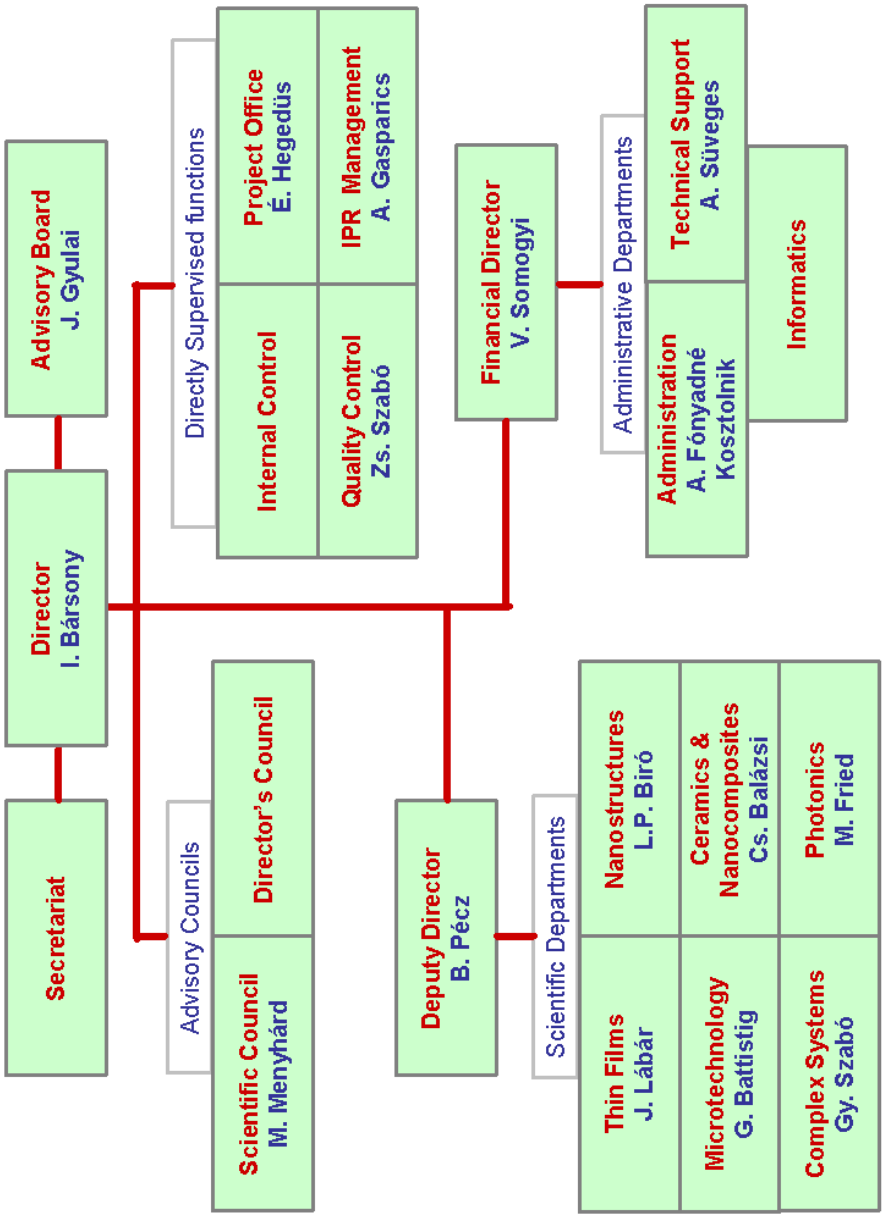

Key Financial Figures

The total budget of MFA in the last couple of years was leveling around € 6million, but in 2008 exceeded a value of € 6.5million. The relatively high success rate of MFA participation in domestic projects and the substantial increase of successful R&D contracts as well as international projects facilitated in the recent years the overcompensation of stagnating or even decreasing subsidies.

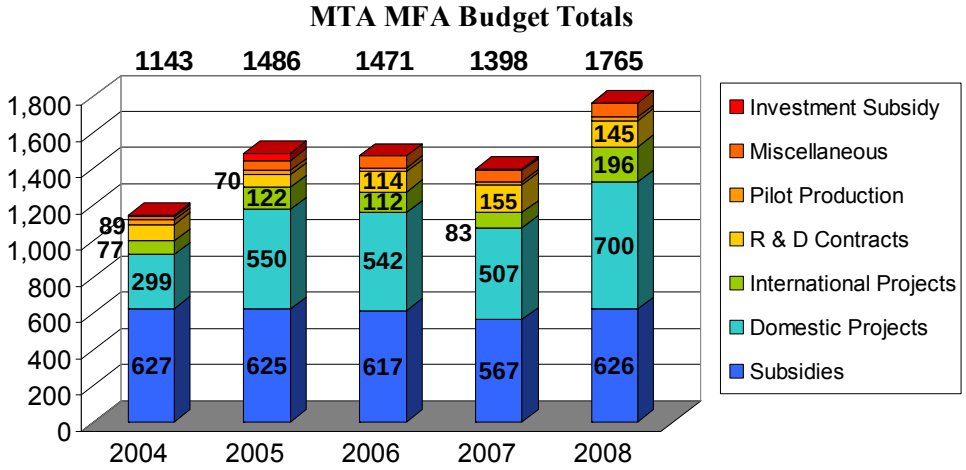

Despite the marginal central investment support, in the last period the research infrastructure of the Institute developed substantially year by year.

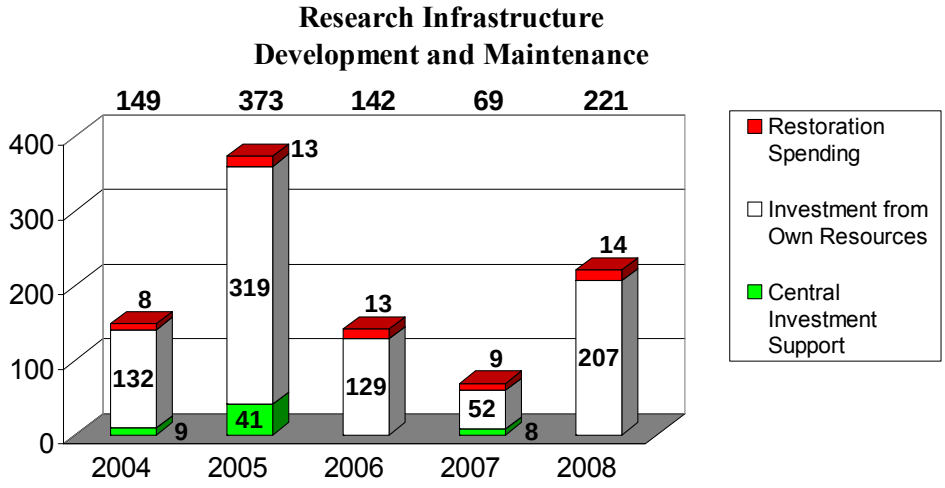

Scientometry (International Impact)

According to the independent database of *The Thomson Reuters*, the institute in the last decade maintained an average publication activity of above 100 scientific papers per year. 2008 has brought a substantial increase. This justifies the strategic decisions of the previous several years, the establishment of new research groups, the development of infrastructure and fields of activity.

Publications of MFA (source: ISI Web of Science)

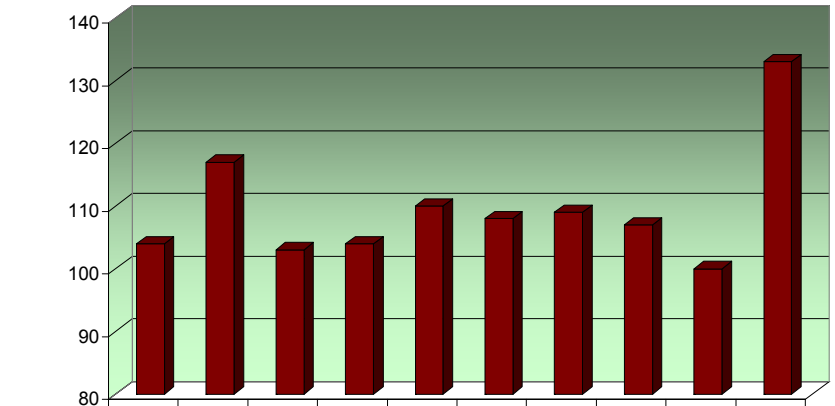

	1999	2000	2001	2002	2003	2004	2005	2006	2007	2008
publications	104	117	103	104	110	108	109	107	100	133

A good measure of the recognition of MFA's scientific activity is the steady yearly growth of independent citations as well as the *h-index* value of 42.

Citations of MFA (source: ISI Web of Science)

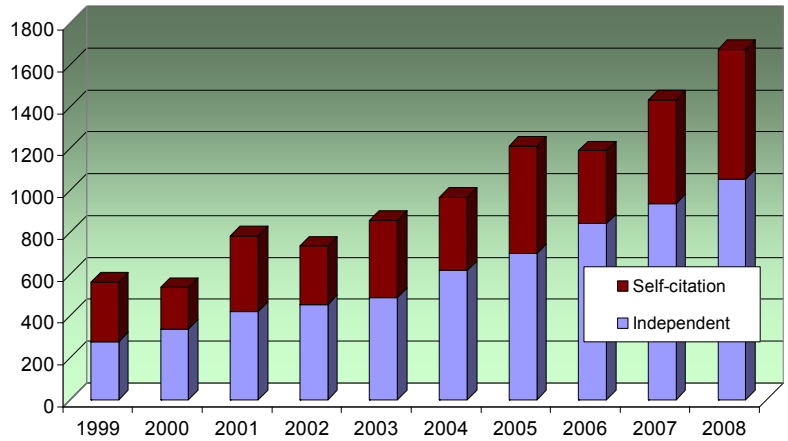

Prizes, Honours and Scientific Promotions

Research Institute for Technical Physics and Materials Science
Kármán Tódor Prize

István Bársony: Order of Merit of the Hungarian Republic - Officer's Cross
Gábor Dénes Prize

Gábor Vásárhelyi: Tactologic Kft The Best Spin-off and Start-up Company – 2008

György Szabó: Outstanding Referee of the American Physical Society 2008

Levente Tapasztó: Junior Prima prize in the category of „Hungarian Science"
Certificate of merit of the Hungarian Academy of Sciences for young researchers

Béla Szentpáli : HTE Pollák-Virág Prize

Péter B. Barna: "Life for Thin Films", European Vacuum Coaters, Anzio, 2008

György Gergely: ELFT Medal 2008

András Kovács: Hungarian Electron Microscopy Society Prize

Krisztián Kertész: Certificate of merit of the Hungarian Academy of Sciences for young researchers

György Kadar: was elected Secretary-general of Roland Eötvös Physical Society

László Bartha: was elected Chair of Chemical and Metallurgical Comitte of HAS.

László P. Biró: was elected Honorary professor of the University of Szeged

Csaba Balazsi: was promoted Associate Professor at Pannon University.

Zsolt E. Horváth and **Gábor Battistig**
MFA Prize

Anita Pongrácz
MFA junior prize

Csaba Daróczi
MFA special prize

Successful Ph.D. defences in 2008:

Norbert Nagy

Gréta Gergely

György János Kovács

Anett Sebestyén

Conferences and Symposia Organized with MFA Contribution

Magnetic Measurements 2008 Conference, September 21-24, 2008, Budapest, Hungary, Chair, Gábor Vértesy

55th IUVSTA Workshop on Electron Transport Parameters Applied in Surface Analysis, September 14-17, 2008, Siófok, Hungary, Chair: Miklós Menyhárd

IUVSTA Executive Council Meeting 104, September 26–28, 2008, Budapest, Hungary, Chair: György Radnóczi

INNOVATIAL School on the usage of the ProcessDiffraction method, May 5-10 2008, Budapest, Hungary, Director: János Lábár

E-MRS Spring Meeting, Symposium A: "Carbon-based nanostructured composite films - 08", May 26-30, 2008, Strasbourg, France, Scientific Committee member: György Radnóczi

1st International Conference on Functional Nanocoatings, 30 March - 2 April, 2008, Budapest, Hungary, Scientific Advisory Board member: Péter Barna

14th International Conference on Thin Films & Reactive Sputter Deposition, Nov. 17 - 20, 2008, Gent, Belgium, International Advisory Board member, Péter Barna

14th European Microscopy Congress, EMC2008, September 1-5, 2008, Aachen, Germany, International Advisory Board member: Péter Barna

12th Joint Vacuum Conference, 10th European Vacuum Conference, 7th Annual Meeting of the German Vacuum Society, September 22-26, 2008, Balatonalmádi, Hungary, Co-Chair of the Programme Committee: Béla Pécz , International Organizing Committee, Chair: Péter Barna

3rd International Conference "Fractography of Advanced Ceramics", in the ACADEMIA Congress Center, September 7-10, 2008, Stara Lesna, Slovakia, International Organizing Committee member: Csaba Balázsi

Notable Events in Year 2008

The MFA Summer School for High School Students

„Let's learn from each other" was the motto of the first Summer School for high school students in June 2008. organised ever by a research institute of the Hungarian Academy of Sciences. The mission of the one week program was to provide a comprehensive overview about the scientific work in the real research environment for talented young students. By using the facilities of MFA under supervision of researchers the hands on experience should improve the attractivity of the studuies in natural sciences and engineering. The tailor-made topics were focused to different fields of materials science. By the end of the week the sixteen participants presented the summary of their activity at a mini-conference and were awarded by the institute a certificate of merit. Besides the studies and work in the labs, several get-together programs were organized: hiking in the forest surrounding the Institute, Budapest sightseeing, visit the telescope at the Konkoly Observatory of the Hungarian Academy of Sciences, etc.

Among others this initiation of this successful program at MFA was honoured with the Tódor Kármán Prize of the Minister of Education and Culture.

Participants, mentors, and organizers of the first Summer School in front of the main building of MFA. The opening ceremony was honored by the president of the Hungarian Academy of Sciences, Prof. József Pálinkás.

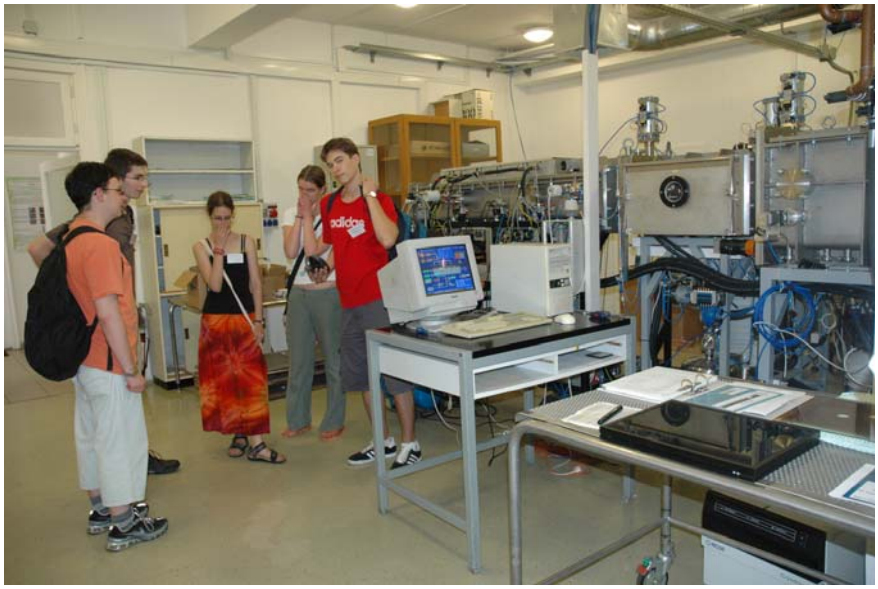

Summer School students visiting the thin-film solar cell laboratory at MFA.

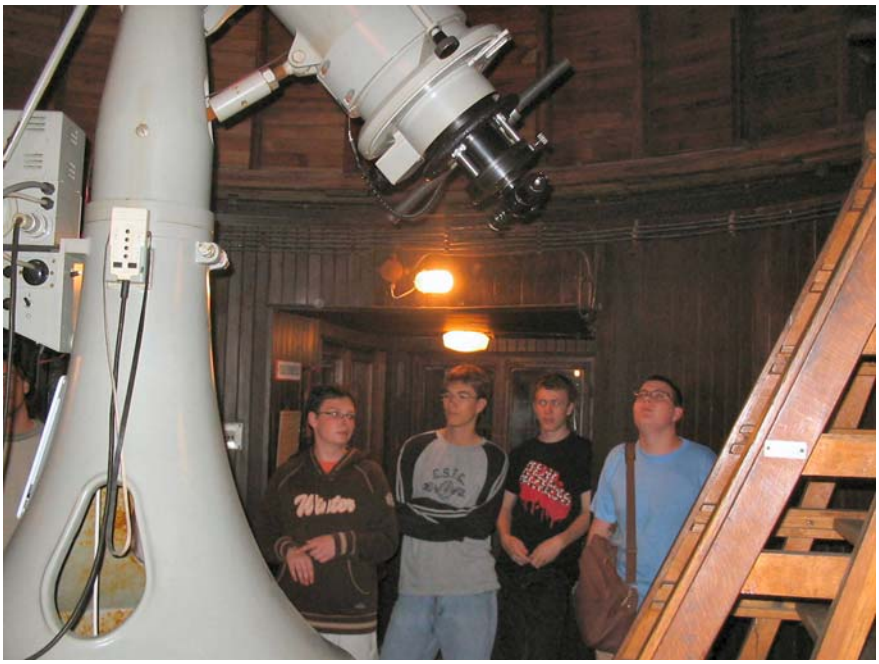

Visit of the telescope at the Konkoly Observatory of the Hungarian Academy of Sciences.

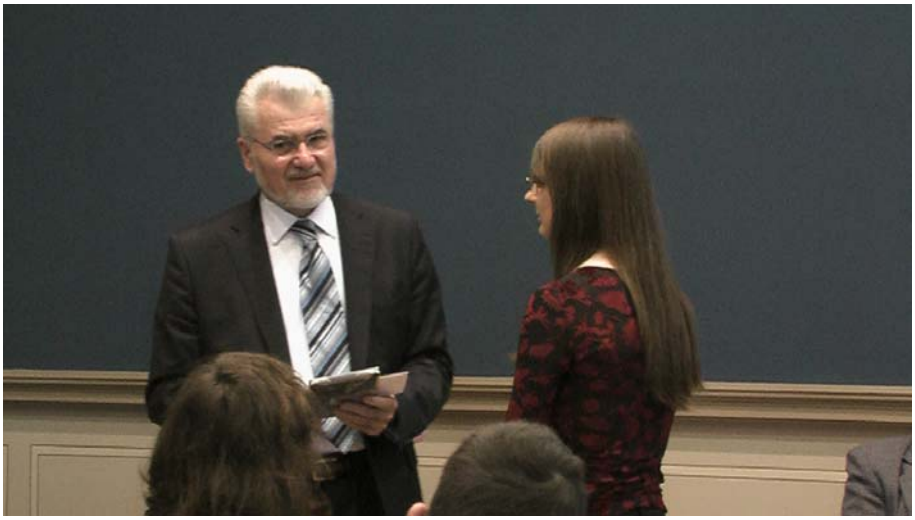

The most successful Summer School students were distinguished by Prof. József Pálinkás, the President of HAS.

The director of MFA receives the Tódor Kármán Prize from the Secretary of state of the Ministry of Education and Culture.

Junior Prima Prize to Levente Tapasztó

"For his outstanding scientific research activity performed in both theoretical calculations and experimental studies, we offer Levente Tapasztó to be honoured by the Junior Prima Prize."

Levente Tapasztó, young researcher of the Nanostructures Laboratory of MFA, was awarded in 2008 the prestigious Junior Prima Prize for young and talented physicist nominated by the members of HAS, József Pálinkás and József Gyulai. Pictured is Levente flanked by Prof. József Gyulai, the former and Prof. István Bársony, the acting director of MFA.

.

Highlights

The influence of influential players in Prisoner's Dilemma

(Hungarian Scientific Research Fund under Grant No K-73449)

G. Szabó, A. Szolnoki, I. Borsos, J. Vukov

The evolutionary Prisoner's Dilemma (PD) games have been widely used for 15 years to study the emergence of cooperative behavior among selfish individuals. In the simplest spatial models players are distributed on the site of a square lattice. The players income comes from PD games played with the neighbors. In these models the players can follow only two strategies: cooperation *C* and defection *D* and their payoff depend on their strategies. Namely, for the two-player game the highest total payoff is shared equally by the cooperators, while for their opposite choices they share the minimal total income. However, both players are enforced to choose defection providing higher individual payoff independently of the co-player's decision (and that is the reason of dilemma).

In the evolutionary games the players try to maximize their total income by imitating those neighbors having higher income. Ten years ago we have introduced a model with a strategy adoption probability dependent on the payoff difference between two neighbors chosen at random. Up to now, we have studied the effect of noise, payoffs, and connectivity structure on the frequency of cooperators in the final stationary state developed when repeating strategy adotions many times. Now this model is extended by distinguishing two types of palyers. The influential players (type *A*) are capable to convince their neighbors to follow their own strategy. On the contrary, the convincing capability of the players of type *B* is reduced by a multiplicative prefactor ($w<<1$).

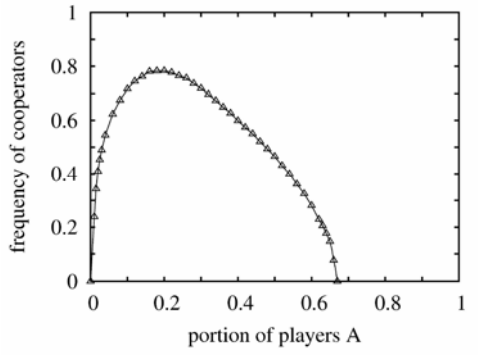

Figure 1 *Typical variation in frequency of cooperators when tuning the portion of A players for w=0.1.*

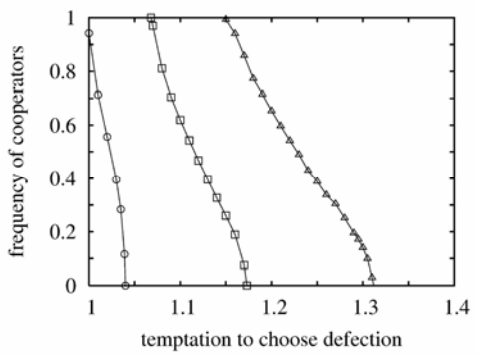

Figure 2 *Frequency of cooperators vs. temptation to choose defection for w=1, 0.05, and 0.005.*

Figure 1 shows that the presence of influential players (type A) can enhance significantly the portion of cooperators and also the strongly related average payoff for an optimum ratio of players *A* and *B* if the number of neighbors is 24. Figure 2 demonstrates how the frequency of cooperators vanishes when increasing the temptation to choose defection. Notice that cooperators have higher chance to survive for lower values of *w*. These phenomena can be explained by the particular distribution of strategies (*C* and *D*) and types (*A* and *B*).

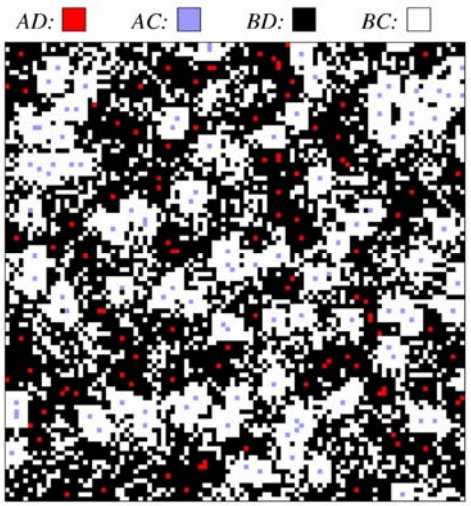

Figure 3 *Typical snapshot of strategy and type distribution if only 2 percent of players belong to type A and their position is fixed.*

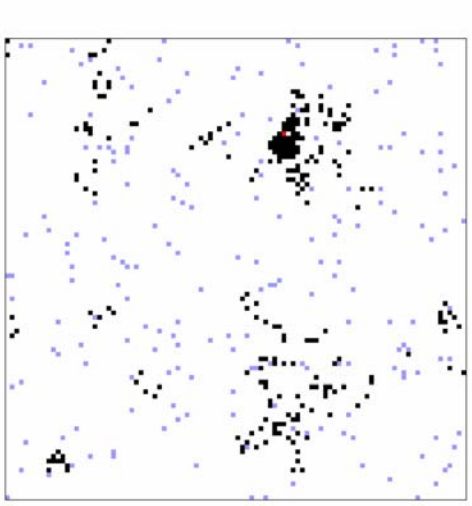

Figure 4 *Typical snapshot if players A are allowed to migrate with a low probability for the same parameters as in Figure 3.*

The above snpashots illustrate that the influential players (type A) convince their neighbors to follow their own strategy. This effect is beneficial for the cooperators and disadvantageous to the defectors. In Figure 3 the *AC* players cannot convince the *AD* players (to become *AC*) because of the absence of direct links between them. The latter shortage disappears if the influential player can move and the strategy adoption is supported through the temporary connections between the *AC* and *AD* players. In the light of this mechanism we could suggest other ways to hepl the maintenance of cooperative behavior.

Device for detecting liquid hydrocarbon derivatives floating on water

(NKTH - Aquanal)

M. Serényi, J. P. Makai, A. Hámori

Natural water bodies are often contaminated by liquid hydrocarbon derivatives (for example oil) or, at higher temperatures, by greases passing into the soil, streams and still water. Since oil is used in almost all industrial fields as well as in transportation, the contamination may occur in the most unexpected places and can cause widespread danger and damage. Accidents during the extraction of the oil and during oil transportation by tankers, trucks or pipelines usually cause large scale isolated environmental problems. The long term leakage of oil from industrial plants, transport vehicles, underground and surface storages may also cause, on the whole, environmental damage of a similar magnitude. Consequently, the fast detection of the pollution in the water bodies, ecologically and hygienically, is an absolute necessity.

Our measurement procedure (patent pending) is based on two physical phenomena: Fresnel reflection and the change in the total angle of reflection at the surface of a solid caused by the adhesion of a layer of different refractive index. The summation of the contributions of both of these phenomena to the transmission and reflection coefficients is possible. If a body submerged in water incorporates a light source which irradiates the body's surface with a diverging beam at an angle close to that of total reflection, and the axis of this beam reaches the surface at approximately the level of the water, then an oil film on the surface produces the above mentioned change in reflection and transmission. By the measurement of the change in beam intensity a contaminant can be detected.

The outline of an oil film detector is shown in Fig. 1. The device is comprised of a LED light source (1), a surface (2) that reflects the radiation beam of the source to the test (3) and reference (4) surfaces as well as a test (5) and a reference detector (6) positioned to detect the test and reference beams, respectively. The radiation beams reaches the test (3) and reference (4) surfaces at an angle of incidence approximately equal to the angle of total internal reflection and close to the level of the water. To achieve comparative measurements a water container (8) is attached to the reference surface (4). Also an electronic unit (7) is connected to the radiation source (1), test (5) and reference detectors (6) for powering, measurement and data evaluation.

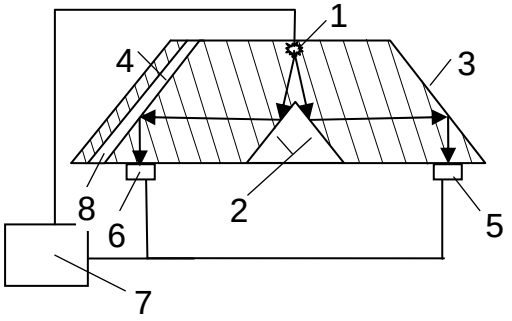

Figure 1
Cross section of the oil film monitor

Several complete equipments for detecting liquid hydrocarbon derivatives film appearing in monitoring wells were constructed (see Fig. 2.) and produced by WESTA-T Ltd. (Budakalász-Hungary).

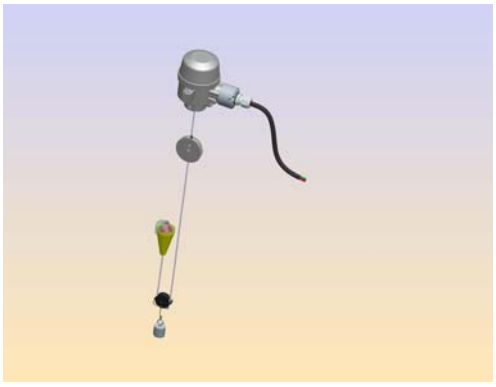

Figure 2 *Complete equipment for detecting liquid hydrocarbon derivatives film*

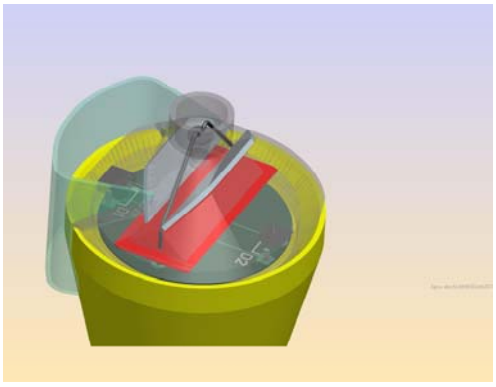

Figure. 3 *Design of the optical monitor part*

Six complete equipments are under test in an MOL plant located in Szajol (Hungarian Plain). The WESTA-T Ltd. made the arrangements for further serial production. The optical monitor part and the electronic unit were officially tested and certificated for use in potentially explosive atmospheres. The designs of these parts are shown in the Fig. 3. and 4, respectively.

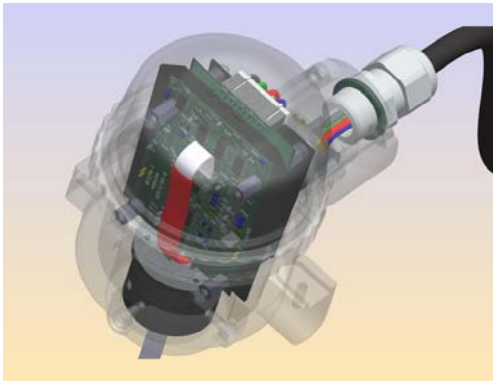

Figure 4 *Design of the electronic unit tested for use in potentially explosive atmospheres*

SCIENTIFIC REPORTS

Nanostructures Department

Head: Prof. László Péter BIRÓ, D.Sc., scientific advisor

Research Staff

Zsolt Endre HORVÁTH, Ph.D., Deputy Head of Department
Prof. József GYULAI, Member of the HAS (Professor Emeritus)
Antal Adolf KOÓS, Ph.D. (on leave)
Géza István MÁRK, Ph.D.
Zoltán OSVÁTH, Ph.D. (on leave)
Levente TAPASZTÓ, Ph.D. (on leave)
Zofia VÉRTESY, Ph. D.

Technical Staff

Zoltánné SÁRKÁNY, technician

Ph.D. students / Diploma workers

Gergely DOBRIK, Ph.D. student
Enikő HORVÁTH, Ph.D. student
Krisztián KERTÉSZ, Ph.D. student
Péter NEMES-INCZE, Ph.D. student
Péter Lajos NEUMANN, Ph.D. student
István TAMÁSKA, Ph.D. student

Gábor MAGDA, diploma worker
Péter VANCSÓ, diploma worker

The Nanostructures Department has an almost two decades expertise in the production and characterization of various nanostructures. In recent years in the focus of work were various carbon nanostructures (carbon and haeckelite nanotubes, nanotube junctions, graphene and few layer graphite) their nanoarchitectures, bioinspired photonic nanoarchitectures and potential applications of these nanoobjects and nanoarchitectures in various fields in nanotechnology, nanoelectronics, sensorics and environmental protection. The most relevant results in 2008 are detailed below:

We developed the first truly atomic resolution lithographic method allowing crystallographic control of the orientation of graphene nanoarchitectures.

Graphene samples on SiO_2 substrate were contacted by In spikes and investigated by STM/STS before and after ion irradiation. The effect of irradiation on the electronic structure and on the Fermi velocity was evidenced.

Carbon nanotubes functionalized in HNO_3 were imaged in atomic resolution by STM. Superstructures were evidenced in atomic resolution images and their origin was explained.

Photonic nanoarchitectures occurring in the scales of various butterflies were shown to be suitable for selective and quantitative gas/vapor sensing in ambient atmosphere.

Our free-access, web-based simulation software for numerically solving the Schrödinger equation was upgraded to allow the users to edit and save their work.

For more details, please feel free to visit the webpage of the Nanostructures Department at: http://www.mfa.kfki.hu/int/nano/index.html.

Graphene nanoarchitectures

(OTKA-NKTH grants K-67793 & NI-67851)

L. Tapasztó, G. Dobrik, P. Nemes-Incze, P. Neumann, Z. E. Horváth, L. P. Biró

Due to its excellent electrical and mechanical properties and due to the sheet like structure compatible with lithographic patterning, graphene is perhaps the most exciting and technologically the most promising carbon nanomaterial of the last decades [A. K. Geim And K. S. Novoselov, *The rise of graphene*, Nature Materials 6 (2007) 183.].The availability of a single atomic layer thick sheet, which exhibits ballistic electron transport and can withstand without damage current densities of the order of 10^8 A/cm^2 can solve the problem of physical limits that is more and more seriously affecting the microelectronic industry.

Graphene has a particular electronic structure [A. K. Geim And K. S. Novoselov, *The rise of graphene*, Nature Materials 6 (2007) 183.] that makes it a zero gap semiconductor, which means that a FET made of graphene does not have an "off" state. The way to overcome this, is to pattern graphene sheets into graphene nanoribbons (GNRs) down to a few nanometers in width. Additionally the control of the crystallographic orientation is needed, as the GNRs with zig-zag edges will always stay metallic.

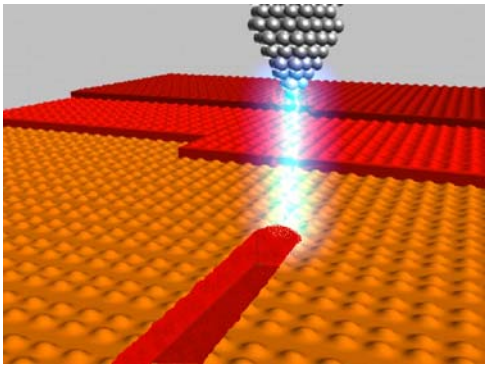

Figure 1 *Principial scheme of STM lithography of graphene. The tunneling current induces the local oxidation of the graphene sheet.*

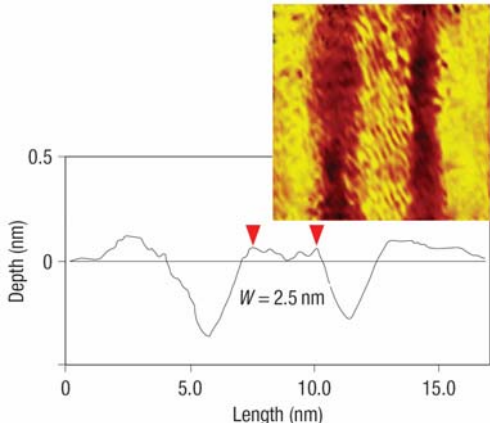

Figure 2 *The narrowest graphene nanoribbon, of only 2.5 nm in width. This width generates a gap of 0.5 eV, large enough to allow room temperature operation of nanoelectronic devices.*

To achieve the lithographic patterning of graphene with such an unprecedented resolution – atomic resolution, in the full sense of the word – and simultaneously having a precise control of the crystallographic orientation, a fundamentally new lithographic technique had to be developed [L. Tapasztó, G. Dobrik, Ph. Lambin, L. P. Biró, *Tailoring the atomic structure of graphene nanoribbons by scanning tunnelling microscope lithography*, Nature Nanotechnology 3 (2008) 397.]. The scanning tunneling microscope (STM) by its very basic construction principles can fulfill both requirements. An atomic resolution image is acquired in topographic mode which allows the precise definition of the crystallographic orientation of the nanorachitecture to be cut. In a subsequent step, by increasing the tunneling voltage to a few volts, the lithographic conditions are achieved, inducing the local oxidation of the sample (Fig. 1). If the conditions are suitably chosen, GNRs down to a few nanometer width can be cut (Fig. 2). The gap induced by the quantum confinement of the electrons scale inversely with the width in the case of armchair edge GNRs, so a GNR of 2.5 nm in width (10 benzene rings) will already possess a gap of the order of about 0.5 eV comparable to that of germanium, allowing the room temperature operation of nanoelectronic devices. A further advantage of the technique is that it does not produce contamination by resist residues. More complex shapes, like triangles (three terminal devices) (Fig. 3), networks of GNRs and 3D nanoarchitectures of few layer graphite (FLG) (Fig. 4) can be equally achieved.

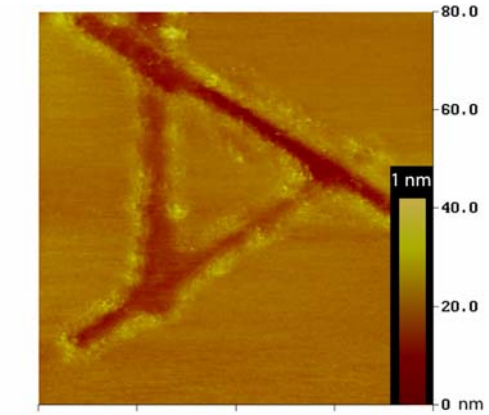

Figure 3 *Triangular nanoarchitecture of graphene.*

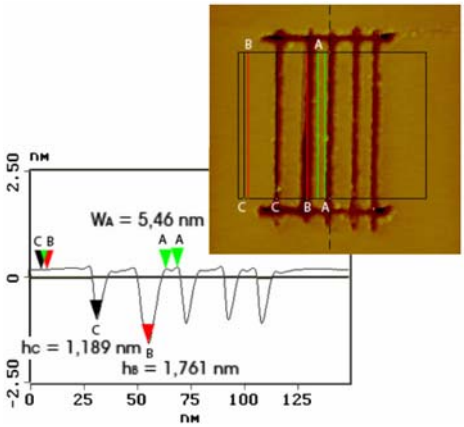

Figure 4 *3D nanoarchitectures of FLG, the line-cut shows the different thicknesses.*

Given the possibility to engineer nanoarchitectures in 3D with atomic resolution and with precise crystallographic orientation control offers an extremely broad field of research that will very likely generate both new physical knowledge and useful practical applications.

STM and electrical study of indium contacted graphene

(OTKA-NKTH grants K-67793 & NI-67851)

L. Tapasztó, P. L. Neumann, G. Dobrik, P. Nemes-Incze, G. Vértesy, Z. E. Horváth, G. Molnár and L. P. Biró

Thin graphite sheets with lateral dimensions of up to a few hundred microns can be prepared by mechanical cleavage of highly oriented pyrolytic graphite (HOPG) with adhesive tape. Here we report the electrical and scanning tunneling microscopy/spectroscopy (STM/STS) investigation of different graphene and few layer graphite (FLG) samples contacted with indium using the mask- and resistless method developed by Girit and Zettl [C. O. Girit, A. Zettl: Appl. Phys. Lett. 91, 193512 (2007)].

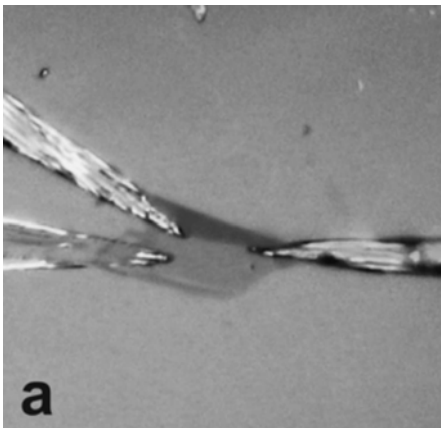

Figure 1 *Optical microscopy image of a graphene flake on Si/SiO_2 substrate contacted with indium solder spikes.*

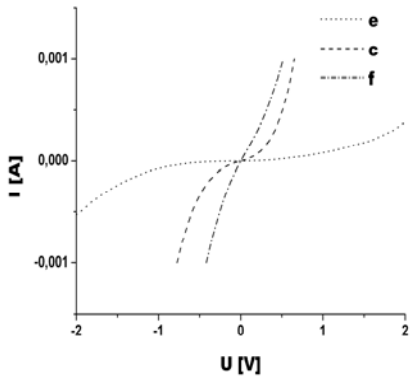

Figure 2 *I-V curves of three typical In contacted graphene flakes showing nonlinear characteristics.*

All graphene and FLG samples were fabricated by mechanical exfoliation of HOPG and deposited on SiO_2 (90nm)/Si substrates. The number of graphene/graphite layers was estimated by optical microscopy from the colour of the flake and then the thickness of suitable selected flakes was checked by tapping mode atomic force microscopy (TAFM). The contacting method uses a micromanipulator to deposit pure indium solder spikes on the desired positions under the optical microscope, see a graphene flake with three electrodes in Fig. 1. In our case, the solder process was performed at 170°C. I-V curves of the as prepared and Ar^+ ion irradiated (30 keV, $5*10^{11}$ ion/cm^2) samples were measured at room and elevated temperatures, furthermore the effect of white light illumination on the resistance was studied. In contrast to bulk graphite, I-V curves of most of the graphene and FLG samples showed more or less nonlinear character, resembling the resultant curve of two

reversely connected Schottky diodes. We the found intensity dependent increase of the conductivity as an effect of illumination in case of both graphene and FLG samples but not in the case of bulk graphite. Ar^+ irradiation could change the rate but not the presence of the effect.

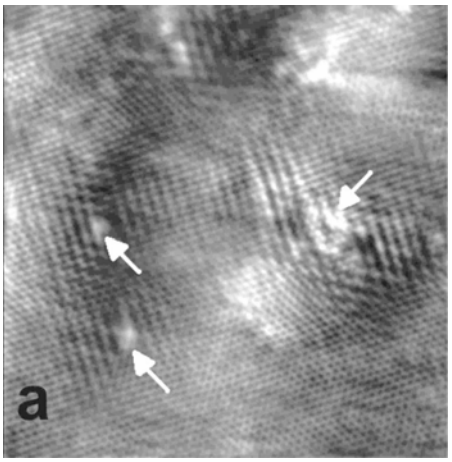

Figure 3 *Atomic resolution STM image of an Ar^+ irradiated graphene sample. White arrows denote the defect sites.*

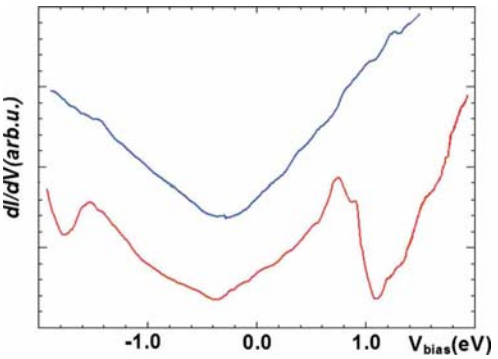

Figure 4 *STS spectra of graphene taken on the defect-free region (upper) and at a defect site of the irradiated graphene (lower).*

STM and STS measurements have been performed under ambient conditions both before and after irradiation on In contacted graphene. The STM tip was positioned under an optical microscope on the contacted graphene flake in order to avoid the crashing of the tip into the insulating SiO_2 substrate. Fig. 3. shows an atomic resolution STM image of an irradiated sample. The honeycomb lattice characteristic to a single graphene layer is clearly seen in the defect-free parts, in contrast to few-layer graphite flakes where a triangular lattice is imaged by STM. Defect sites on the STM images of the irradiated graphene appear as bright spots corresponding to hillocklike protrusions with 0.2–0.5 nm height and 1 nm width, denoted by white arrows in Fig. 3. Oscillations in the electronic density distribution with a period much larger than that of the graphene lattice can clearly be identified in their close vicinity. The origin of these oscillations can not be explained simply by the interference of the electrons scattered by the defect site, the change of the Fermi velocity due to the fluctuation of nearest-neighbor hopping amplitudes also has to be considered. The bias dependence of the oscillation periodicity and the additional peaks in the STS spectra (see fig 4.) support this interpretation, see details in [L. Tapasztó, G. Dobrik, P. Nemes-Incze, G. Vertesy, Ph. Lambin and L. P. Biró: *Tuning the electronic structure of graphene by ion irradiation*, Phys. Rev. B 78, 233407 (2008)].

Scanning tunneling microscopy investigation of functionalized multiwalled carbon nanotubes, the study of circular electronic superstructures

(OTKA-NKTH Grants no: K67793 & NI67851)

P. Nemes-Incze, L. Tapasztó, Al. Darabont, Ph. Lambin, L.P. Biró

Carbon nanotubes (CNTs), these 1D graphene cylinders, or nanowires, have been one of the hot topics of nanoscience since the early nineties. The semimetallic properties of graphene, from which the properties of CNTs can be derived, coupled with the cylindrical structure of the tubes gives rise to the interesting properties of this material. Depending on the crystallographic wrapping direction of the graphene sheet the tubes can be either metallic or semiconducting. This, along with other exciting properties of the tubes offers the possibility of interesting device applications [M.C. LeMieux, et al., *Self-sorted, aligned nanotube networks for thin-film transistors*, Science 321 (2008), 101–104]. However, the immense challenge of separating the semiconducting tubes from the metallic ones, in the as prepared sample, only recently started to be overcome [M.C. LeMieux, et al., *Self-sorted, aligned nanotube networks for thin-film transistors*, Science 321 (2008), 101–104].

One method of solving the before mentioned problem and exploiting the properties of CNTs is to functionalize their sidewalls. Chemically functionalized CNTs may have mechanical, electrical properties that are different from the properties of the as grown tubes. But importantly these properties are largely defined by the functional groups attached to the CNTs. These groups may also be used to tailor the interaction of the tubes with their surroundings. The properties of functionalized CNT are as varied as the functional groups attached to their walls.

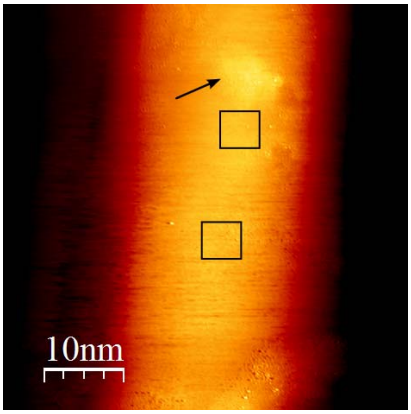

Figure 1 *STM image of a CNT having a protrusion due to the attachment of a functional group (shown by arrow). STM images were taken at the sites marked by squares.*

One of the most common forms of covalent functionalization is the attachment of carboxylic groups to the nanotube sidewalls. In our experiments we have used multiwalled CNTs (MWCNTs) produced by our group, having carboxylic side groups. The samples were measured by scanning tunneling microscopy (STM). Functional groups show up as protrusions on the CNT sidewall (see Fig. 1). We have taken atomic resolution measurements near such a functional group and away from it. In the STM image recorded far away from the defect site, a triangular atomic lattice of the MWCNT is observed. In contrast, in the STM image recorded in the close vicinity of the protrusion, a circular superstructure pattern perturbs the normal atomic resolution image of the carbon

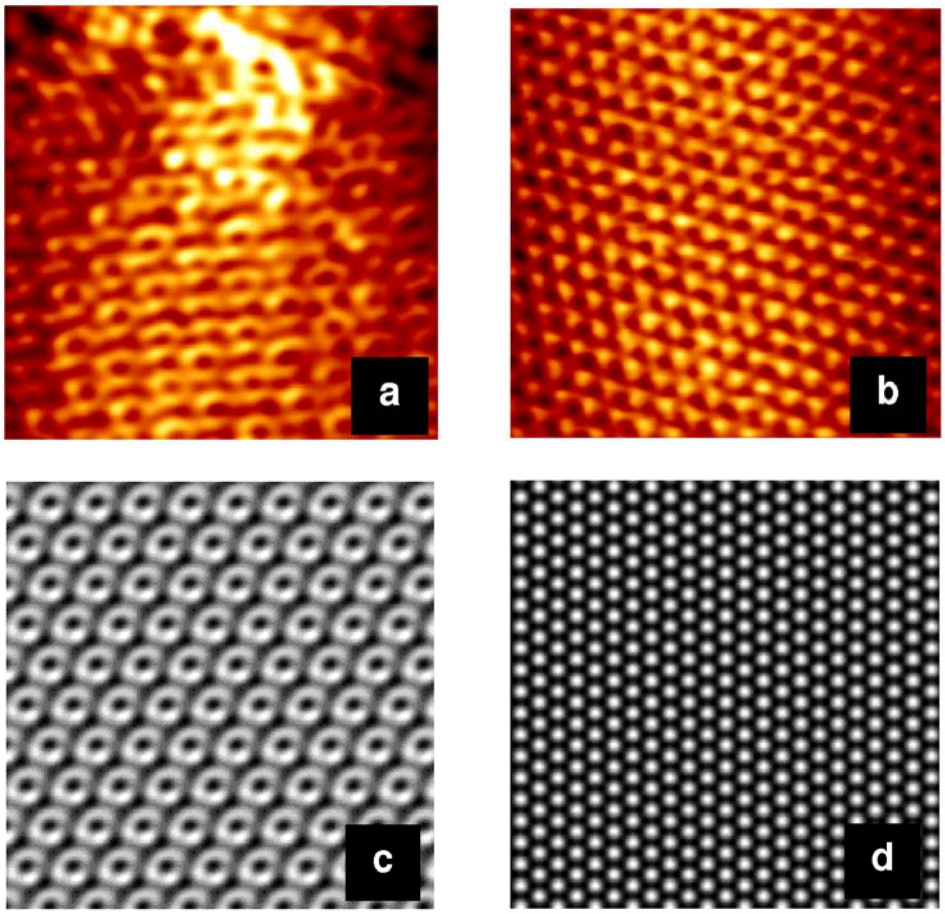

Figure 2 *Atomic resolution STM images of the CNT: (a) near and (b) away from the functional group. (c, d) Simulated STM images of the superstructure and unperturbed atomic resolution image.*

nanotube surface. This pattern is due to the coherent scattering and interference of electrons from the defect in the atomic lattice, at the position of the functional group. Using computer simulation of the scattering and interference phenomena we have successfully reproduced the observed circular superstructure pattern [Nemes-Incze P. et al., *Scanning tunnelling microscopy observation of circular electronic superstructures on multiwalled carbon nanotubes functionalized by nitric acid*, Carbon (2009) in press, doi:10.1016/j.carbon.2008.11.010].

The better understanding of such scattering effects may be of particular importance in the design of nanoelectronic devices.

Biologic and bioinspired photonic nanoarchitectures

(OTKA-NKTH grant K-67793; FP6 BIOPHOT NEST-Pathfinder)

K. Kertész, Z. Vértesy, G.I. Márk, E. Horváth, I. Tamáska, G. Molnár, L. P. Biró

In many millennia, biologic evolution created an extremely complex, self regulating, homeostatic and hierarchically structured environment with well defined organizational levels from nano- to the macro-scale [C. Sanchez, H. Arribart and M. M.Giraud Guille, *Biomimetism and bioinspiration as tools for the design of innovative materials and systems*, Nature Materials 4 (2005) 277.]. The major advantages of biologic "design principles" are the low cost, mild synthesis processes, the multifunctionality of materials and the genetically coded structures with a high level of stability and mild level of variability. Due to the fact that biologic evolution acts in a "trial and error" manner instead of using a very wide range of different materials like technical evolution does, biologic evolution uses a limited number of materials but in infinitely more complex structures as compared to technical evolution. Therefore, the simpler structures evolved biologically, like scales giving structural colors on butterfly wings or beetle elytra with photonic nanoarchitectures (photonic crystal type structures built of chitin and air), can be used both as produced in nature or as "blueprints" for man made nanoarchitectures and devices.

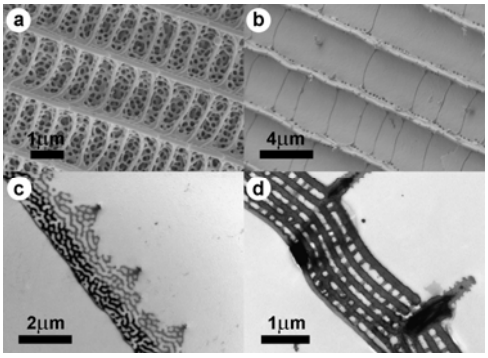

Figure 1 *Electron micrographs showing the nanoarchitectures occurring in the dorsal cover scales of the* Pseudolycena marsyas *(a, c) and of the* Chrysiridia ripheus *(b, d). SEM images (a, b), TEM images (c, d).*

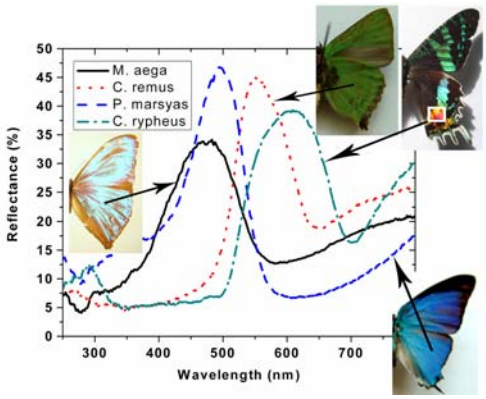

Figure 2 *(Color on-line) Reflectance maxima of the four investigated wing pieces at 45° in backscattering geometry, recorded to white diffuse standard.*

We successfully showed that pieces of the wings of various butterflies which have scales with photonic nanoarchitectures can be used very effectively as selective and concentration sensitive gas/vapor sensors in normal, room ambient [Biró LP, Kertész

K, Vértesy Z, Bálint Zs: *Photonic nanoarchitectures occurring in butterfly scales as selective gas/vapor sensors*, in: The Nature of Light: Light in Nature II, edited by Katherine Creath, Proc. of SPIE Vol. 7057 (2008) 705706-1.]. The butterfly scales with photonic crystal type nanoarchitectures (Fig. 1), may exhibit various colors, covering the full visible range (Fig. 2). We used a very simple setup: the wing pieces were placed in a flow cell with quartz window (Fig. 3) and a small membrane pump was used to pass the ambient air, or ambient air/vapor mixture through the cell.

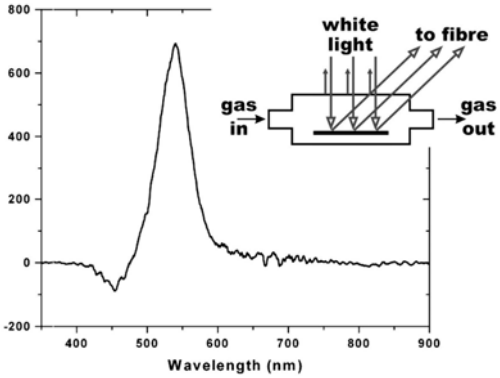

Figure 3 *Difference of the spectra when flowing air, or air/ethanol mixture through the cell. The inset in the right upper corner shows schematically the measurement arrangement*

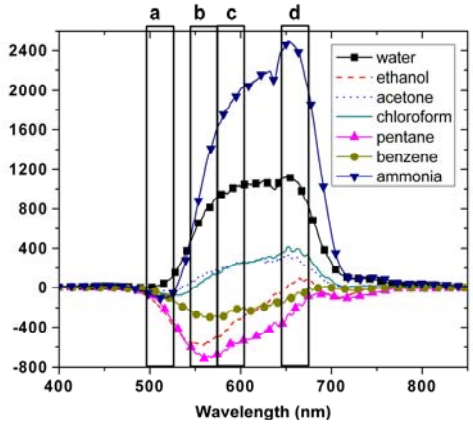

Figure 4 *(Color on-line) Difference signals for the Chrysiridia ripheus wing for seven different vapors. Selecting the area under the curves of the difference signal in the four labeled regions: (a), (b), (c) and (d), one may unambiguously identify which vapor is present in the ambient air.*

As shown in Fig. 3 and Fig. 4 very clear and gas specific difference signals can be recorded for all vapors and all butterfly wings used. This clearly offers the possibility to realize cheap, highly sensitive, selective detectors operating on similar principles like we reported earlier for chemically functionalized carbon nanotubes [Horváth ZE, Koós AA, Kertész K, Molnár G, Vértesy G, Bein MC, Frigyes T, Z. Mészáros, Gyulai J and Biró LP: *The role of defects in chemical sensing properties of carbon nanotube films*, Applied Phys. A, 93 (2008) 495.].

The major advantage of using butterfly wings as gas sensors is given by the very low cost production of nanoarchitectures. The color generating nanoarchitectures have role in sexual signaling, so that they have a high degree of reproducibility.

Web-Schrödinger 2.0, an Internet based tool for the study of electron motion in nanosystems

(OTKA-NKTH-K-67793, Belgian FNRS-MTA)

Géza I. Márk, Philippe Lambin, and László P. Biró

In order to construct nanoelectronic devices we need to study the motion of electrons inside nanostructures. The most important difference of the macroworld and nanoworld is that electronic motion in the nanoworld is governed by the laws of quantum mechanics. During the last decade we developed a wave packet dynamical (WPD) simulation package for the investigation of electron tunneling- and transport through nanosystems. This software is based on the solution of the time dependent two- and three dimensional Schrödinger equation. The program proved to be a considerable help at the interpretation of the STM images of carbon nanotubes. During the year 2007, we prepared an Internet based user interface for our WPD simulation. The program can be accessed through a simple Web browser. The Internet address of this software, named Web-Schrödinger is:

http://www.nanotechnology.hu/online/web-schroedinger/index.html

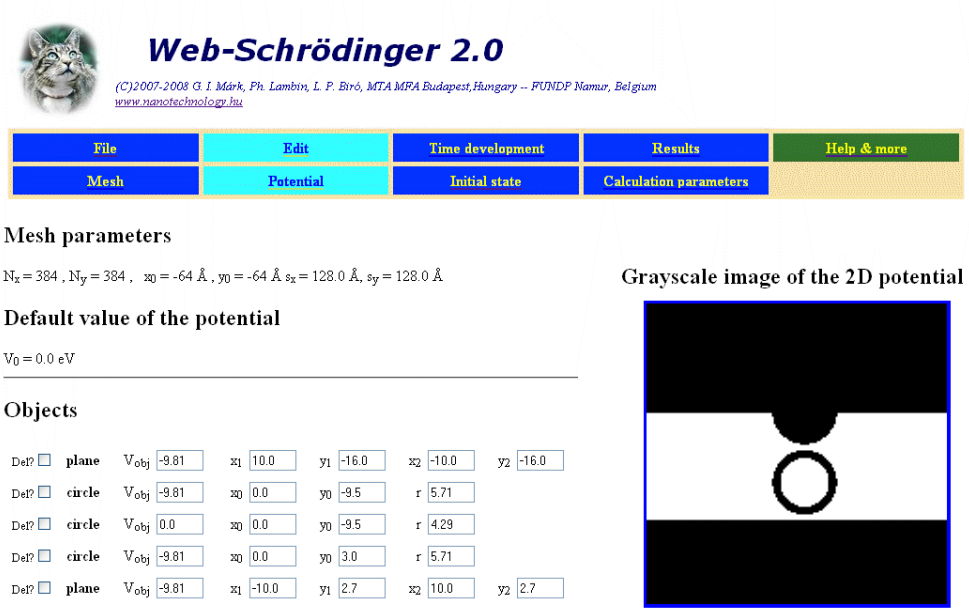

Figure 1 *This screenshot from Web-Schrödinger 2.0 shows the construction of the potential used for modelling the electron tunneling through the STM tip–nanotube–support system.*

In 2008 we created a new user interface for Web-Schrödinger, the user is now capable to edit, load and save potential and initial state parameters (cf. Fig. 1). An example library also comes with this version, which illustrates several important phenomena in quantum mechanics, including allowed and forbidden bands, tunneling, scattering, quantum revival, etc. An example from "real research" is also there, namely the simulation of scanning tunneling microscope investigation of a carbon nanotube. Web-Schrödinger 2.0 is quite useful in education of quantum mechanics and nanoelectronics. Numerical solution of problems on a computer drastically widens the assortment of the problems that can be solved analytically, and it opens the possibility for the study of more realistic systems as well. By performing "computer experiments" and studying the outcomes of computer simulations students can get a certain "personal" experience in the nanoworld. The presentation of the results in graphical form may contribute to a large extent to the understanding of the concepts and phenomena studied. Fig 2. illustrates the complexity of phenomena occurring in a nanosystem. The "nano Christmas tree" studied in this example was composed of thin potential walls. Scattering and interference phenomena similar to those seen in this example also occur in real nanodevices.

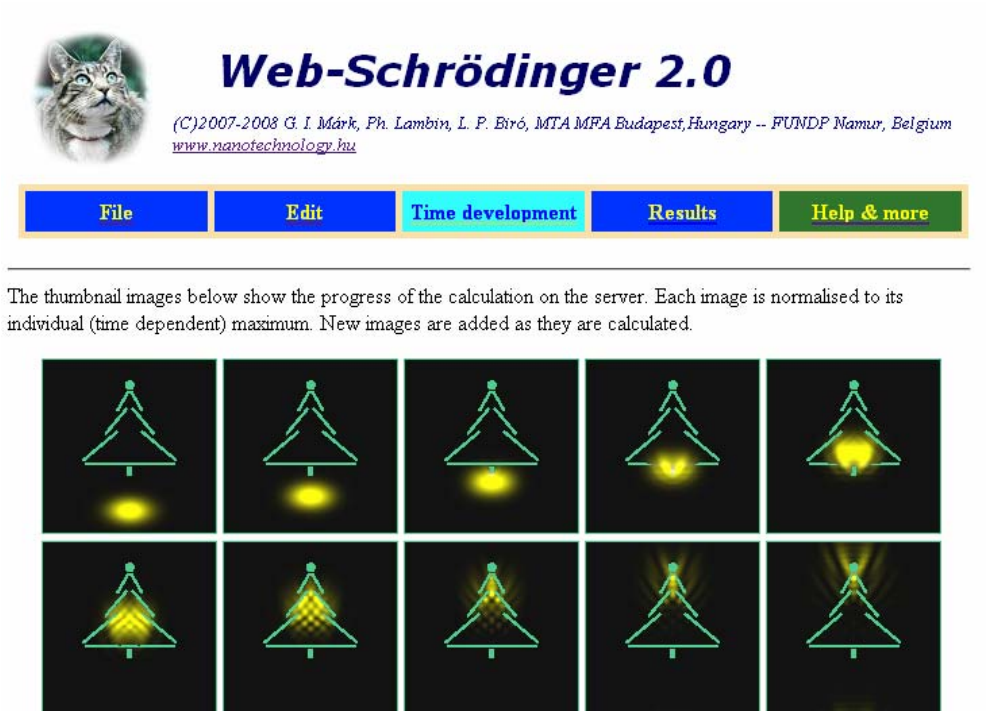

Figure 2 *Tunneling of an electronic wave packet with 5 eV energy through a „nano Christmas tree" built of potential walls of 0.1 width and 2 eV height. Total size of the tree is 3 nm. Note the complicated interference and scattering patterns.*

Photonics Department

Head: Fried Miklós, D.Sc., scientific advisor

Research Staff

Petrik Péter, Ph.D., Head of Ellipsometry Laboratory
Serényi Miklós, CSc., Head of Semiconductor Photonics Laboratory
Balázs János, Ph.D (part-time)
Gasparics Antal, Ph.D.
Hámori András, dr univ.
Horváth Róbert, Ph.D
Juhász György, dr univ.
Kádár György, DSc
Kurunczi Sándor, Ph.D
Laczik Zsolt, Ph.D. (on leave)
Lohner Tivadar, CSc.
Makai János, CSc (part-time)
Nagy Norbert, Ph.D.
Polgár Olivér, Ph.D
Rácz Miklós, Ph.D (part-time)
Riesz Ferenc, Ph.D.
Török Péter , DSc. (on leave)
Vértesy Gábor, DSc

Ph.D. students / Diploma workers

Kozma Péter, Ph.D. student
Major Csaba, Ph.D. student

Technical Staff

Jankóné Rózsa Márta, technician

Main results: In the frame of several collaborations, we have made the spectral version of the wide-angle ellipsometer. International patent (PCT) process was started.

Magnetic measurements were performed on low-carbon-containing steel in the frame of an international collaboration (Universal Network for Magnetic Non-destructive Evaluation) which aims to disseminate magnetic methods in the practice, mainly in power plants. Our methods prove the most sensitive to show the changes.

Optical waveguide lightmode spectroscopy has been used to observe successfully the deposition of bacterial flagellar filaments of mean length 350 nm from bulk solution onto a smooth planar substratum, chemically modified to covalently bind the flagellar filaments on contact.

We have two pending patents in the frame of Aquanal-project to detecting liquid hydrocarbon derivatives floating on water. Six complete equipments are under test in an MOL plant located in Szajol (Hungarian Plain). The WESTA-T Ltd. made the arrangements for further serial production. The optical monitor part and the electronic unit were officially tested and certificated for use in potentially explosive atmospheres.

We are involved in two “National technology development” projects: “Development of integrated process monitoring metrology for the 32 nm technology node of IC processes” and “Development of metrology tools based on electrical and optical techniques for in-line and laboratory qualification of thin film solar cells”

Self-assembly of rodlike receptors from bulk solution

(Marie Curie Actions of the EC (OPTICELL, at Carnfield U.), OPTIBIO (at MFA) and the OTKA postdoctoral fellowship (at MFA) "Optical resonances in functionalized protein assemblies for label-free sensing")

S. Kurunczi, R. Horváth, Y.-P. Yeh, A. Muskotál, A. Sebestyén, F. Vonderviszt and J. J. Ramsden

Optical waveguide lightmode spectroscopy has been used to observe the deposition of bacterial flagellar filaments of mean length 350 nm from bulk solution onto a smooth planar substratum, chemically modified to covalently bind the flagellar filaments on contact. At the highest practicable bulk concentration, the filaments follow the theoretically predicted kinetics of random sequential addition of highly elongated rigid rods to the substratum, but addition terminates with the rods almost perpendicular to the substratum. Rod-rod correlations in the bulk anomalously accelerate the rate of arrival of the filaments at the surface of the substratum, relative to spheres. At lower concentrations, this effect is absent, and the rods have time to order themselves on the substratum, forming a two-dimensional array.

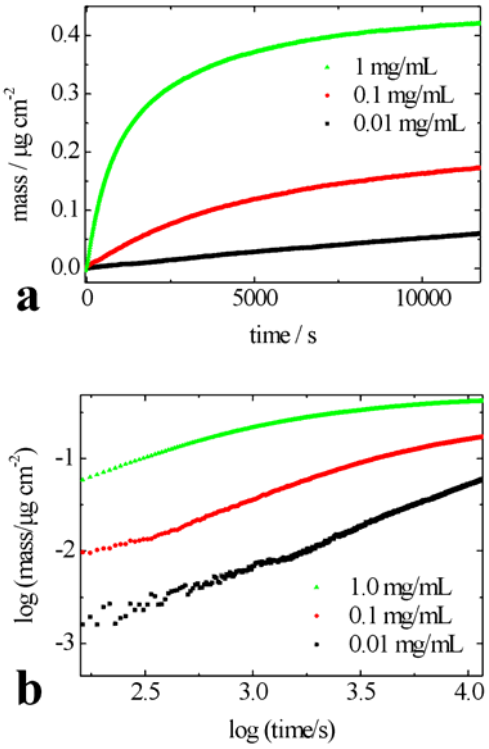

Figure 1 *Plots of the amounts of deposited flagellar filaments vs time, calculated from the OWLS data, adsorbed on Si0:6Ti0:4O2. From bottom to top, bulk solution concentrations for 0.01, 0.1 and 1 mg/L. Top panel (a), lin-lin plot; bottom left panel (b), log-log plot of the same data; bottom panel*

Development of integrated process monitoring metrology for the 32 nm technology node of IC processes

(NKFP-07-A2-ICMET_07)

M. Fried, G. Juhász, P. Petrik

The aim of this project (leaded by Semilab Inc.) is to develop measurement technology and equipment, which enables the process control of the 32-65nm generation integrated circuit production complying with the clean room and automatization standards. The equipment, which will be delivered by the project, enables one of the most important technological processes in the semiconductor dopant (resistance and type adjustment) monitoring in several steps: after the implantation and thermal activation of the dopant species.

MFA's task is in the project to prepare ion-implanted reference samples (ultra-low-energy implantation, ULE-imp), and to perform reference measurements.

Ellipsometry is very sensitive for changes but the detection is limited from two directions. The lower limit is the minimum detectable lattice-disorder depending on the atomic mass of ions and the implantation energy. The upper limit is the full amorphization, also depending on the atomic mass and energy, two orders of magnitude higher than the lower limit. Precision is better than 1 % within the two limits if calibrated with ion-backscattering technique (RBS, available in MFA). RBS needs expensive accelerator and vacuum system but ellipsometry being an optical method can be used in-situ or in-line. Unfortunatly, ellipsometry cannot be applied for the determination of electrically active dopants after high temperature annealing.

Ellipsometry shows increasing damage thickness with increasing energy. Similarly, the series of increasing dose show an increasing damage.The used energies are less than 10 keV which results in less than 20 nm range.

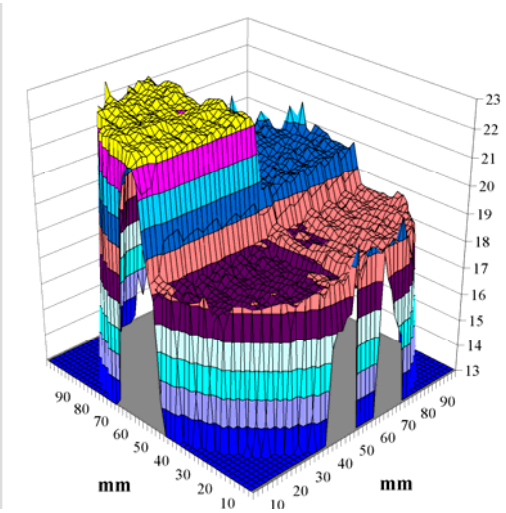

Figure 1
Pseudo-dielectric function-map measured by wide-angle ellipsometry on a sample implanted with 10 keV boron at doses of 0, 1, 3, 5e15 B/cm2

Development of metrology tools based on electrical and optical techniques for in-line and lab qualification of thin film solar cells

(TECH_08_ D2(2008) PVMET_08)

M. Fried, C. Major, G. Juhász, P. Petrik

The aim of this project (lead by Semilab Inc.) is to develop an equipment and measurement technology family capable to perform electrical and optical measurements for in-line and laboratory qualification of thin film solar cells. MFA's task is in the project to make applicable spectroscopic ellipsometry for this purpose.
We develop optical models for transparent conductive oxides (ZnO:Al) Figure 1 shows a photo of the sample where the measured points are indicated by numbers from 1 to 9. Spectroscopic wide-angle ellipsometry measurements of ψ at the measured points are shown in Figure 2. These points have different physical properties such as transparency, conductance and thickness.

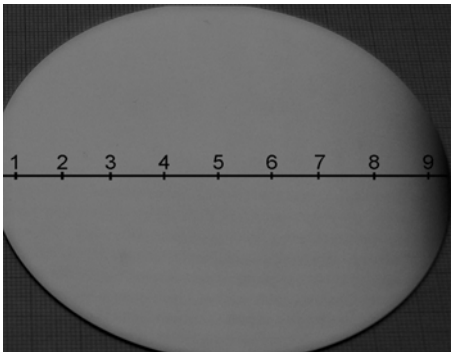

Figure 1 *Measured points on a 4" sample*

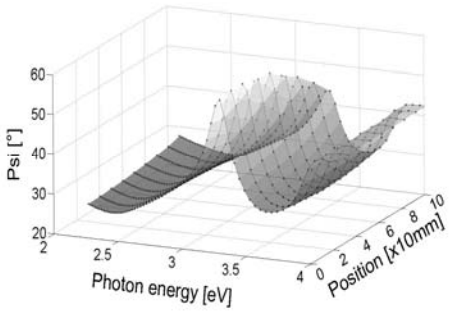

Figure 2 *Spectra of measured Psi*

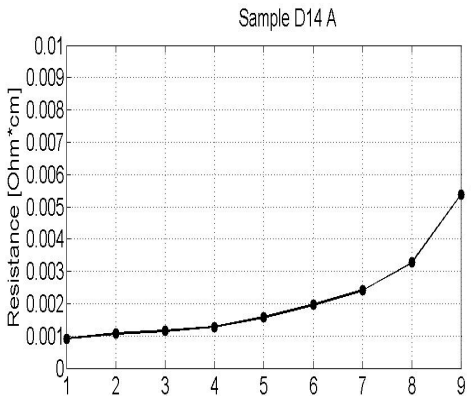

Figure 3 *Specific resistance distributon*

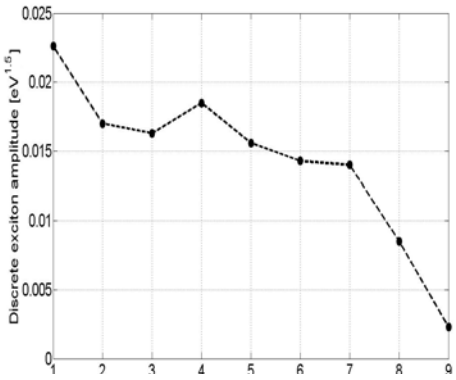

Figure 4 *Discrete exciton amplitude distr.*

Inspection of steel degradation by Magnetic Adaptive Testing

(OTKA K62466)

G. Vértesy

A new, nondestructive magnetic measurement method has recently been developed, based on systematic measurements of minor magnetic hysteresis loops. This technique can serve as a powerful tool for comparative measurements, and for detection of changes, which occur in structure of the inspected samples during their lifetime or during a period of their heavy-duty service. It has been shown previously that this method, Magnetic Adaptive Testing (MAT), is significantly more helpful than that of the traditional major loop studies. It is highly suitable for very sensitive nondestructive characterization of structural changes in such materials. Another advantageous and independent outcome of the tested method is the confirmation, that without magnetic saturation of the samples, measuring a series of minor loops and performing the MAT method on the obtained data-pool, reliable and very sensitive parameters can be determined. Moreover, the relative measurement can be done with a ferromagnetic yoke attached to the sample, and the yoke does not even have to be large and very special.

In the present work MAT was applied for a series of degraded steel, and the measurements were performed both on magnetically closed and open samples. Structural degradation of the compressed (cold rolled) steel samples was examined and correlation was studied between the nondestructively measured MAT results and the Vickers hardness (HV) and the ductile-brittle transition temperature (DBTT) determined destructively, in the traditional way.

Three series of low carbon steel samples, each containing five samples, were prepared for the magnetic measurement. The material of them is low-carbon steel with 0.16 wt.% of C, 0.20 wt.% of Si, 0.44 wt.% of Mn, with the rest of Fe. Convenient pieces of the material were cold-rolled down to plastic deformation, ε, of 0, 5, 10, 20 and 40%, and then the samples of desired dimensions and shapes were carefully machined from the deformed steel. Three types of shapes were prepared: picture-frames, rectangular plates and rectangular bars. Vickers hardness, HV, of the deformed material was measured with the standard Vickers indentation technique. Charpy impact test was performed on bar samples in the 201÷363 K temperature range. The ductile-brittle transition temperature, DBTT, was defined as the midpoint between the low toughness brittle- and the high toughness ductile-fracture regimes.

A specially designed Permeameter was applied for measurement of families of minor loops of the magnetic circuit differential permeability. The picture-frame samples were magnetized and the induced signal from the time-change of their magnetization was recorded with the aid of magnetizing and pick-up coils, respectively, wound directly on each of the samples. The magnetically open plate- and bar-samples were measured by attached magnetizing/measuring heads, namely by U-shaped yokes equipped with magnetizing and pick-up coils each. The samples were magnetized with step-wise increasing magnetic field and the signal of pick-up coil

was used for characterization of the sample. The Permeameter works under full control of a PC computer. The computer registers data-files for each measured family of the minor "permeability" loops. The recorded signal data were processed by a data-evaluation program, one family of minor loops for each measured sample. The data-pools of the minor loops determined for every sample made possible to calculate the optimal MAT descriptors. The most sensitive and reliable MAT descriptors were taken for each series of samples. In each measurement series, all the descriptors were normalized by data of the virgin (not rolled) sample, which made it possible to compare numbers measured on the different series

Representative sets of the optimal MAT descriptors are plotted in Fig. 1 for the frame-, for the plate- and for the bar-shaped samples, as functions of destructively measured quantities. Regular, linear correlation, with low scatter of values was found between the optimally chosen MAT descriptors and the ductile-brittle transition temperature (see Fig. 1).

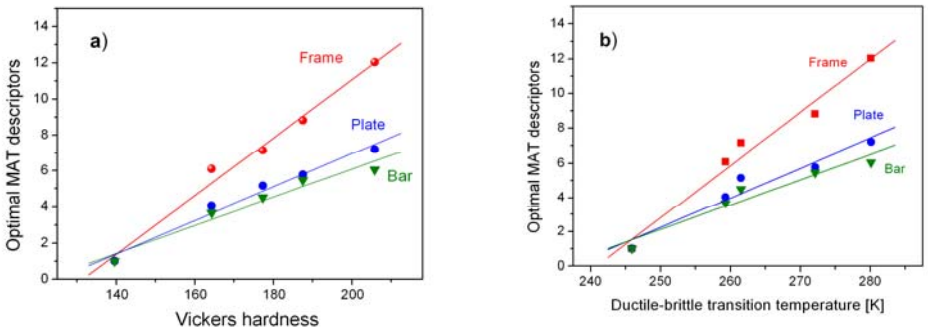

Figure 1. *Optimal MAT descriptors versus Vickers hardness (a) and DBBT (b) for different shape compressed steel samples*

As expected, the highest sensitivity was obtained in the case of magnetically closed samples, which follows from the most perfect magnetizing and sensing conditions in this measurement. But it is also evident that qualitatively the same relationships were obtained for all the three sample series. It is clearly seen from results of the measurements, that the consecutive series of the nondestructively determined MAT descriptors well describe magnetic reflection of the investigated material modifications. The presented figures demonstrate, that in the case of the low carbon steel samples, plastically deformed by cold rolling, MAT feels the difference between the most compressed and the not compressed samples approximately as 6:1, in the case of bar samples, in contrast to 1:1.8 sensitivity as it is felt by the Vickers hardness and ductile-brittle transition temperature measurement, respectively.

The presented results give a good chance to determine the level of embrittlement of ferromagnetic steel objects (e.g. of the nuclear pressure vessel surveillance specimens) due to their heavy-duty industrial service period, with the aid of the non-destructive method of Magnetic Adaptive Testing.

Magnetic nanoparticles combined with submicronic bubbles and dye for oncologing imaging (NANOMAGDYE)

(EU FP7, CP-FP 214032-2)

Gábor Vértesy, Antal Gasparics

The objective of the project consists in developing tailored biocompatible magneto-optical nanosystems based on magnetic iron oxide nanoparticles. The project will comprise elaboration of the nanosystems and characterisation of their structural, optical and magnetic properties. In vitro and in vivo tests will be carried out to test their biocompatibility. The combination of magnetic and optical properties will be achieved through hybrid nanoparticles made of a magnetic iron oxide core on which an organic layer (dye) will be grafted through a dendrimer molecule and a phosphate entity. This grafting strategy will be extended to bubbles on which magnetic nanoparticles will be glued. The grafting sites will be controlled in order to design new geometries and architectures from rings up to submicronic magnetic spheres. Magnetic nanoparticles with monodisperse size between 2 and 100 nm will be elaborated in order to increase the possible range of properties. The opto-magnetic nanoparticles will be tested in a medical application and a dedicated magneto-optical probe will be fabricated. Current methods for labelling the lymph node system use a dye (vital blue) or radio nuclide injection detected through optical or Gamma probes, respectively, or a combination of both types of markers. Combining optical and magnetic labelling into a single biocompatible nanosystem will provide higher spatial resolution than presently and avoid using ionising radiation to improve patient safety and medical effectiveness. Stabilized submicronic bubbles labelled with the optical-magnetic nanoparticles will play the role of a contrast agent currently used in ultrasound imaging and facilitate the uptake of the iron nanoparticle, and therefore improve node imaging.

Role and contribution of MFA to the project: a new method and new measuring probe will be developed for determining magnetic susceptibility of super-paramagnetic particles. The method is based on a high sensitivity magnetic field sensor, developed in the institute.

Fabrication and investigation of diffractive optical elements using ion implantation

(Hungarian Scientific Research Fund under Grant No. K68688)

T. Lohner, I. Bányász, M. Fried, C. Major, F. Pászti, A. Watterich

Tellurite glasses have gained a widespread attention because of their potential as hosts of rare-earth elements for the development of fiber and integrated optic amplifiers and lasers covering all the main telecommunication bands. Er^{3+} doped

tellurite glasses in particular are very attractive materials for the fabrication of broadband amplifiers in wavelength division multiplexing around 1.55 μm, as they exhibit large stimulated cross sections and broad emission bandwidth. Furthermore, tellurite glasses have low process temperature, good chemical durability and nonlinear properties.

Fabrication of channel waveguides in Er-doped tungsten-tellurite glasses using ion impantation was recently demonstrated. In order to get a deeper understanding of the process and to optimize the characteristics of the waveguides, we fabricated a set of planar waveguides, each of 7 mm x 7 mm lateral dimensions, in an Er-doped tellurite glass sample by implantation of 1.5 MeV nitrogen ions. Doses of the implanted ions ranged from $1x10^{16}$ to $8x10^{16}$ ions/cm^2. The samples were studied using interference phase contrast microscopy (Interphako), m-line spectroscopy and spectroscopic ellipsometry. The results show that a barrier layer of reduced refractive index was created around the range of the implanted ions at every dose. It is hoped that combination of the results obtained in these experiments with simulations for channel waveguides will make it possible to optimize ion-implanted fabrication of integrated optical components in this tellurite glass.

To complement the results obtained with dark-line spectroscopy, the sample was measured using a SOPRA ES4G spectroscopic ellipsometer with microspot facility (about 0.15 x 0.35 mm). The wavelength range was 300 – 750 nm. Evaluation of the ellipsometric spectra measured on the unimplanted glass surface was performed using a three-phase optical model consisting of ambient (air), a surface roughness layer and the substrate (glass). The roughness layer was taken into account on basis of effective medium approximation; the roughness layer consists of 50% of glass and 50% of void.

The Cauchy dispersion relation was employed to describe the refractive index and the extinction coefficient of the glass. The five parameters of the Cauchy dispersion relation and the thickness of the surface roughness layer were considered as free variables. For the analysis of the spectroellipsometric data we applied the evaluation software WVASE32 created by the Woollam C., Inc. The measured and the best-fitted spectra are displayed in Figure 1. The evaluation yielded 7.90 ± 0.06 nm for the thickness of the surface roughness layer and 2.081 for the refractive index of the non-implanted glass substrate for the wavelength of 635nm.

The optical model applied in the evaluation of the spectroscopic ellipsometry data for different ion-implanted areas consisted of three layers on top of the glass substrate. The layer adjacent to the non-implanted tellurite-glass substrate ($layer_1$) represents the depth region where the nitrogen ions come to rest. The second layer ($layer_2$) corresponds to the depth region where the implanted nitrogen ions lose their energy while traversing the glass before they stop in $layer_1$. The surface roughness film was considered as the third layer. The dielectric functions of $layer_1$ and $layer_2$ were described by Cauchy dispersion relation. The parameters of the Cauchy dispersion relations and the layer thicknesses were considered as free parameters. Figure 2 shows the measured and the best-fitted spectra for the case of the $4{\cdot}10^{16}$ ions/cm^2 irradiation dose. The evaluation yielded a thickness value for $layer_1$ and

layer$_2$ 97±19 nm and 1779±16 nm, respectively, and different refractive index from the bulk. The agreement between the measured and generated spectra is good [*Banyasz et al: Nitrogen-ion-implanted planar optical waveguides in Er-doped tellurite glass: fabrication and characterization, (ed.: Digonnet MJF, Jiang S, Glesener JW and Dries JC) SE: PROCEEDINGS OF THE SOCIETY OF PHOTO-OPTICAL INSTRUMENTATION ENGINEERS: (SPIE), Conference on Optical Components and Materials V, JAN 21-23, 2008, San Jose, CA, SP: SPIE, BN: 978-0-8194-7065-2, 6890(2008) A8901-A8901*]

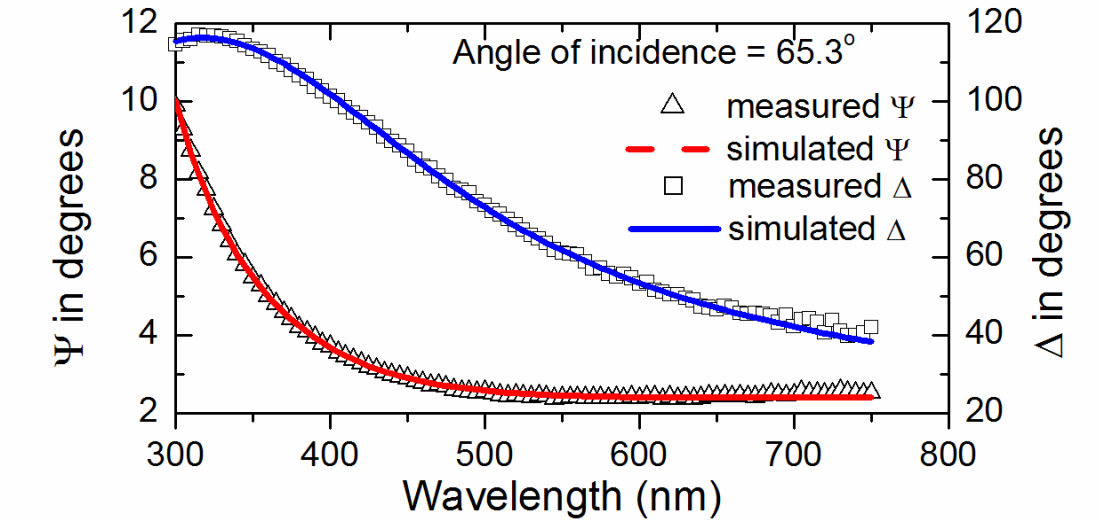

Figure 1 *Measured and simulated ellipsometric spectra for the unimplanted glass*

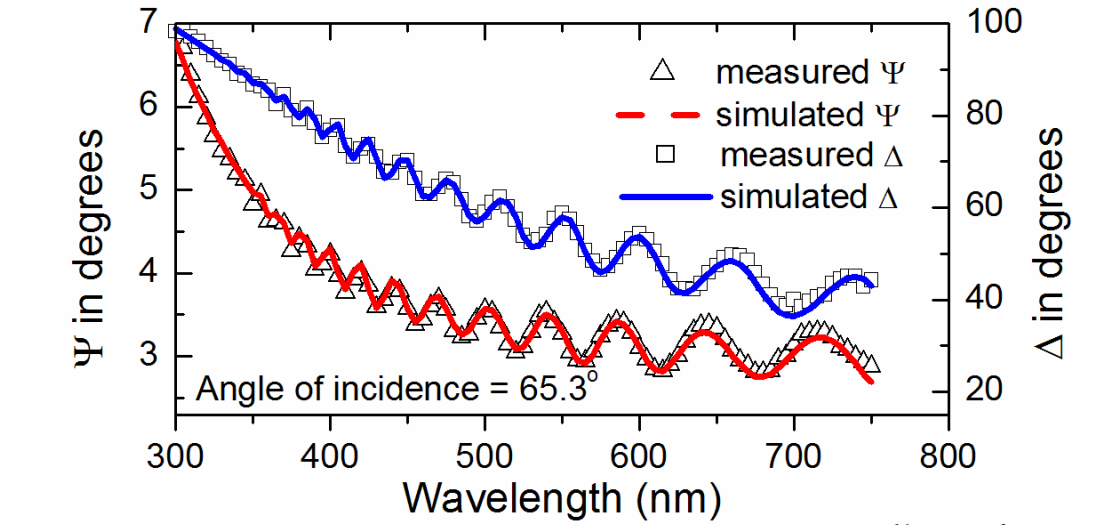

Figure 2 *Measured and simulated ellipsometric spectra for ion dose of 4x10^{16} ions/cm^2).*

Nanocrystals and nanolayers characterized by ellipsometry

(EU I3, ANNA Project Nr. 026134,OTKA K61725)

P. Petrik, M. Fried, T. Lohner

Nanocrystalline materials are intensively studied worldwide because of the wide range of applications from microelectronics through photonics, to photovoltaics. We improved our main characterization method, ellipsometry, in order to be able to characterize nanocrystalline semiconductors in a more accurate and sensitive way [P. Petrik, "Ellipsometric models for vertically inhomogeneous composite structures", physica status solidi (a) 205:(4) 732-738 (2008) (Drude Award speech http://www.icse4.se/awards/).].

This task was part of a European project (EU I3, ANNA Project Nr. 026134), the aim of which was to form a virtual laboratory for special characterization tasks, to unify the input, the workflow, and to check, correlate and improve all the methodologies offered in the consortium. This system should work in a way that allows easy access to the infrastructures for all users. Details can be found on the homepage of the project: **http://www.i3-anna.org**.

We improved both the parametrization of the dielectric function and the layer structure to properly describe thin and ultra-thin layers of nanocrystals or dielectrics. We used different parametrizations including the model dielectric function of Adachi (Fig. 1, [Petrik et al, "Nanocrystals characterization by ellipsometry in porous silicon using model dielectric function", accepted for publication in the Journal of Applied Physics.]) and the generalized critical point model (Fig. 1). We are using grid supercomputing on the 128-node "atxblade" cluster of MFA, because of the large computation need of multi-parameter models. We not only develop the parametrization of the dielectric function, but also the models for a multi-layer structure to properly describe the transition of properties at layer boundaries and surfaces. This is especially important when modeling ultra-thin layers like silicon oxides on SiC [Szilágyi et al, „Oxidation of SiC investigated by ellipsometry and Rutherford backscattering spectrometry"; JOURNAL OF APPLIED PHYSICS v.104, Article Number: 014903, 2008]. Using a combination of ellipsometry and backscattering spectrometry the density of the layer could be determined as well. This is a unique combination, because ellipsometry provides the physical thickness, while backscattering spectrometry provides the number of atoms per unit area.

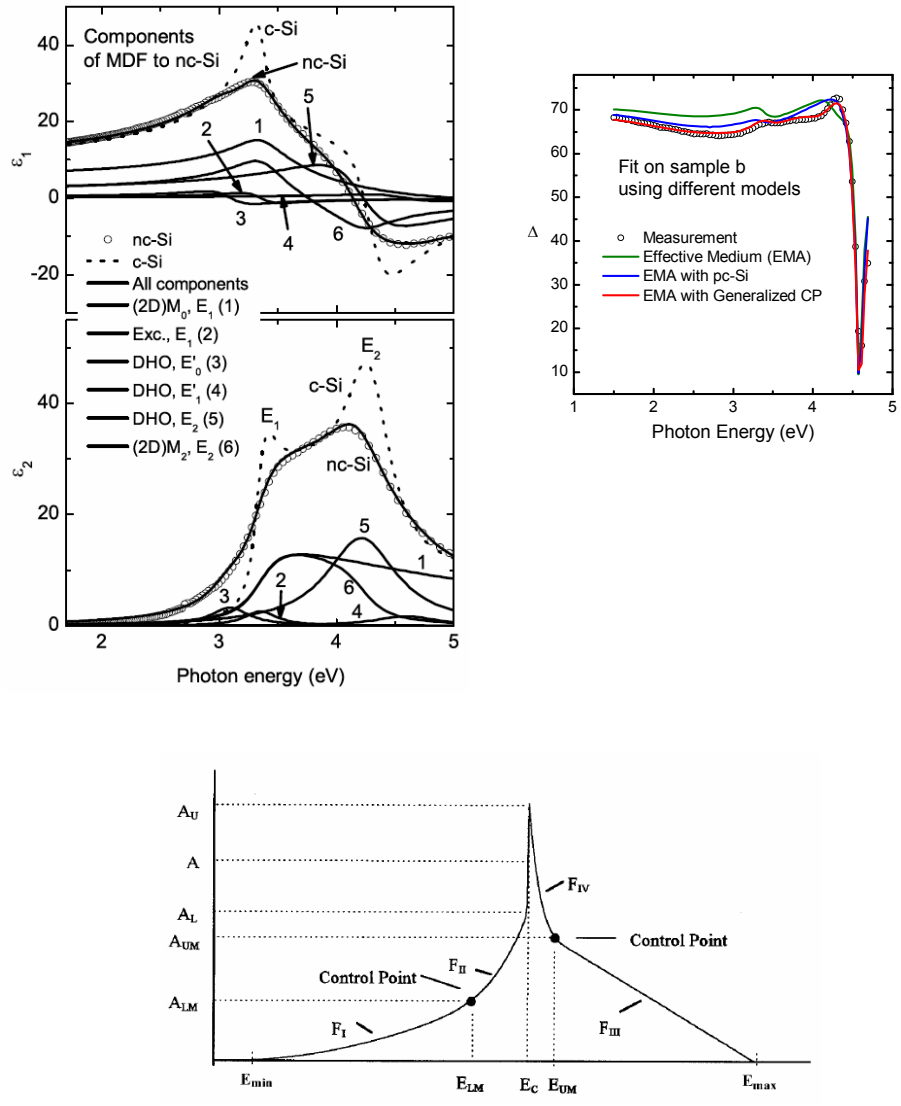

Figure 1 *Top-right: Fit on the dielectric function of nanocrystalline silicon using the „model dielectric function" parametrization of Adachi (Ref. 1)i. The direct inter-band transitions are described using distinct oscillators depending on the type of the critical point. "nc-Si" is a fine-grained nanocrystalline silicon generally used as an EMA ("Effective Medium (EMA)") component to simulate polycrystalline and porous silicon materials. Top-left: Ellipsometric fit on porous Si using effective medium approximation (EMA) with single-crystalline and nanocrystalline ("EMA with pc-Si") components, and with the generalized critical point model ("EMA with Generalized CP). The bottom figure demonstrates how the critical point features are approximated within the Generalized CP model.*

Parametrization and profiling of disorder in semiconductors by ellipsometry

(EU I3, ANNA Project Nr. 026134,OTKA K61725)

P. Petrik, M. Fried, T. Lohner, Z. Zolnai, N. Q. Khánh, O. Polgár

We developed optical models and improved the methods of ellipsometric characterization of ion implanted structures. We investigated different materials from Si [Petrik et al, "Ellipsometric models for the near-surface disorder in silicon ion implanted by 10-keV helium at high dose", IBMM 08 - 16th International Conference on Ion Beam Modification of Materials, from August 31 to September 5, 2008, Dresden, Germany, poster presentation.;.Petrik et al, „Ellipsometry on ion implantation induced damage", 16th International Conference on Advanced Thermal Processing of Semiconductors – RTP2008, September 30 – October 3, 2008, Las Vegas, USA, IEEE Proceedings Catalog Nr. CFP08TPS-PRT, ISBN: 978-1-4244-1950-0, page 93-101. – invited talk] through SiC [Lohner, et al, "Complex dielectric function of ion implantation amorphized SiC determined by spectroscopic ellipsometry", physica status solidi (c) Volume 5 Issue 5, May 2008 (p 1374-1377] to CdTe [Petrik et al, „Ion implantation induced disorder in single-crystal and sputter-deposited polycrystalline CdTe characterized by ellipsometry and backscattering spectrometry", physica status solidi (c) Volume 5 Issue 5, May 2008 p 1358-1361]. We focused on the investigation of the near-surface region, because of the enhanced sensitivity. The ellipsometric measurement is especially sensitive near the surface (e.g., in Si, down to 5-20 nm), because of the limited penetration depth of light around the critical point (CP) energies. We used wedge masks to bring the damaged region close to the surface [Fried et al, "Defect profiling by ellipsometry using ion implantation through wedge masks", physica status solidi (c) Volume 5 Issue 5, May 2008 p 1227-1230].

The investigation of Si implanted by low energy (10 keV) He at high fluences (up to 10E17 cm^{-2}) was important, because using this method point defects are created. The problem was, that the penetration depth of He is large (compared to the above mentioned sensitive region of the top 5-10 nm in Si), so we used wedge masks to create damage near the surface. Using models with proper reference materials the depth profile of the structure without using masks could also be investigated (Fig. 1). We were able to sensitively characterize the depth distribution of disorder and voids (down to a depth of 200 nm).

Using a sputter-deposition technology for CdS/CdTe, a solar cell efficiency of 14 % was demonstrated. For accurate fitting of the optical properties of sputter deposited CdTe films, parameterization of the critical point structures is needed for samples of grain sizes covering a broad range. The optical response of a polycrystalline material as a function of grain size is analogous to the optical response of ion implanted material as a function of fluence, whereby the grain size can be described in terms of an effective defect density, Thus, both polycrystallinity and implantation damage influence the long range order in the material and hence the lifetime of excited

carriers. We used ion implantation to create defects in a controlled and reproducible way, as first attempts towards the development of models, parameterizations, and ultimately databases for polycrystalline CdTe characterization. We investigated the optical response of bulk single-crystal CdTe (c-CdTe), sputter-deposited polycrystalline CdTe films (pc-CdTe), and single-crystal Si ion implanted with different ions and fluences covering defect densities starting from single-crystalline and ranging to highly disordered. We used second derivative analysis (Fig. 2) to measure the broadening of the CP features as a function of fluence (disorder). This method can in turn be used to estimate track sizes of impinging ions [Polgáret al, "Determination of ion track and shapes with damage simulations on the base of ellipsometric and backscattering spectrometric measurements", physica status solidi (c) Volume 5 Issue 5, May 2008 p 1354-1357].

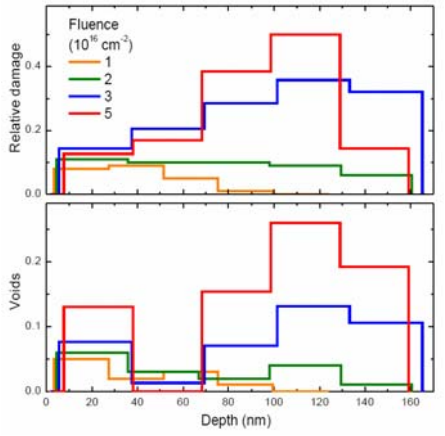

Figure 1 *Near-surface damage and void distribution in Si implanted by 10-keV He ions with different fluences. Note the near-surface accumulation of voids.*

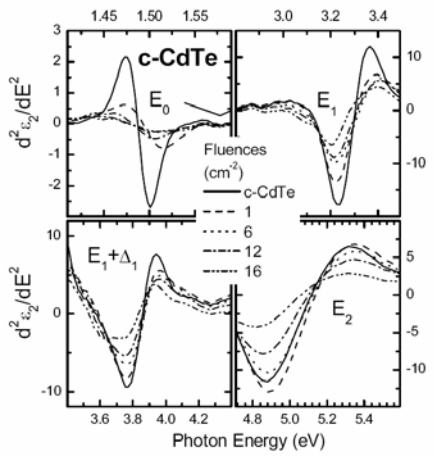

Figure 2 *Second derivative spectra around the critical point energies of single-crystalline CdTe ion implanted with 350 keV Xe using different fluences.*

Makyoh topography

(OTKA K 68534; HYPHEN, EU FP6 IST 027455; ANNA, EU 026134 (RII3))

F. Riesz, J. P. Makai

Makyoh topography is an optical tool for the flatness testing of specular surfaces, based on the defocused detection of a collimated light beam reflected from the tested surface. By inserting a square grid into the path of the illuminated beam, the height

map can be calculated by integrating the gradients obtained from the distortion of the grid's reflected image.

Research activities in 2008 were concentrated mainly on applications, partly within the framework of the ANNA transnational access program. Strain and morphology measurements were performed on Si substrates and SiC/Si heterostructures grown by vapour phase epitaxy at IMEM–CNR, Parma. It was shown that the pre-growth carburisation of the surface induces etch pits (Fig. 1). A large amount of curvature of the heteroepitaxial samples was observed (typically, 20 m curvature radius). The results were completed with AFM and SEM measurements of the surface morphology with the final aim to optimise the growth parameters.

Morphological features of Ti substrates of various preparation technologies for hydroxyapatite growth were studied (in collaboration with the Institute of Solid State Physics, Sofia) (see Fig. 2 for an example of a Ti substrate exhibiting traces of lapping).

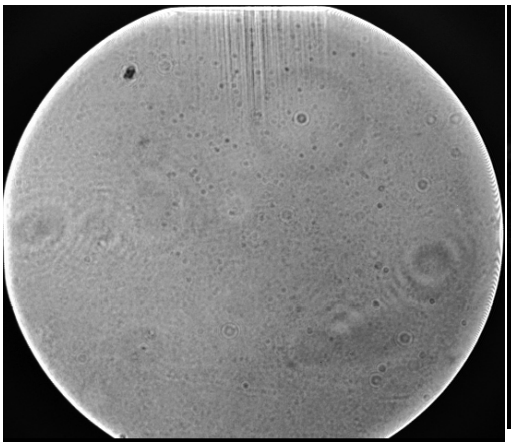

Figure 1 *Makyoh image of a Si substrate prepared for SiC growth showing pits induced by carburisation*

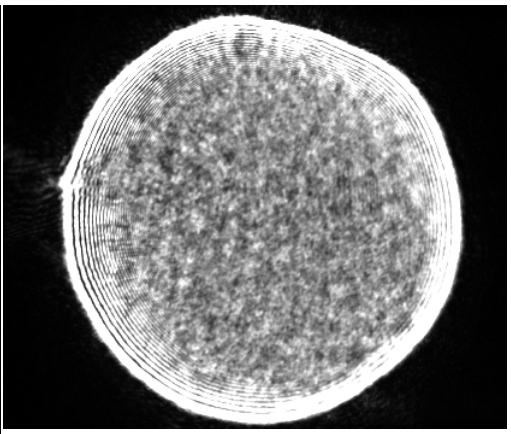

Figure 2 *Makyoh image of a Ti substrate for hydroxyapatite growth showing lapping marks*

The study of the surface morphology of PbI_2 crystals for nuclear detector applications was continued (in collaboration with Institute of Photonics and Electronics, Prague).

Deformation and morphology measurements were also performed on Si/SiC-based hybrid substrates used for GaN growth (within the HYPHEN project).

The deformation of Si wafers was measured to assess the stress-modifying effect of annealing of the deposited oxide layer as well as that of the doping of homoepitaxial layers (within the ANNA project).

In addition, our previous model for the height sensitivity was extended for isolated surface defects and two dimensions.

Comparative investigation of the Si/SiO_2 interface layer containing SiC crystallites using spectroscopic ellipsometry, ion beam analysis and XPS

(EU I3, ANNA Project Nr. 026134,OTKA K68688)

T. Lohner, A. Pongrácz, N. Q. Khánh, O. H. Krafcsik, K. V. Josepovits, and P. Deák

3C-SiC is an attractive wide band gap semiconductor for high-temperature, high-frequency power electronics since it has high thermal conductivity and high electron saturation velocity. 3C-SiC can be grown epitaxially on single-crystalline silicon substrates by chemical vapour deposition.

The first step is the carbonization of the Si surface to produce seeds for epitaxial growth. Krafcsik et al. [Krafcsik OH „Void-free epitaxial growth of cubic SiC crystallites during CO heat treatment of oxidized silicon", MATER SCI FORUM 389-393: 359-362, 2002] presented a method for the synthesis of 3C-SiC crystallites at the Si/SiO_2 interface. Since carbon enters silica only in the presence of oxygen, heat treatments in CO containing atmosphere were applied in order to introduce carbon into the Si/SiO_2 system. It was shown that SiC crystallites had appeared at the Si/SiO_2 interface after the annealing. The nanometer sized SiC grains could have further importance in the optoelectronic applications.

In our experiments first 100 nm thick SiO_2 layers were thermally grown on <100> Si substrates. The Si/SiO_2 structures were heat treated in CO containing atmosphere for 20 and 102 hours at 1190°C for investigation. Spectroellipsometry was applied to study the microstructure of the heat-treated samples.

A four-phase optical model (air, $layer_1$, $layer_2$, single crystalline silicon substrate) was constructed to interpret measured spectra. $Layer_1$ represents the thermally grown silicon dioxide layer, $layer_2$ represents the interface layer containing the SiC crystallites formed during the heat treatment in CO at 1190°C for 20 hours. $Layer_2$ was considered as a mixture of SiC and crystalline Si. The fit quality σ exhibits a low value of 0.052. Fig. 1 shows the measured and calculated spectra for this model.

For the sample annealed for 102 hours the best model is a two-layer model with a top silicon dioxide layer and a mixed interface layer with crystalline Si and SiC components. A thickness value of 25.7 nm ± 0.3 nm was obtained for the interface layer and a volume fraction of 89% ± 1% were found for the percentage of SiC in it. Figure 2 shows the measured and calculated spectra for this model.

To confirm the results of the ellipsometry characterization we applied ion beam analysis and X-ray photoelectron spectroscopy. For determination of the carbon content $^4He^+$ ion beam of 3.5 MeV was selected taking the advantage that the scattering cross section of carbon at this energy at 165° detection angle is about six times larger than the Rutherford type one [Lohner et al; Comparative investigation of the Si/SiO2 interface layer containing SiC crystallites using spectroscopic ellipsometry, ion beam analysis and XPS. physica status solidi (c), 5 (2008) 1337-1340].

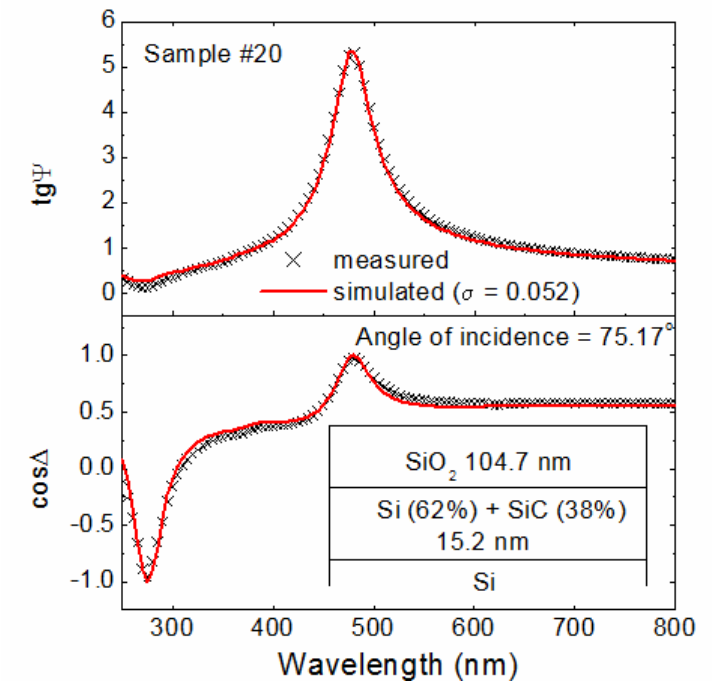

Figure 1
Measured and best-fitted ellipsometric spectra for sample annealed for 20 hours. The inset shows the optical model with the results of the evaluation.

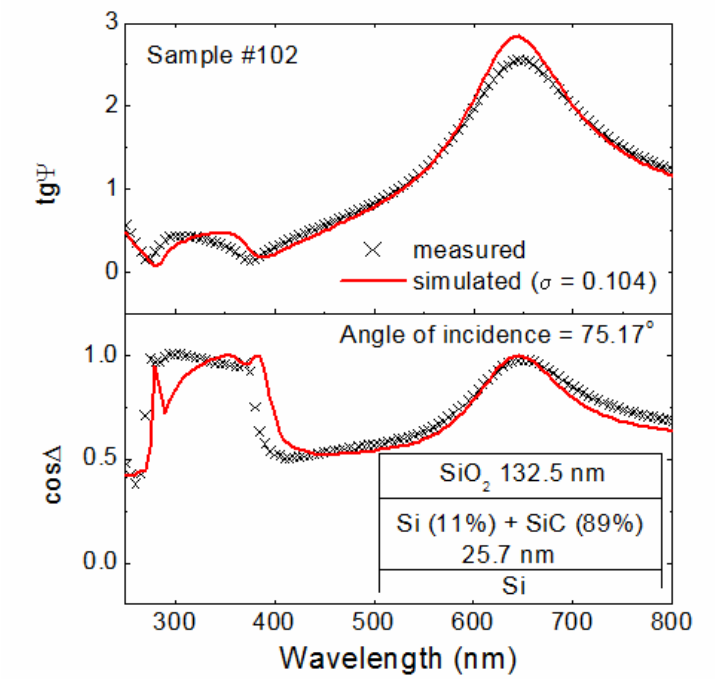

Figure 2
Measured and best-fitted ellipsometric spectra for sample annealed for 102 hours. The inset shows the optical model with the results of the evaluation.

Microtechnology Department

Head: Gábor Battistig, Ph.D.

Research Staff

G. **Battistig**, Ph.D.
I. **Bársony**, Ds.C.
Cs.S. **Daróczi**, dr. univ.
L.**Dózsa**, Ph.D.
P. **Fürjes**, Ph.D.
Z.J. **Horváth**, Ph.D.
Z. **Lábadi**, Ph.D.
G. **Molnár**, Ph.D.
A.E. **Pap**, Ph.D.
V. **Rakovics**, Ph.D.
G. **Vásárhelyi**, Ph.D.
Z. **Zolnai**, Ph.D.

M. **Ádám**, M.Sc. (part time)
F. **Beleznay** Ds.C. Prof. Emeritus
A. **Karacs**, M.Sc. (part time)
T. **Mohácsy**, M.Sc. (part time)
G. **Pető**, Ds.C. Prof. Emeritus
I. **Pintér** , Ph.D. (part time)
B. **Szentpáli**, Ph.D.
É. **Vázsonyi**, M.Sc. (part time)
Á. **Nemcsics**, Ph.D. (part time)
B. **Pődör,** Ph.D. (part time)

Vo Van **Tuyen**, Ph.D., (on leave)

Ph.D. students / Diploma workers

P. **Basa**, Ph.D. student
Á. **Németh**, Ph.D. student
Zs. **Baji** Ph.D. student
A. **Pongrácz**, Ph.D. student
K. **Gillemot** Diploma worker

Technical Staff

E. **Badalján**, engineer
Á. **Debreczeny**, engineer
J. **Ferencz**, engineer
Cs. **Lázár**, engineer
Á. **Majoros**, engineer
S. **Püspöki**, dr. techn. engineer (part time)
Zs. **Püspöki**, engineer
I. **Réti**, engineer
I. **Szabó**, dr. univ. engineer (part time)
T. **Szabó**, engineer
Á. **Szendrey**, engineer
J. **Waizinger**, engineer
K. **Veresné Vörös**, engineer
T. **Jászi**, engineer (on leave)

G. **Altmann**, technician
G. **Bíró**, technician
S. **Csarnai**, technician
M. **Erős**, technician
Cs. **Faragó**, technician
A. **Gondos**, technician
G. **Lehel**, technician
A. **Nagy**, technician
M. **Payer**, technician
M. **Varga**, technician

R. **Hodován**, diploma worker

T. **Berkó**, engineer (left)
V. **Kulin**, engineer (left)

The Microtechnology Department of MFA operates a 300 m^2 clean lab (Class 100-10000) with a complete Si-CMOS technology together with a mask shop. Another large facility of the Department is the CIGS solar cell laboratory equipped with a pilot line of a sputtering, an evaporation and a laser scribing module connected together with a sophisticated conveyor line for 30×30 cm^2 glass substrates.

The main tasks of the laboratory:

Research and development of physical, chemical/biochemical sensors and integrated systems:
- MEMS and MEMS related technology, with special emphasis on development of Si CMOS driving and readout circuitry.
- Development and applications of well tuned near IR light emitting diodes and detectors.
- Solar cells and their novel technology.
- Acoustic wave devices and their application.

Fundamental research on:
- novel sensing principles,
- novel materials and nanostructures,
- novel 3D fabrication techniques,
- and ion-solid interaction for supporting MEMS development are performed.

Device and material characterization:
- Various ion beam analysis methods.
- IR and Raman scattering.
- Scanning Microprobes.
- SEM, TEM, EDX, XRD.
- Spectroscopic Ellipsometry.
- Electrical characterisations.

The infrastructure of the clean lab is further developed in 2008, a new closed loop water cooling system has been installed. In order to increase the technical capabilities of the lab and to introduce new technologies (nanoimprinting, wafer bonding) into the MEMS developments, new equipments were purchased (Figures 1, 2, 3 and 4):

- SÜSS MicroTec MA 6 Manual Mask aligner for 3” and 4” wafers (4” and 5” masks)
    - manual loading
    - 0.7 μm precision
    - back side alignment
    - alignment toolset for wafer bonding
    - toolset for UV cured nanoimprint technology

- SÜSS MicroTec CB6L high vacuum anodic bonder
  - offering flexibility and accuracy for production and/or laboratory wafer
  - anodic bonding of two Si wafers of Si wafer to glass substrate,
  - aligned bonding of two or more wafers,
  - Supports thermo-compression bonding
  - with user friendly software allowing unlimited variations of process
  - bonding of aligned substrates up to 150mm in diameter.

To increase the quality of photolithography:

- Brewer Science Cee Model 200CB Spin Bake Unit
  - automated and programmable spin coater (0-12000 rpm)
  - programmable hotplate (<400°C)

- Brewer Science Cee Model 200 Spray Developer
  - for automatic and programmable developing of exposed photoresist.

In the next pages brief descriptions of the different tasks running in the lab are given. Some are not mentioned here because patenting processes of new sensing principles, technologies and devices are going on.

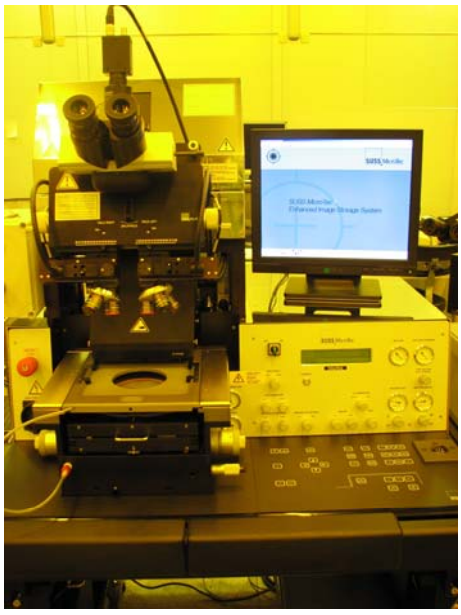

Figure 1 *SÜSS MicroTec MA 6 Manual Mask aligner with nanoimprint toolset*

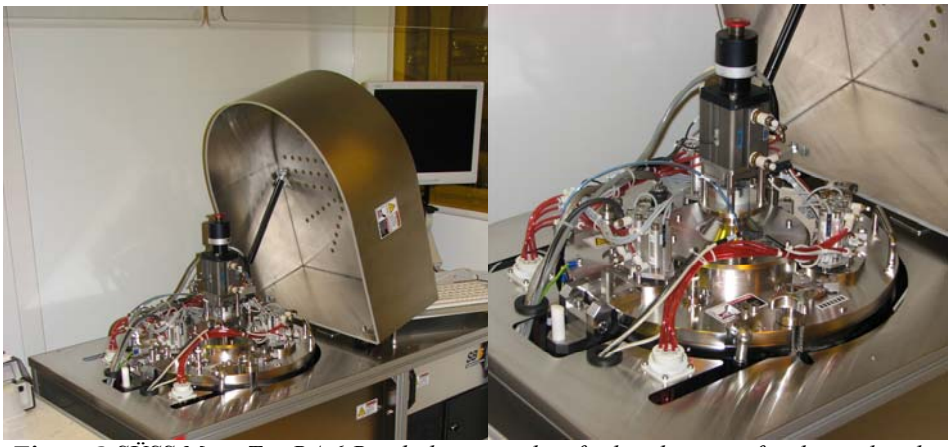

Figure 2 *SÜSS MicroTec BA 6 Bond aligner and wafer bonding unit for thermal and anodic bonding*

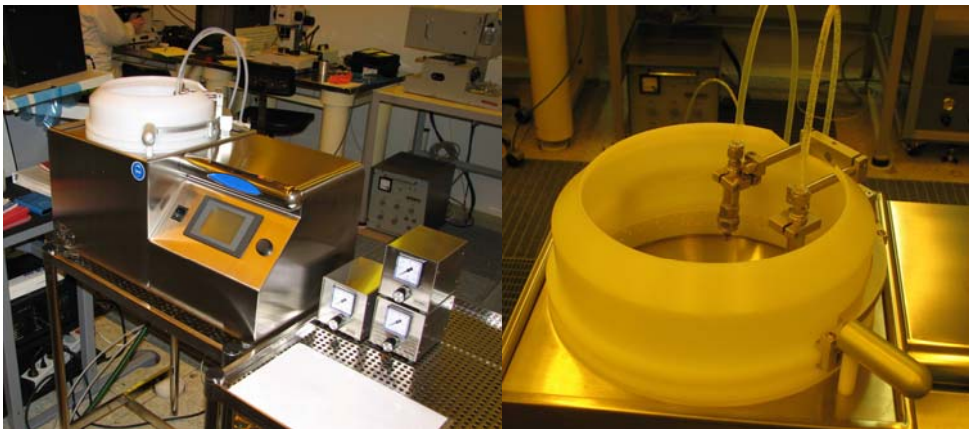

Figure 3 *Brewer Science Cee Model 200 Spray Developer for automatic and programmable developing of exposed photoresist*

Figure 4 *Brewer Science Cee Model 200CB Spin Bake Unit, automated and programmable spin coater and hotplate for photoresist*

Chemically Modified Solid-State Nanopores for Sensing

(Supported by Hungarian Scientific Fund (OTKA) NF69262)

P. Fürjes, A. L. Tóth, R.E. Gyurcsányi

Sensing with chemically-modified nanopores is an emerging field that is expected to have major impact on bioanalysis and fundamental understanding of nanoscale chemical interactions down to the single-molecule level. The main strength of nanopore sensing is that it implies the prospect of label-free single-molecule detection by taking advantage of the built-in transport-modulation-based amplification mechanism. At present, fabrication and application of solid-state nanopores are becoming to the focus of attention because, compared with their biological counterparts, they offer greater flexibility in terms of shape, size, and surface properties, as well as superior robustness.

We have reported on the fabrication of single channel solid-state nanopores fabricated by Focused Ion Beam etching, as well as on their chemical functionalization for selective detection of proteins and nucleic acids. Figure 1 represents the realisation method of solid-state nanopore combining the silicon bulk micromachining technology and nanoscale fabrication by FIB. The nanopores were etched in a free-standing silicon-nitride / gold layer structure manufactured by 3D MEMS technology.

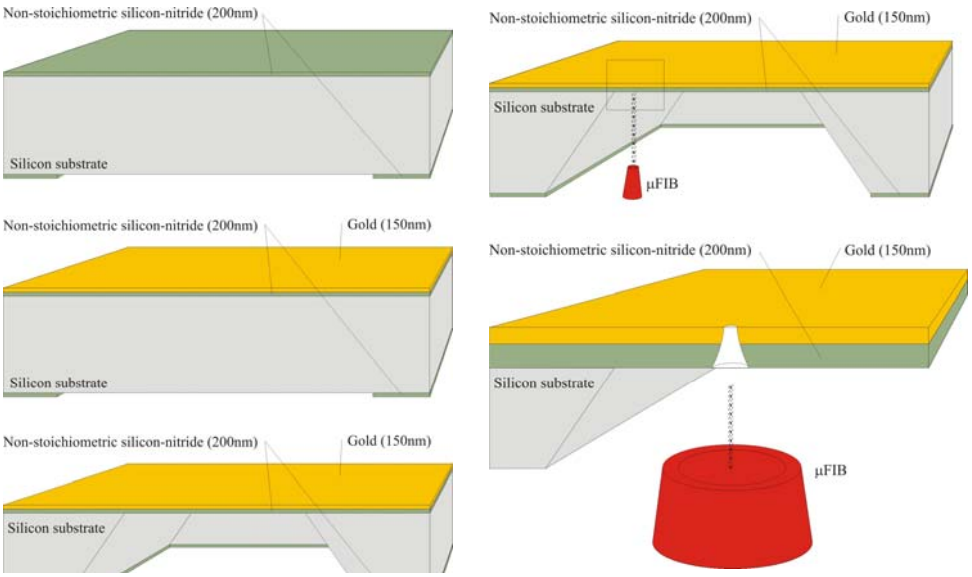

Figure 1 *Schematic representation of the fabrication process of the solid-state single nanopore by FIB*

The functionalisation of the nanochannels (Figure 2) passing through the gold layer and the method of transport-modulation-based selective molecule detection were developed by the Research Group for Technical Analytical Chemistry of the Hungarian Academy of Sciences at Budapest University of Technology and Economics. The transport-modulation based detection utilize the amplification mechanism i.e. species entering in the nanopore are acting on the electrical field or concentration induced flux of marker species (mostly, small ions provided by an electrolyte solution). In addition, to the label-free determination of target species, new hyphenated methods are introduced for signal amplification.

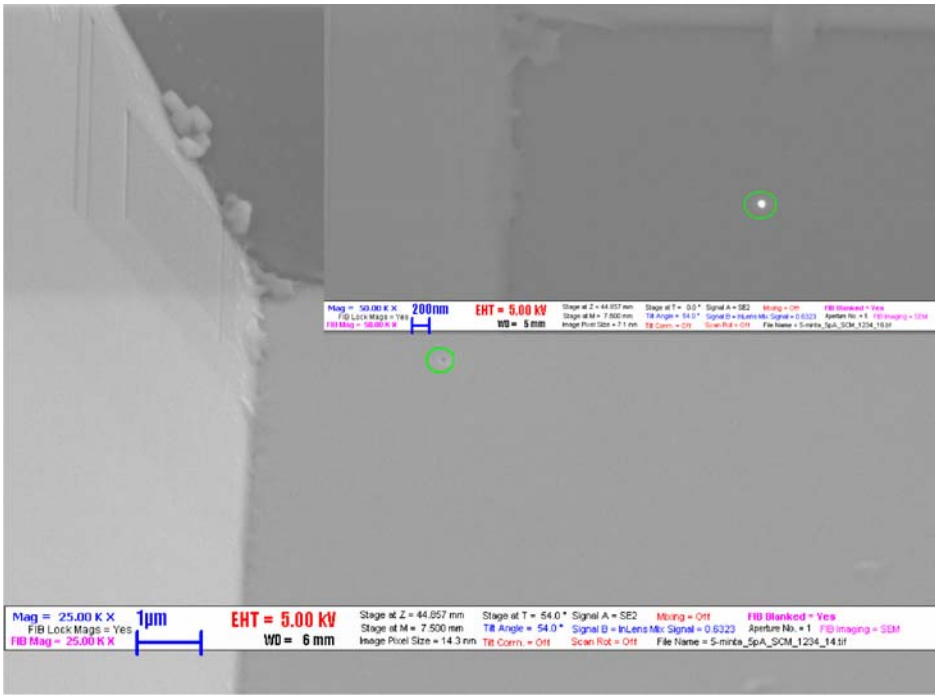

Figure 2 *SEM view of the single nanopore etched by FIB via the SiN_x / Au membrane (magnified in the inset))*

The capabilities of nanopore based sensors in terms of detection limit are explored by using random walk simulation and multiphysics modelling. Apparently, the detection limit of single nanopore based affinity sensor is determined by the probability of a successful encounter between the nanosensor and the solution. Since a single molecule can be in principle detected by nanopore sensors the limit of detection of such sensors has also explored in terms of concentration. However, significant improvements are obtained upon directing the solution by means of an electrical field or pressure gradient into the sensing zone of the nanopore.

Investigation of Actuation Phenomena and Controllable Moving Microstructures for Microfluidic Application

(Supported by Hungarian Scientific Fund (OTKA) F61583)

P. Fürjes

Realisation and application of controllable moving microstructures are the milestones of development microfluidic systems. The integrated microfluidic elements are essential components of lab-on-a-chip devices consisting of various elements: opened or embedded channels and cavities, fluid mixers and reactors. Smart devices are built up with additional active elements, typically heaters, sensors of various type and valves containing moving components for injection or facilitating the fluid flow in the required direction or in the reactor micro-vessel. To establish the research and development of complex microfluidic systems the investigation of actuation possibilities is essential.

The practicability of the actuation phenomena (electrostatic, magnetic and thermal) and the predictable functional parameters of the designed structures (deformation, driving frequency, residual stresses of the layer structures) were analysed by Finite Element Modelling. Test structures were manufactured by development and application the adequate MEMS techniques and analysed considering the functional aspects. The thermal actuation phenomena were analysed by realisation and investigation of a microfluidic valve system presented by Figure 1. The active part of the 3D MEMS structure were manufactured by silicon bulk micromachining applying platinum microheaters embedded in CVD deposited layer structure. The microchannels were formed by porous silicon micromachining and PDMS formation. Figure 2 shows the manufactured valve structure.

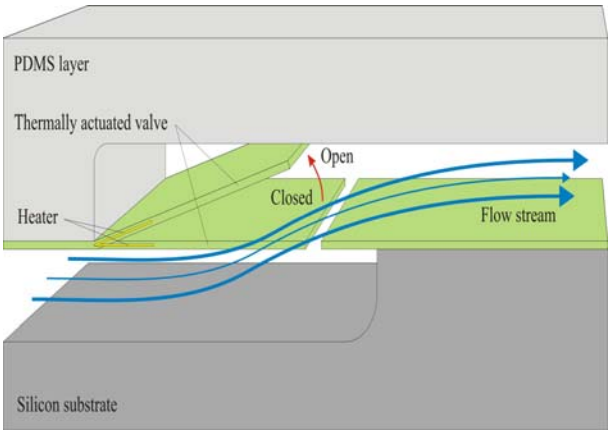

Figure 1 *Schematic representation of a thermally actuated microfluidic valve. The microfluidic channels are realized by the combination of 3D silicon micromachining and PDMS formation.*

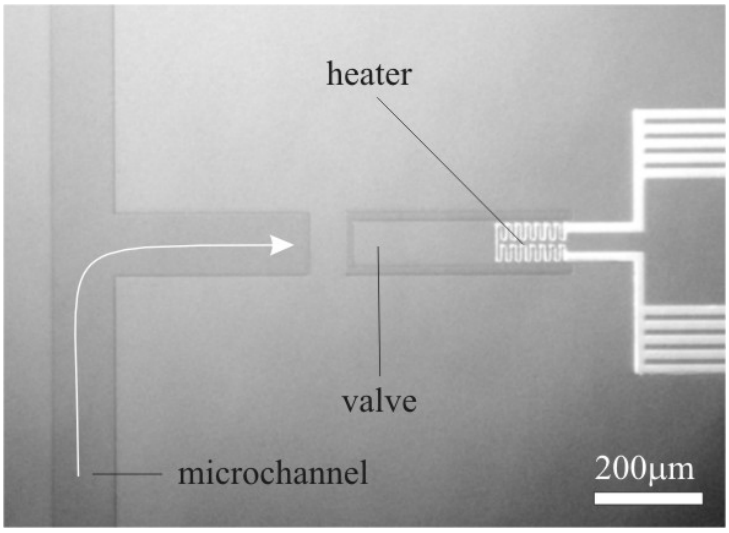

Figure 2 *Micrograph of the realized microfluidic system consisting valves*

Micro-heaters are basic components of sensors and lab on a chip devices, e.g. as sensors of calorimetric principle, or heaters in chemical micro-reactors. The most frequently used structural materials are silicon-nitride, non-stoichiometric silicon-nitride, silicon-oxinitride, silicon-dioxide and multilayered combination of these materials.

In the micro-heater design the most important parameters to be considered are the thermal conductivity, the thermal capacitance, linear expansion and the residual stress in the applied layers in order to select the optimum functionality of the device. While appropriate data are available for the widely used materials (SiO_2, Si_3N_4) this is far not being the case for the non-stoichiometric materials or deposited poly-crystalline silicon, diamond and DLC layers. Their properties are process dependent, i.e. both their composition and structure are determined by the given individual process. Therefore, relatively simple methods for determination of thermo-mechanical properties are essential in functional design. These thermo-mechanical properties were extensively analysed for proper prognostication of the functional parameters and behaviour of the active elements of the microstructures.

Si Micro-turbine by Proton Beam Writing and Porous Silicon Micromachining

(Supported by Hungarian Scientific Fund (OTKA) T047002)

P. Fürjes, Cs. Dücső, Z. Fekete, I. Rajta (ATOMKI, Debrecen)

Lab-on-a-chip MEMS are fabricated by various techniques: hot embossing, pressure moulding, laser ablation, LIGA or thick layer processing. Devices with complex functions are preferably formed from Si or combination of Si and other materials. The alternative key technologies are the alkaline etching of the bulk Si or the surface micromachining technique where the actuated membrane is formed from deposited polycrystalline Si or metal layers. The most promising technique for the formation of crystalline silicon components is the DRIE (Deep Reactive Ion Etching).

In the last few years proton beam writing in combination with porous silicon processing has been proposed for formation of high aspect ratio fixed 3D Si structures. Our group indicated that membranes of high displacement can also be fabricated by this technique. In the present work conventional microtechnology processes (thin layer deposition of non-stoichiometric silicon-nitride, polycrystalline Si and Al, double side photolithography, dry and wet etching techniques) are combined with PBW and porous Si micromachining for the fabrication of a silicon micro-turbine (Figure 1).

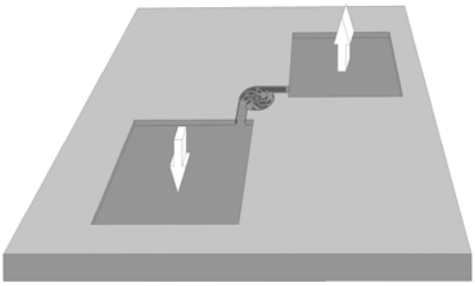

Figure 1 *The structure of the micro-turbine Si chip*

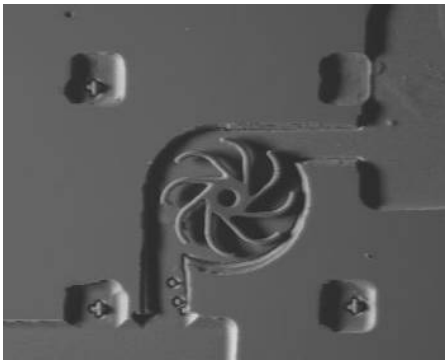

Figure 2 *SEM view of the processed micro-turbine chip*

A 3D Si micro-turbine (Figure 2) characterized by high aspect ratio vertical walls was formed by the combination of proton beam writing (PBW) and subsequent selective porous Si (PS) etching. Crystal damages generated by the implanted protons result in increased resistivity, thereby limit or even prevent the current to flow through the implanted area during electrochemical etching. Characteristic feature of the proposed process is that the shape of the micro electro-mechanical (MEMS) components is defined by two implantation energies. A higher energy is applied for defining the

housing of the device while the lower energy is used to write the moving components. The electrochemical etching is driven until the sacrificial PS layer completely underetches the moving components, but the etch-front does not reach the bottom of the housing.

This work is the first demonstration of a silicon device containing a moving part made by proton beam writing. The operation of the encapsulated device fabricated is successfully demonstrated (Figure 3-4).

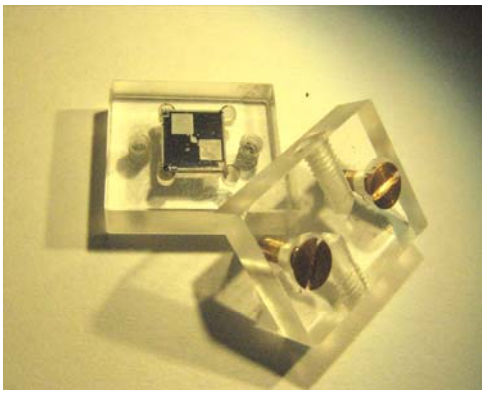

Figure 3 *Plastic housing of the micro-turbine chip*

Figure 4 *The rotating micro-turbine (see http://www.atomki.hu/atomki/VdG/ibaweb/video/)*

The aligned, two-energy proton beam implantation can provide high aspect ratio, completely or partially released microelements embedded in a cavity or a channel, thereby enabling us to form mobile components in the microfluidic MEMS.

Preliminary research for integrated Photo-acoustic Gas Detector System

(Supported by National Research and Development Programme NKFP3-00021/2005)

P. Fürjes, Z. Bozóki (Univ. Szeged)

An extremely sensitive photo-acoustic gas detector system is developed for analysis the methane and ammonia circulation of living forests. This method is based on the detection of the pressure wave generated by the selective energy absorption of the interested gas component excited by adequate laser-pulse in the test chamber. Beyond development of a micro cantilever microphone capable to detect the interested gas presenting in ppm range through the deformation of the suspended reflective micro-membranes, the applicability of an integrable microscale excitation source was considered.

3D MEMS structures including two optical microphones (Figure 1) were designed, developed and manufactured by double-side bulk micromachining silicon technology, fitting these structures to the active and reference flow chambers of the optoacoustic measuring system. The circumspect geometric and material design of the suspending multilayer microstructures is a crucial object of the research.

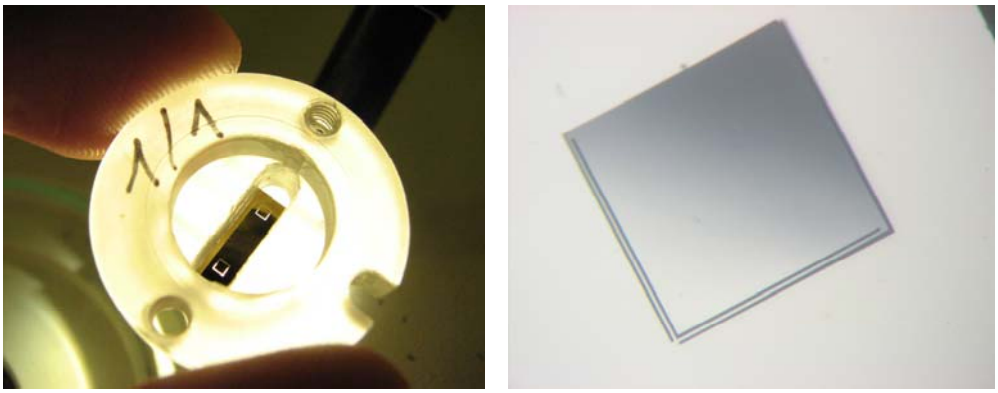

Figure 1 *Optical microphone structure (left) consisting cantilever membranes (right)*

Development and reliable realisation of a micro-scale excitation source is crucial for integration and miniaturisation of the photo-acoustic chamber and detection system. Adequate radiation spectra, integrability, long term stability, reliable operation are the basic requirements which have to meet the functional behaviour of the microheater structure. The special technology developed previously at MFA MEMS Laboratory for realisation microheater structures has completely improved (Figure 2). The manufactured suspended 3D micro-scale source (Figure 3) can fulfil the strict requirements of decreased power dissipation (reaching the temperature of 600°C at 20mW) due to the enhanced thermal insulation achieved by porous silicon sacrificial technology.

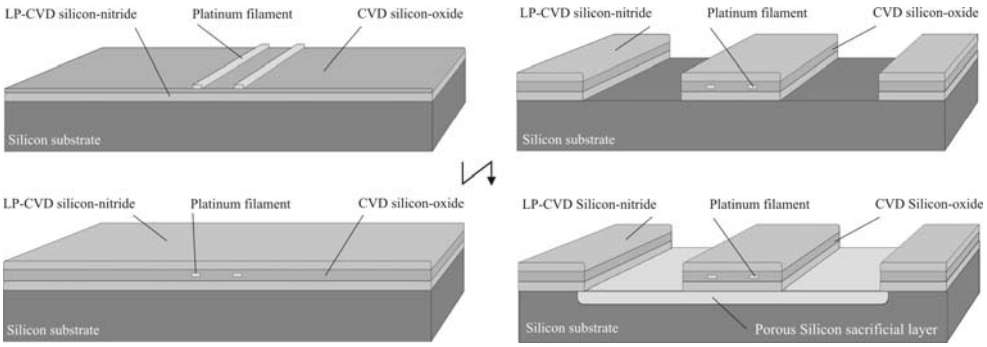

Figure 2 *Fabrication process of the integrable multi-layer microheater*

The adequate structural materials have selected by applying sophisticated finite element modelling for decreasing residual thermo-mechanical stress, and deformation as presented in Figure 4. The formerly applied simple non-stochiometric silicon-nitride suspension was improved by a symmetrical stacked layer structure consisting additional silicon-oxide layers decreasing deformation and mechanical instability of the source.

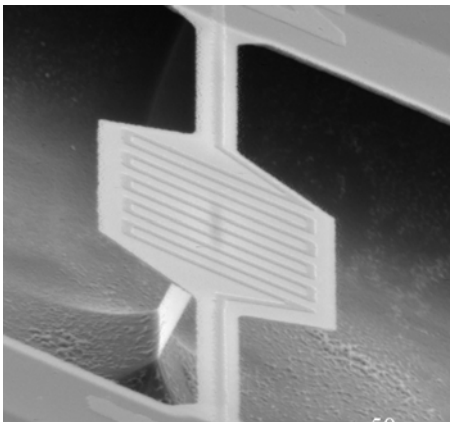

Figure 3 *Suspended structure applied as excitation source of photo-acoustic system*

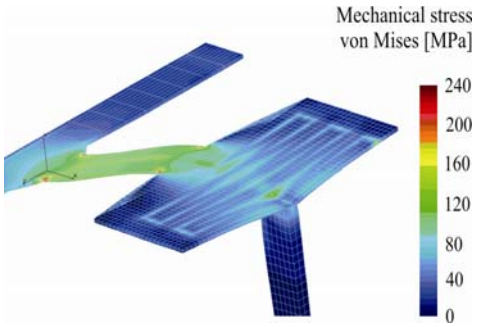

Figure 4 *Thermo-mechanical stress distribution of the heated structure*

Beyond the frequently applied structural materials, protective coating of MEMS elements used in harsh environment is essential for their reliable operation. The best candidates for such application are diamond, diamond-like-carbon (DLC) or SiC because of their superior chemical and abrasion resistance in aggressive chemicals. Applying a unique technique developed in corporation with BUTE a special micro-heater was manufactured replacing the structural materials by micro- and ultrananocrystalline diamond deposited by SAD (Selective Area Deposition) PE-CVD technique.

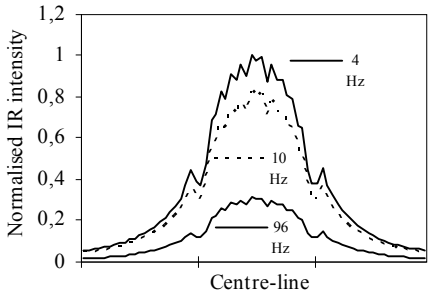

Figure 5 *IR intensity distribution along the centre-line of the source as the function of the driver frequency*

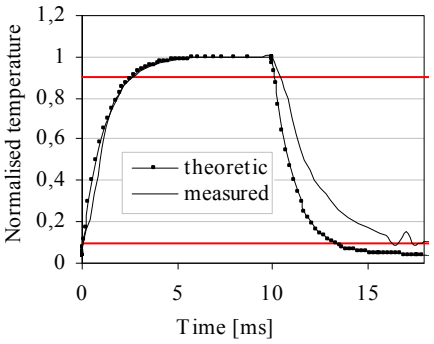

Figure 6 *Transient response of the heater driven by 10ms square wave excitation*

To ensure functional applicability of the micro radiation source the emissivity behaviour of the coating layers were investigated. The emission spectra of the source was analysed by using different top coating layers as doped poly-crystalline and amorphous silicon deposited by LP and PE CVD techniques, respectively.

The low power dissipation, high operating temperature and excellent transient behaviour are the significant requirements for the applicability of integrated micro sources. The transient response of the microstructure was tested by lock-in thermograpy recording the lateral distribution of the IR intensity using different driver frequencies. Figure 5 presents the frequency dependence of the radiated intensity distribution. The time response (Figure 6) of the structure was also analysed, the time constant of the thermal system was calculated for 1.1ms, and the frequency limit of the operation is several 10Hz.

Formation of SiC Nanocrystals in Si Based Systems by Reactive Annealing

A. Pongrácz, G. Battistig, D. Beke

Epitaxial formation of SiC nanocrystals on single crystal silicon surfaces by a simple and cheap reactive annealing in CO has been discovered and patented by BME AFT and MTA MFA. We have investigated the CO diffusion and SiC nanocrystal formation on different silicon based systems after 100% CO treatment at elevated temperatures (T>1000°C).

In cooperation with Institut des NanoSciences de Paris, SAFIR SiC nanocrystal formation was investigated by X-ray Photoelectron Spectroscopy at SOLEIL synchrotron. We identified the nc-SiC peak in the Si 2p XPS spectra. SiC was grown by heat treating single crystal silicon with 2.5 nm chemical oxide in 100% CO at 1100°C for 90 min at atmospheric pressure. Si-C binding energy was found at 100.56-100.61 eV after flashing off the oxide and the water vapor related contaminations. Fig. 1. shows the Si 2p peak deconvolution (Si-OH, Si-C, Si 2p ½, Si 2p 3/2 and surface states from left to right).

A continuous polycrystalline SiC layer formation as protective coating can have a great interest in harsh environment MEMS applications. Polycrystalline silicon unlike epitaxial Si can be deposited on arbitrary substrates and does not need exposed silicon underneath. Its good thermal stability, good interface to silicon dioxide, good conformality and ease of deposition and processing have made it a mainstay of silicon microelectronics technology. Single crystal silicon, polycrystalline silicon with 300 nm grain size and polycrystalline silicon with 100 nm grain size were used as a base structure for SiC growth in CO annealing. The comparison of the three samples after 3 hr CO heat treatment at 1100^{o}C is shown on Fig 2-4.

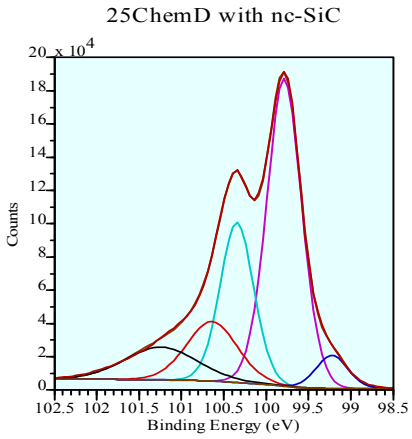

Figure 1 *Si 2p XPS peak from a single crystal Si surface covered with SiC nanocrystals*

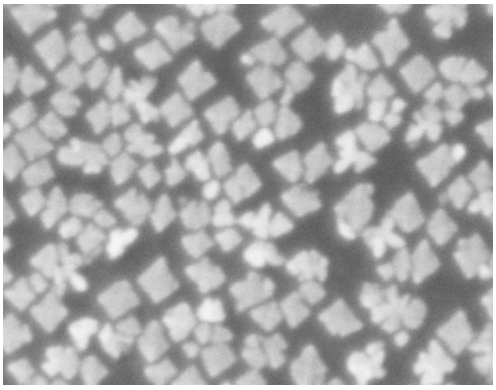

Figure 2 *SEM image of SiC nanocrystals on single crystal Si surface after oxide removal. Samples were heat treated in CO for 3 hrs at 1100°C.*

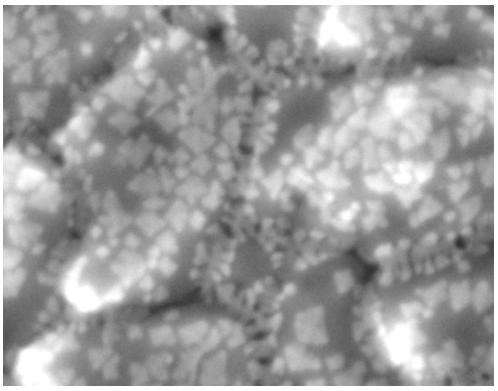

Figure 3 *SEM image of SiC nanocrystals on poly Si surface after oxide removal. Average grain size of poly-Si was 300 nm. Samples were heat treated in CO for 3 hrs at 1100°C.*

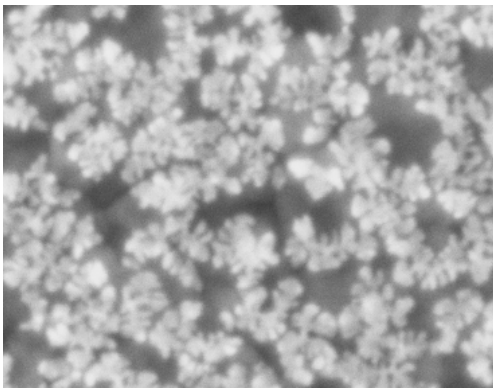

Figure 4 *SEM image of SiC nanocrystals on poly Si surface after oxide removal. Average grain size of poly-Si was 100 nm. Samples were heat treated in CO for 3 hrs at 1100°C.*

While on single crystal silicon the average grain size is 32 nm, on 300nm poly-Si the average SiC crystal size is 25 nm and on 100 nm poly-Si the typical SiC grain size is 20 nm.

SiC nucleation on poly-Si takes place on two characteristic areas: nucleation on the grain area and nucleation on grain boundaries. Nucleation density can be calculated on the grain area on 300nm poly-Si sample. Nucleation density is in the same range on the grain area as compared to the single crystal sample; however the growth rate is smaller. Nucleation at grain boundaries became the dominant phenomena as the grain

size is decreasing. On 100 nm poly Si sample nucleation on the grain area is almost never happen, while nucleation on grain boundaries shows a very high nucleation density and dendrite like crystal growth.

Semiconductor Nanocrystals in Dielectrics

(Supported by Hungarian Scientific Fund (OTKA) T048696)

Zs. J. Horváth, P. Basa

Semiconductor nanocrystals (NCs) are widely studied for non-volatile memory purposes. During this year our activity in this field was devoted to study $Si/SiO_2/Si_3N_4/Si$ NC/Si_3N_4 structures.

Three different samples were prepared. The first sample (GSR) was a reference structure without NCs. In the second one Si NCs were deposited for 60 s (SK) onto the thin Si_3N_4 layer. For the third sample (SN) Si NCs were deposited for 120 s onto the Si_3N_4 layer, but they were oxidized after deposition by the same HNO_3 treatment, as the tunnel oxide was prepared. After these steps the samples were covered with a 35 nm thick Si_3N_4 control layer. The cross-section of samples SK and SN are shown in Fig. 1.

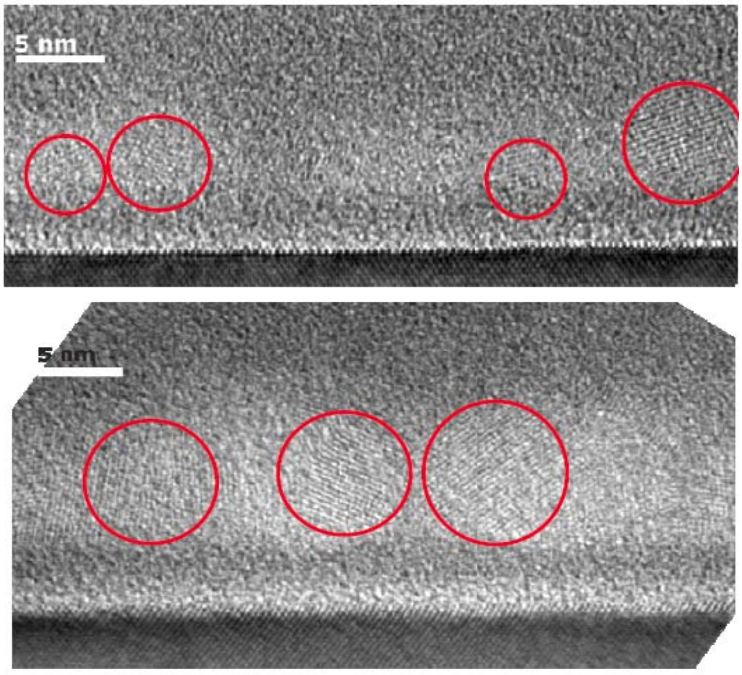

Figure 1 *High resolution transmission electron microscope images of two $Si/SiO_2/Si_3N_4/Si$ NC/Si_3N_4 structures*

Extremly good injection properties were obtained for samples SK and SN containing Si NCs, as presented in Fig. 2: the memory window width was about 3 V for charging pulses of ±6 V, 10 ms, and 15 V for pulses ±15 V, 10 ms. But the retention time was

very poor, a few seconds only. Nevertheless, due to the extremly good charge injection properties, similar structures can be good candidates for DRAM applications.

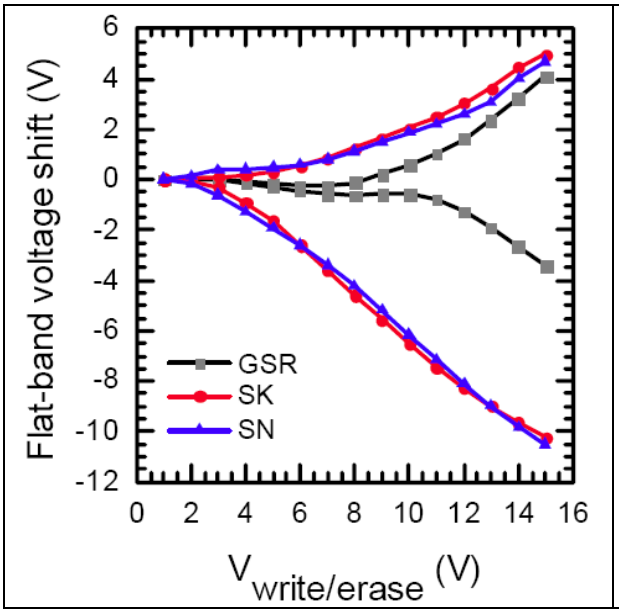

Figure 2 *The memory window of the two Si/SiO_2/Si_3N_4/Si NC/Si_3N_4 strucures referred in Fig. 1 (SK and SN. The memory window of the reference structure without Si NCs is also shown (GSR).*

Table 1. *The Ge nanocrystal deposition duration, the initial memory window width, its extrapolated values for 1 and 10 years, and the retention time for the studied SiO_2/Si_3N_4/Ge NC/Si_3N_4 structures for writing/erasing voltage pulses of ±15 V, 10 ms.*

Sample No.	NC deposition duration (s)	Initial memory window width (V)	Memory window width after 1 year (V)	Memory window width after 10 years (V)	Retention time (years)
G000	0	7.43	1.17	0.55	77.07
G025	60	7.93	1.88	1.35	3947.98
G050	120	7.68	0.86	0.22	21.64

Similar to the SiO_2/Si_3N_4/Si NC/Si_3N_4 structures, SiO_2/Si_3N_4/Ge NC/Si_3N_4 structures containig Ge nanocrystals were also prepared. In this case the duration of Ge NC depositon was studied as well (25 s and 50 s - samples G025 and G050, respectively). Opposite to the results obtained for similar structures with Si NCs, the Ge NC deposition improved the charging behaviour insignificantly, but the retention behaviour were very good (see Table 1). SiO_2/Si_3N_4/Ge NC/Si_3N_4 structures with Ge NC depostion duration of 25 s exhibited the best extrapolated retention time of about 4000 years.

Functionalization of Medical Implant Surfaces by High Energy Laser Pulses

(Supported by National Research and Development Programme NKFP 3/A 058-04/2004)

G. Pető, A. Karacs, G. Molnár

Although ”Development and Application of Functionalized Surfaces in Specific Biochemical and Chemical System” Project, has formally ended in 2007, we continued this work for developing optimal human implant surface structures by laser assisted surface modification. The investigation of Ti surface structures has attracted interest because of can be applied as a material of medical implants, due to its excellent mechanical properties and its native oxide that is the reason of its biocompatible properties. The aim of this work was to modify the Ti surface in order to turn it into bioactive besides its biocompatibility. Pulsed laser surface treatment was used to achieve the desired bioactive properties. The resulted surface morphology of Ti implants depends on the energy and incidence angle of the laser pulses and on the pressure of the surrounding gases. Formation of different surface morphologies falling in the size range of 10 and 30 micrometer (Fig. 1(a)) may enhance the bonding between the implant material and the cells. Moreover, size of the proteins that are adsorbed on the surface typically falls into the nanometre size range (10-30 nm) (Fig. 1(b)) therefore a roughness with such a characteristic length can influence the process positively. On this way, bioactive behaviour was achieved, which results in faster and stronger osseo integration in medical practice.

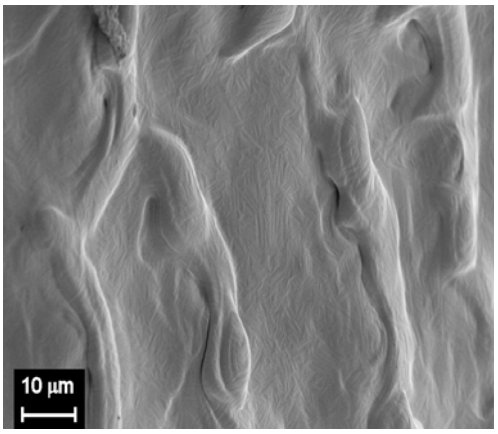

Figure 1(a) *SEM image of periodic micron-size waves on the surface of a screw shaped Ti implant after Nd:YAG pulsed laser treatment*

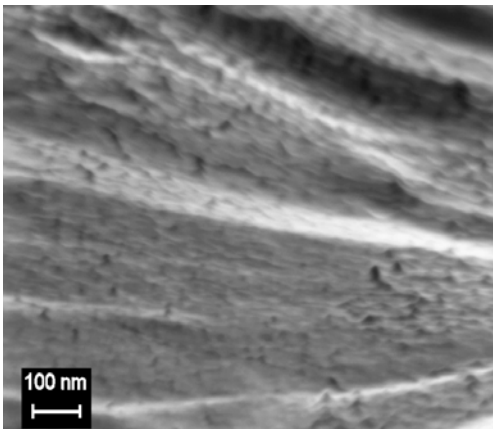

Figure 1(b) *SEM image of nano-sized morphology on the surface of a screw shaped Ti implant after Nd:YAG pulsed laser treatment*

Tactile sensor development and applications

TactoLogic Ltd.

G. Vásárhelyi

2008 was a successful year regarding tactile research and development at MFA. Through supports from our freshly founded spin-off, TactoLogic Ltd, we could continue our long-standing tactile sensor development with many different projects.

Our porous Si based piezoresistive MEMS technology has already stood the test of time through our general 4-element tactile arrays, capable of measuring 3D surface forces. These sensors have already been integrated into commercialized general tactile sensor products (TactoPad 2×2 and TactoFlex 2×2) through TactoLogic Ltd., and proved to be successful among the first users. In 2008 we also enhanced our measurement setup and techniques for high quality standardization of our sensors. We constructed a new measurement setup for precisely determining the functional properties (temperature dependence, multi-component response, linearity etc.) of our sensors.

Other development directions include the fabrication of 64 element integrated tactile arrays, where we combine MEMS and CMOS processes through a novel and unique patented technology. The first prototypes of the 8×8 type chips have been developed, the product integration processes are still running.

The last main development trend of the year is the construction of a single element miniature 3D tactile sensor, which is suitable for catheter applications mainly in the medical field. TactoLogic also realizes products based on this sensor, under the name TactoPoint 1×1.

TactoLogic Ltd. has started its evolution in 2007 and after one year of functioning could already realize profit from the commercialization of tactile sensors, which is an outstanding result among spin-off companies. Partly because of this, partly due to the great potential it holds, TactoLogic Ltd. has won this year's "Best spin-off/start-up Award" from the Hungarian Spin-off and Start-up Association, with the sponsorship of Ernst and Young.

Our future development trends include the integration of other modalities (e.g. temperature, humidity) into tactile sensing, the exploitation of viscoelastic properties of the elastic cover of the tactile sensors for bio-inspired and neuromorphic product development, and the construction of novel application-specific prototypes based on the current well-known technology.

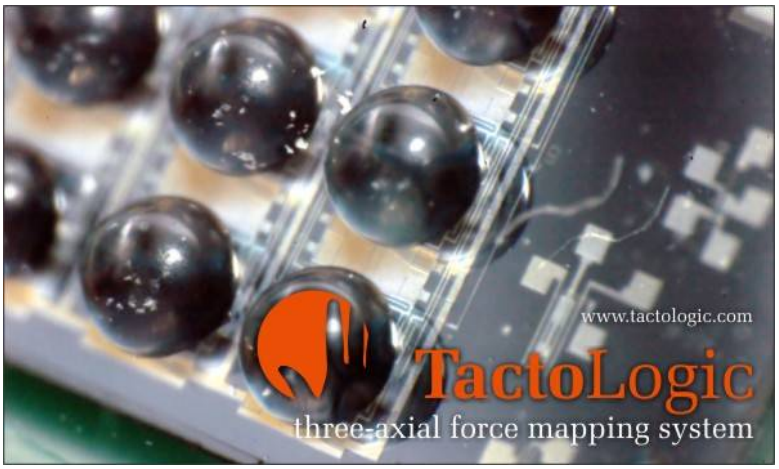

Figure 1 *Details of a 8×8 tactile sensor array with elastic covering plastic hemispheres (and TactoLogic Ltd's logo).*

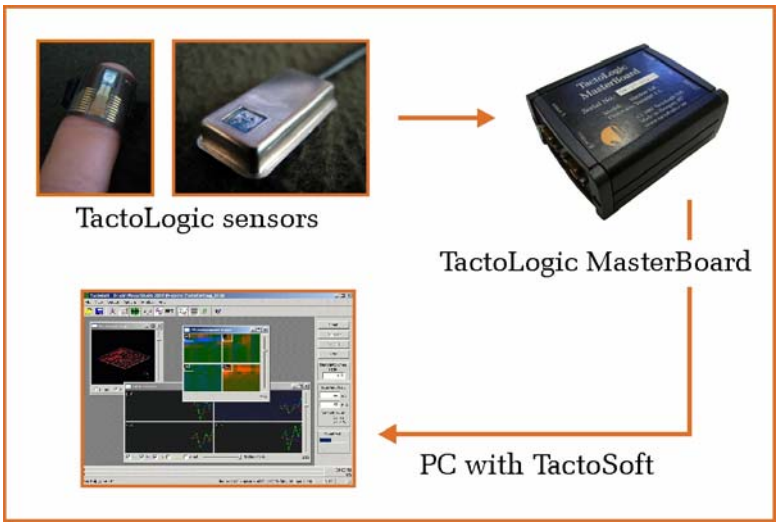

Figure 2 *Tactile development system based on MFA's 3D tactile sensors*

Tactile Sensor Development in the Microtechnology Lab in 2008 was mainly supported by TactoLogic Ltd., a spin-off founded in 2007 partly by MFA, with the mission of tactile R&D and commercialization. Throughout this year we developed and qualified several new tactile sensor prototypes for a wide range of commercial applications.

Increased Sensitivity Measurement of Point Defects by DLTS

L. Dózsa, G. Molnár, J. Ferencz, and S. Lanyi

The detection and identification of contamination in silicon is of technological importance. We have investigated microscopic, structural, and electric properties if FeSi2 layers. [Vouroutzis N, et al., Journal of Alloys and Compounds 448 (2008) 202, Tsormpatzoglou A, et al., J. Appl. Phys 100 (2006) 0733139]. Scanning probe capacitance microscope (SCM) was found to give information on silicon surface contamination [Dózsa L, ET AL., Appl. Surf. Sci. 234 (2004) 60]. For understanding the electrical properties, measurements with high spatial resolution are needed. The modern devices of few micron size require measuring apparatus of increased sensitivity.

In this work we suggest a method of point defect identification. The corresponding electrical characteristics are measured by the conventional DLTS system but with using a preamplifier.

The method is illustrated by measurement of Fe contaminated silicon. $FeSi_2$ quantum dots were grown on n-type (100) silicon. In the Fe deposited layer a resistive layer with high concentration of Fe related defects dominate the characteristics. The concentration of the Fe related deep level defects outside the Fe deposited region is comparable to the shallow dopant concentration near the silicon surface as it is shown in Figure 1 by a series of frequency scan DLTS spectra of a large area Schottky junctions. The defect is attributed to Fe contamination.. Capacitance-voltage characteristics and capacitance DLTS frequency scan of the measuring tip positioned at 5 micron distance from the silicon surface is shown in Fig.2. Both the C-V and DLTS characteristics are equivalent to them measured in macroscopic Schottky junctions. By measuring small junctions the preamplifier increases the sensitivity capacitance 200 times, while the current sensitivity increases 1000 times, which enables measurement of junctions of small area. The realization of the surface scale requires nanopositioning of the preamplifier and the measuring tip in the DLTS cryostat.

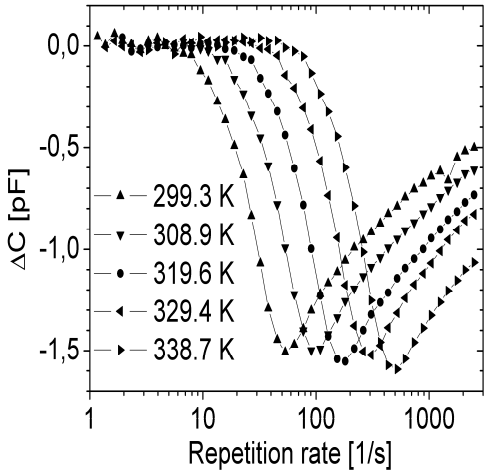

Figure 1 *DLTS frequency scan spectra measured in DLS-83D system at 299.3 K, 308.9 K, 319.6 K, 329.4 K, and 338.7 K temperatures.*

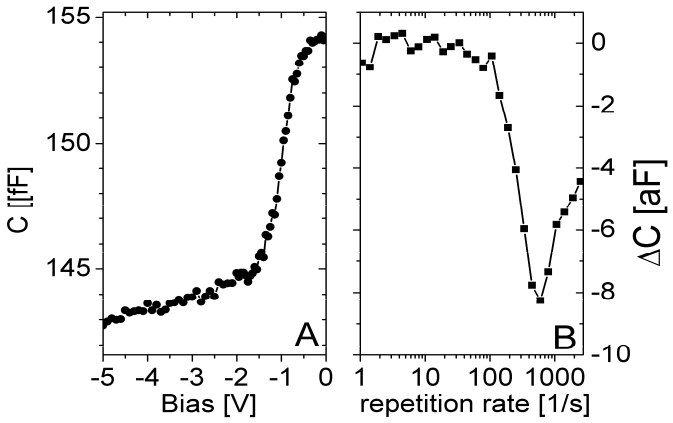

Figure 2 *C-V characteristics (A) and DLTS frequency scan (B) measured by the capacitance preamplifier with a 50 μm diameter tip positioned at 5 μm distance from the free silicon surface*

Si Surface Preparation and Passivation by Heavy Water Vapour

A.E. Pap, G. Battistig

Due to the shrinking feature size, the characteristics of the interface under the gate dielectrics play a crucial role in the performance of MOS devices; therefore, interface engineering is a key issue in processing. In cooperation with Mattson Technology, Inc. we investigated the stability of the H and D passivated Si surfaces against native oxidation in normal air.

We demonstrated that deuterium adsorbs on Si surface at room temperature much stronger than hydrogen. Moreover, in case of deuterium passivated wafers the vacuum storage can be omitted without risking the non–controlled native oxidation of silicon for up to 5 hours or more. It could be a suitable and more robust surface cleaning and passivation process for the industry, but heavy water is expensive. As a cheaper procedure, we presented that 1 min vapour phase treatment at 65 ºC of heavy-water (D_2O) + 50% HF (e.g. 20:1) mixture was enough to remove the native oxide and to passivate the Si surface without any degradation of the atomic surface flatness. The surface evolution of the D-passivated surface was followed by contact angle measurements, by spectroscopic ellipsometry (SE), by atomic force microscopy (AFM), by X-ray photoelectron spectroscopy (XPS), by transmission electron microscopy (TEM) and by infrared absorption spectroscopy (IR) qualification and the results were compared to the H-passivated Si surface.

Combination of D passivation with rapid thermal process (RTP) based on the thermal desorption kinetics of the adsorbed D and/or H layers on Si is a promising method for improved interface engineering and for better initial reactions in case of ultra thin dielectric layer formations. In order to confirm this statement we created Si_xN_y thin layer on D (Fig. 1.) and H passivated Si surface by using RTP. The typical Schottky-like current-voltage characteristics obtained on the studied Al/SiN_x/n-Si structures are. Both H and D treatments influenced the I-V behaviour much, but in opposite way: H treatment yielded lower current through the structure, while D treatment resulted in much higher current level, than that obtained for the untreated structure. In addition, the shape of the forward branch of the I-V curves (Fig. 2.) changed and its slope became more abrupt after both H and D treatments. The results indicate that the current flow through the structures is limited by the conductance trough the SiN_x layer and by the potential barrier at the Si surface. The parallel shift of the curves along the current (vertical) axis is due to the effect of H and D treatment on the density of interface states at the SiN_x/Si interface, while the change of the shape and slope is probably connected with the effect of treatments on the conductivity of the SiN_x layer. Taking into account the Al and Si work function difference, the charge in interface states increased after H treatment, while it decreased significantly after D treatment indicating an affective passivation of Si surface.

These results confirmed that using D passivation on Si surface is a promising method in the MOS technology and the interface engineering processes.

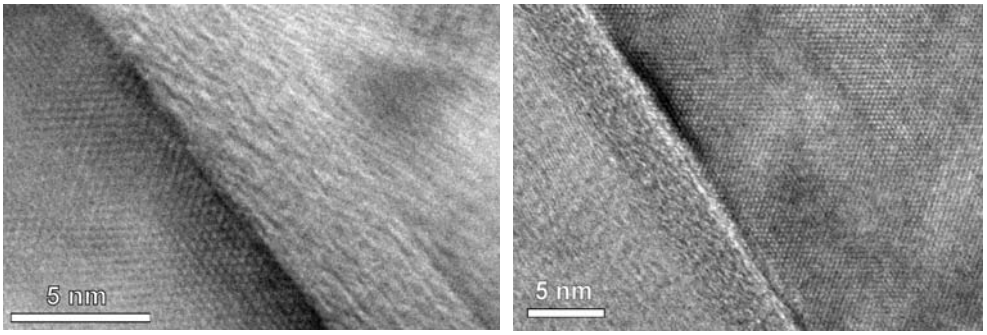

Figure 1 *Oxy-nitride layer thickness on (a) H-passivated wafer 4.35 nm and on (b) D-passivated 3.5 nm.*

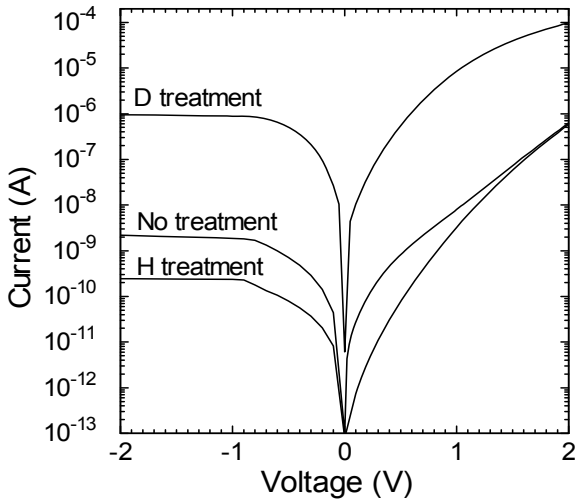

Figure 2 *Typical current-voltage characteristics of the studied Al/SiN_x/n-Si structures.*

The Effect of Ion Irradiation on Ordered Colloidal Nanoparticulate Masks

Z. Zolnai, A. Deák, N. Nagy and A.L. Tóth

In nanotechnology, fabrication represents the first and one of the most significant challenges to the realization of nanostructures. A promising method to create arrays of small objects on a substrate is nanosphere lithography (NSL) which was pioneered in the early 1980's [Fischer U C et al, J. Vac. Sci. Technol. 19 (1981) 881] and was further developed by several groups. In NSL, a self-organized layer of colloidal spheres is used as a mask for a lithographic step such as illumination, ion implantation, deposition, or etching. When NSL is used for masking, an array of nanostructures, arranged in closely packed hexagonal symmetry, is left on the substrate surface (deposition) or embedded in the substrate (implantation). NSL is a simple, fast, and inexpensive method to create large arrays of nanostructures.

The Langmuir-Blodgett (LB) technique is commonly used to prepare molecular films from Stöber silica nanospheres. Fig. 1(a) shows a monolayer LB film of ∅ 450 nm Stöber silica nanospheres deposited on (100) Si substrate.

As recent studies show, ion implantation through a LB nanomask leads to the deformation of the mask due to ion-nanoparticle interactions. The nature and the intensity of the deformation process strongly depend on the size of the nanospheres and the implantation parameters (ion energy, mass, and fluence). One of the most striking example of the shaping effect is the deformation of single colloidal particles under MeV energy irradiation with heavier ions [T van Dillen et al, Appl. Phys. Lett. 78 (2001) 910]. In this case spherical silica colloids expand perpendicular to the ion beam and contract parallel to the ion beam changing their shape to oblate ellipsoidal. This phenomenon – called „ion hammering" – is due to the fact that amorphous materials subject to high-energy ion irradiation can undergo anisotropic plastic deformation [Klaumunzer S et al, Phys. Rev. Lett. 51 (1983) 1987]. With the different applications evolving and for fundamental understanding it becomes important to find the key parameters that determine the deformation rate. As our preliminary experiment showed, already at 0.5 MeV Xe^{2+} ion energy ion hammering occurs for ∅ 450 nm silica spheroids, see Fig. 1(b). In this case the average penetration depth (~220 nm) of the ions is comparable to the diameter of the spheres (i.e. both masking and deformation occurs) so that our experiment gives valuable information about the potential and limits of NSL.

Scaling down the diameter of the spheres one has to decrease the energy of the bombarding ions to satisfy the geometrical conditions for masking (selective area patterning). Even so, to date only a few attentions were paid to ion-nanomask interactions in the energy range of 10-100 keV. A recent study [Lindner J K N et al., Nucl. Instrum. Methods Phys. Res. B 242 (2006) 167-169] has shown that the irradiation of ∅ 100 nm silica spheres with 15-75 keV energy C^+ ions leads to different effect than ion hammering. In that case the collective motion and coalescence of the spheres was observed, an effect called „ion beam sintering". In our preliminary study

performed in a focused ion beam (FIB) setup with 30 keV Ga^+ ions we found significantly different behaviour of colloidal silica spheres for ∅ 450 nm than for ∅ 90 nm under similar irradiation conditions, see Fig. 1(c) and (d). For the larger spheres no collective motion and sintering is observed, instead the silica colloids contract perpendicular to the ion beam changing their shape to cylindrical like. For the smaller spheres ion beam sintering occurs.

The details and cause of the size effect and the sintering process are not yet completely understood, however, they play clearly fundamental role in the NSL technique. Our recent plan is to give significant contribution to this research area.

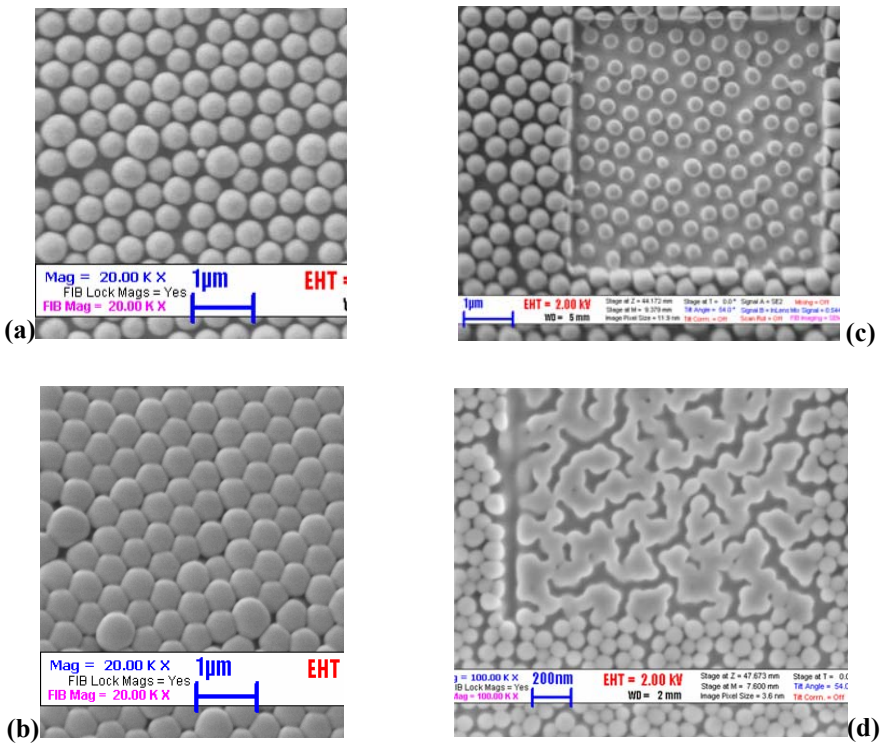

Figure 1 *(a) FESEM image of one monolayer Stöber silica spheres with diameter of 450 nm deposited on Si substrate using Langmuir-Blodgett (LB) technique (unirradiated film). (b) A similar film after irradiation with 500 keV Xe^{2+} ions: shape transformation from spheres to oblate ellipsoids occurs (anisotropic plastic deformation, or ion hammering effect). (c) A similar LB film irradiated with 30 keV Ga^+ ions: size reduction without collective motion of the spheres can be observed. (d) One monolayer of ∅ 90 nm Stöber silica nanospheres deposited on Si substrate irradiated with 30 keV Ga^+ ions: collective motion of the spheres and ion beam sintering can be observed.*

Orientation Dependence of the Thermal Relaxation of Damage in 4H-SiC Introduced by High Fluence Ni Implantation

Z. Zolnai, G. Battistig, A.L. Tóth, J. Garcia López, and Y. Morilla

Nowadays the investigation of single crystalline silicon carbide (SiC) is an intensive research area. The unique physical properties of SiC, especially the wide band gap, make it suitable for spintronics applications. One possibility to introduce magnetic ions (Fe, Co, Cr, Ni, Mn, etc.) with high concentration (ca. 0.1-10 atomic %) into SiC is ion implantation. This process results in the formation of lattice damage which leads to degradation and unstable operation of the devices. The problem to optimize the post-implantation annealing process in order to recover the damaged crystal lattice is not yet solved, however, one have to overcome this obstacle before SiC can be used in spintronics devices. It is an important issue to study the effect of annealing on SiC layers pre-amorphized with high fluence Fe^+, Mn^+, Ni^+, etc, implantation.

We investigated the thermal recovery of 860 keV Ni^+ implantation-induced damage on the surface and throughout the implanted layer in 4H-SiC. The results for two different crystalline orientations, namely the (0001) and (11-20) planes were compared, see Fig 1.

In the FESEM micrographs in Fig. 1, largely different changes in the surface morphology for (0001) and (11-20) orientations can be observed after post-implantation annealing at 1150 ^oC for 1 hour. In the former case a pattern of cracks with trigonal or hexagonal symmetry is formed on the 10 micron scale, while in the latter case parallel cracks appear with a spacing of about 10 micron. For higher magnification in Fig. 1 (b) wire-like structures can be observed by FESEM indicating the formation of a polycrystalline zone during annealing. For (11-20) orientation similar structures cannot be seen as the surface appears to be quite homogeneous. These results are in agreement with previous observations performed on Al^+ ion implanted SiC samples [Battistig G et al, J. Appl. Phys 100 093507 (2006)] showing that for (0001) orientation cubic (3C) polycrystalline inclusions appear after a similar annealing treatment. The recent results on Ni implanted samples show that for (11-20) orientation the hexagonal character – nevertheless, in the presence of planar defects – can be recovered.

The above described qualitative trends were confirmed with 3.5 MeV He^+ ion backscattering/channeling (BS/C) measurements (not presented here) which have shown that despite the high Ni atomic concentration of 0.5 %, i.e. the high implantation fluence (being ca. 20 times higher than the amorphization threshold for SiC), the long range ordered hexagonal character of the (11-20) oriented substrate is preserved throughout the whole 770 nm thick implanted layer after annealing.

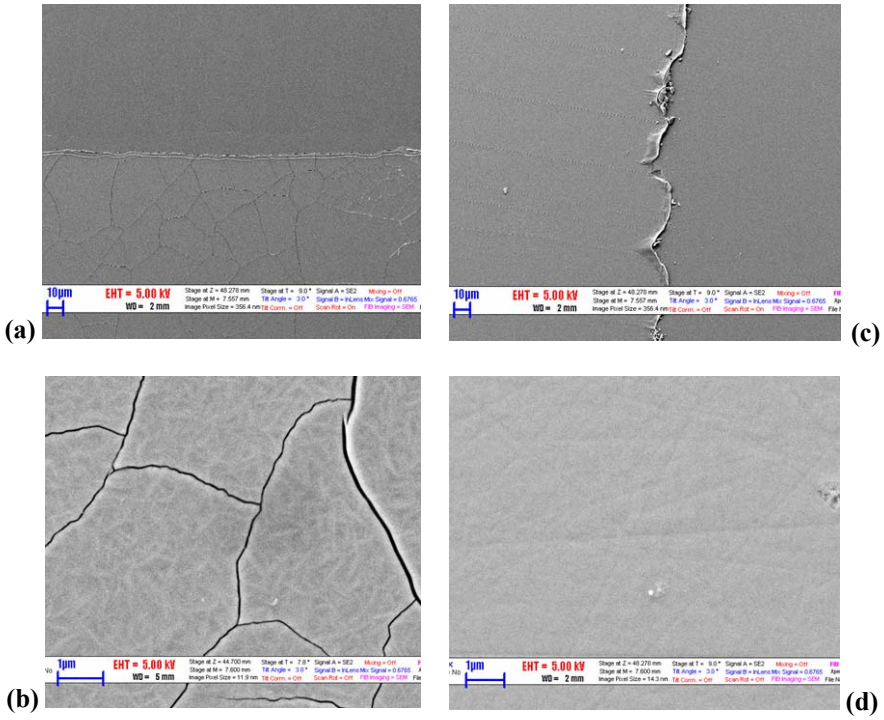

Figure 1 *The effect of post-implantation annealing on the surface morphology of (0001) and (11-20) oriented 4H-SiC samples irradiated with 860 keV Ni^{+} ions to a fluence of 1×10^{16} cm^{-2}. The annealing process was performed at a temperature of 1150 ^{o}C for 1 hour.*
To the top: FESEM micrographs taken at the border of the as-implanted and post-implantation annealed regions for (a) (0001) and (c) (11-20) oriented surfaces.
To the bottom: FESEM micrographs with higher magnification taken on the relaxed surfaces after the annealing treatment. (b) The wire-like structures with diameter of ~50 nm are well visible on the (0001) oriented surface, while (d) they are absent on the (11-20) oriented plane. Here only scratches, probably due to the original surface polishing, are visible.

Bandgap Engineering of Quaternary GaInAsP Semiconductor for Application as Active Layer in Optoelectronic Devices Used for Food Spectroscopy

V. Rakovics

Infrared emitting diodes play an important role in the development of portable spectrometers due to their high efficiency compared to conventional lamps. Quality control in food industry and clinical diagnostics demand powerful, versatile and relatively not expensive spectrometers. Semiconductor light sources are characterized by small dimensions and low power consumption. They can therefore be regarded as suitable components for low price miniature devices.

The GaInAsP/InP alloy system is widely used for fabricating optical devices, because GaInAsP can be epitaxially grown lattice matched on InP substrates over a wide range of band gaps from 1.34 eV (920 nm) to 0.74 eV (1680 nm) at room temperature.

Liquid phase epitaxy (LPE) were used for development of the device structures, as the composition of the active layer can be relatively easily adjust by weighing appropriate amount of the materials into the growing melts. By development of the precise experimental phase diagram, LPE growth of new GaInAsP device structures became fast and reliable fabrication method.

Near-infrared (NIR) spectroscopy is based on the absorption of electromagnetic radiation at wavelengths in the range 780–2500 nm. NIR spectra of foods comprise broad bands arising from overlapping absorptions corresponding mainly to overtones and combinations of vibrational modes involving C-H, O-H and N-H chemical bonds. The concentrations of constituents such as water, protein, fat and carbohydrate can in principle be determined using classical absorption spectroscopy. NIR spectroscopy is used routinely for the compositional, functional and sensory analysis of food ingredients, process intermediates and final products. The major advantage of NIR is that usually no sample preparation is necessary, hence the analysis is very simple and very fast (between 15 and 90 s) and can be carried out on-line. One of the strengths of NIR technology is that it allows several constituents to be measured concurrently. In addition, for each fundamental vibration there exists a corresponding series of overtone and combination bands with each successive overtone band approximately an order of magnitude less intense than the preceding one. This provides a built-in dilution series which allows several choices of absorptions of different intensity containing the same chemical information. Finally, the relatively weak absorption due to water enables high-moisture foods to be analyzed. NIR spectroscopy is well suited for determining the major components of foods such as water, fat, and protein. The reason why NIR spectroscopy is well suited when assessing the presence of water and protein is due to the specificity of O–H and N–H bindings. In the overtone region from 1000 to 1900 nm water can be observed around 1400–1550 nm, and this overlap to some extent with the N–H regions from 1490 to 1600 nm.

GaInAsP/InP is an ideal material system for the fabrication of double heterostructure devices. As InP has higher band gap than the lattice matched GaInAsP active layer, absorption losses inside the devices structure can be minimized. Additionally, waveguide layers, gratings, optical filters, can be grown from the same type of material. However light emitting diodes have narrow spectral bandwith compared to conventional lamps and in most applications a series of different wavelength devices is needed to cover the wavelength range of the analyzed components. For optimal overlapping of the LED array spectra not only the peak emission wavelengths but the spectral widths are equally important to be designed carefully. High quality GaInAsP LEDs have been developed for emission in the 900-1700 nm range and the emitting wavelength of these devices can be tuned by changing the composition of their active layers. Liquid phase epitaxy is a versatile tool for growing thick layers with various composition simply by weighing different amount of materials into the melts. LPE grown infrared emitting diodes have 50-75 meV spectral bandwidth depending on the growth conditions. Small area surface emitting LED chips were prepared to cover the 1000-1700 nm wavelength range completely. These chips were efficiently used for food spectroscopy. Fig 1 shows the infred photo of high brigthness LED chip. Figure 2 shows the relative near infrared transmission spectra of ethanol and water.

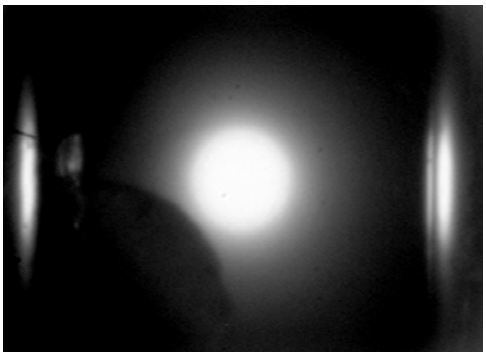

Figure 1 *Infrared photo of high brightness GaInAsP/InP IR-LED chip*

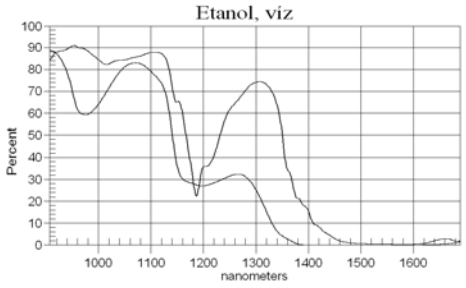

Figure 2 *NIR transmission spectra of ethanol and water*

In 2008 we have developed high brightness IR LED chips for selective spectroscopy of ethanol- water solutions and for photo-acoustic water vapour.

Co-evaporated Four-Component Semiconductor Thin Films for Photovoltaics - Solar Cell Innovation Center

(Supported by Hungarian National Research Fund (OTKA) Project NK 73424)

Z. Lábadi, Á. Németh, I. Bársony

Aim and achievements:

The aim of the Solar Cell Innovation Center is to develop an R&D facility for thin film solar cells with CuInGaSe active layer. The cross-section of the solar cell structure is shown in Fig. 1.

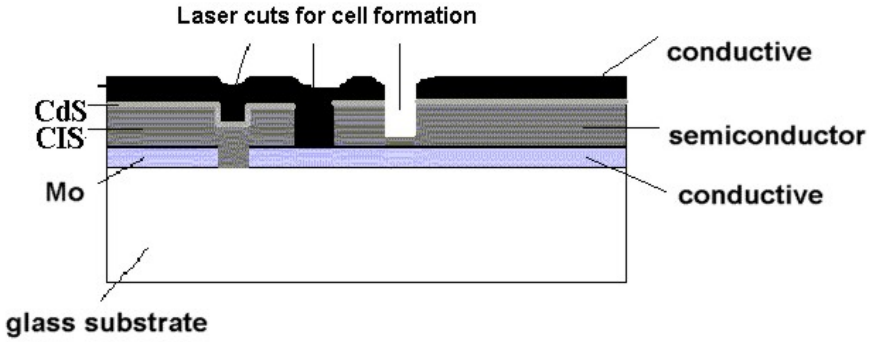

Figure 1 *Structure of CIGS solar cell*

1. Co-evaporated four-component semiconductor thin films for photovoltaics

The research project is aimed at the understanding of fundamental phenomena and the interrelation of composition, structure and optical / electrical properties vs. growth and deposition parameters in the active layer of CIGS PV devices.

The project is aimed to study the main materials related issues in p-type CIGS such as

- Shallow acceptor doping by intrinsic defects in CIGS
- Bandgap engineering in CIGS
- Grain boundary and grain-size
- Na-diffusion effect
- Bandgap matching by the buffer layer
- Buffer layer growth by Atomic Layer Deposition (ALD)

2. Results related to the reactive sputtering of Al doped ZnO contact layers

Reactive sputter deposited ZnO received much attention in the solar cell technology during the past few years due to its cost efficiency. The key issue for its introduction into mass production was the deep understanding of the reactive sputter process.

The most notable difficulty is the well known hysteresis effect of the reactive plasma just in the range of the system parameters necessary for excellent property Al:ZnO TCO thin films.

Detailed study of the deposited layers vs. deposition parameters made possible the identification of different regions in the power vs. oxygen flow chart of the system. These are summarized in Fig 2.

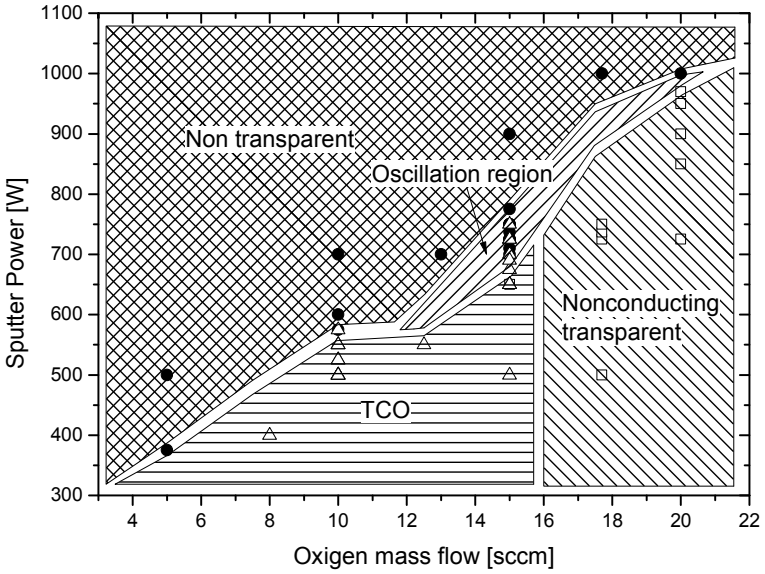

Figure 2 *Detailed study of TCO deposited layers vs. deposition parameters*

A. Metallic region ("non -transparent" in Fig 2.) showed inadequate transparency but high conductivity
B. Above 15sccm oxygen mass flow the layers were transparent but insulating as well. ("Nonconducting transparent" in Fig. 2.)
C. Spontaneous and stable plasma oscillations were observed in the oscillation region (See Fig. 2.). Fig. 3 shows the time dependence of the working pressure and the target voltage in this domain while Fig. 4 shows a cross-sectional TEM micrograph of a sample deposited from oscillating plasma. A qualitative physical model for the oscillation was also developed.

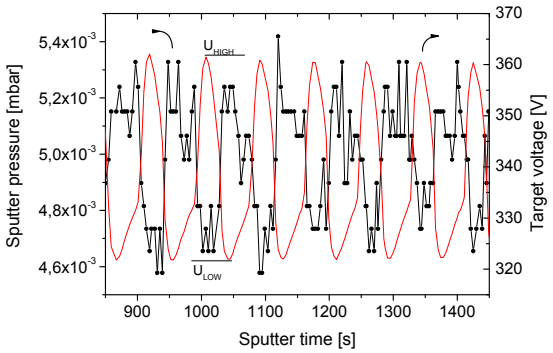

Figure 3 *Time dependence of the working pressure and the target voltage in the oscillation domain*

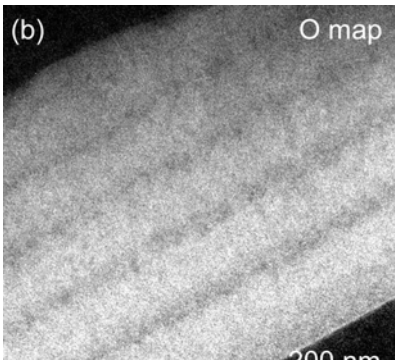

Figure 4 *TEM micrograph of a sample deposited from oscillating plasma.*

D. On the basis of our experimental findings reproducible deposition of TCO layer is possible at target power values below 750 W and at oxygen inlets less than 15 sccm ("TCO in Fig.2.") An optimal working point can be defined in the 550 - 575W power range and at 10/40sccm O/Ar gas flow where 7.7×10^{-4} Ωcm TCO layer with 90% transparency can be deposited without closed loop process control and substrate heating.

Thin Film Physics Department

Head: János L. Lábár, D.Sc., scientific advisor

Research Staff

Katarína BALÁZSI, Ph.D., Deputy Head of Department
Árpád BARNA, D.Sc., Professor Emeritus
Péter B. BARNA, D.Sc., Professor Emeritus
Zsolt CZIGÁNY, Ph.D.
László DOBOS, Ph.D.
György GERGELY, D.Sc., Professor Emeritus
Olga GESZTI, M.Sc.
Sándor GURBÁN, M.Sc.
András KOVÁCS, Ph.D. (on leave)
Viktória KOVÁCSNÉ KIS, Ph.D. (on leave)
Miklós MENYHÁRD, D.Sc.
Béla PÉCZ, D.Sc., Deputy Director of MTA MFA
György RADNÓCZI, D.Sc.
György Zoltán RADNÓCZI, Ph.D.
György SÁFRÁN, Ph.D.
Attila SULYOK, Ph.D.
Péter SÜLE, Ph.D.
Lajos TÓTH, Ph.D.
Bernadett VEISZ, Ph.D. (on leave)

Technical Staff

Sándor CSEPREGHY, engineer
Ferencné GLÁZER, lab assistant *
Andrea JAKAB, technician
Andor KOVÁCS, engineer
Antalné KOVÁCS, technician *
István KOVÁCS, engineer *
László PUSKÁS, technician *

Ph.D. students / Diploma workers

Emil AGÓCS, diploma worker
Róbert GRASIN, Ph.D. student *
László KÓTIS, Ph.D. student
Gyula LESTYÁN, diploma worker
Fanni MISJÁK, Ph.D. student
Marianna RÉDEINÉ SZERENCSI, Ph.D. student
Lajos SZÉKELY, Ph.D. student

*: part time or part of the year

The Thin Film Physics Department concentrates on major aspects of structure and structure development of thin films and their surfaces and interfaces. Activity spans from basic research to industrial applications, from deposition of films to their characterization by TEM, AES and by other complementary methods, including development of both preparation instrumentation and characterization methods. The range of studied materials cover metals, semiconductors and insulators.

Basic research concentrates on two distinct fields. On the one hand, scattering of electrons and ions is studied, including their utilization in spectroscopy, diffraction and ion mixing. On the other hand, the models for structure development are refined.

Research aimed at industrial applications include the study of materials for hard coating, low-friction coatings, semiconductor devices and their contacts, together with various applications of metallic nanoparticles and nanocomposites. The Department is experienced in different forms of cooperation as indicated by our participation in several European and National Research Projects, in education, and in fulfilling specific industrial contracts. .

Members of the Department regularly teach and supervise university students of different levels (starting research (TDK), BSc, MSc and PhD).

Social-professional activities of the members of the Department include participation in National and International Scientific Bodies and Committees, Boards of Societies and Journals, organization conferences and schools and chairing sessions in them.

Structure and morphological development of metal-metal (Cu-Ag) nanocomposite films

(OTKA 048699)

Misják F, Radnóczi G, Barna PB

There is increasing scientific and commercial interest in the development of nanostructured thin films due to their outstanding properties relative to single-phase materials. The Cu-Ag system can be a suitable model for the investigation of structure development in metal-metal nanocomposites and their structure-property relations. Beside this, Cu-Ag alloy materials are also of interest in numerous applications (decorative and deformable coatings, electronic contacts or interconnects).

In thermodynamic equilibrium the two components in the Cu-Ag binary system are practically non mixing with each other. However, the applied growth conditions can create such non-equilibrium situation, in which the Cu and Ag atoms intermix and as a result a new, metastable structure forms. This structure is different from the known equilibrium state structure and may have also new physical properties. The aim of the present work is to reveal the property and the development of this new structure.

Cu-Ag films were prepared by thermal evaporation and co-deposition of Cu and Ag in vacuum of 10^{-5}-10^{-6} mbar onto amorphous thin carbon foils and amorphous SiO_2, held at room temperature. The composition of the films covered the range of 10-60 at % of Ag. Deposition rates were around 1 nm/s. High resolution TEM was performed by a JEOL 3010 operated at 300 kV.

Films of eutectic composition (60 at% of Ag) are composed of columnar grains 30-50 nm in diameter. The columns have a pronounced <111> one axis texture and are nanocrystalline composed of 2-3 nm size zones of Cu and Ag rich solid solutions. (fig 1.)

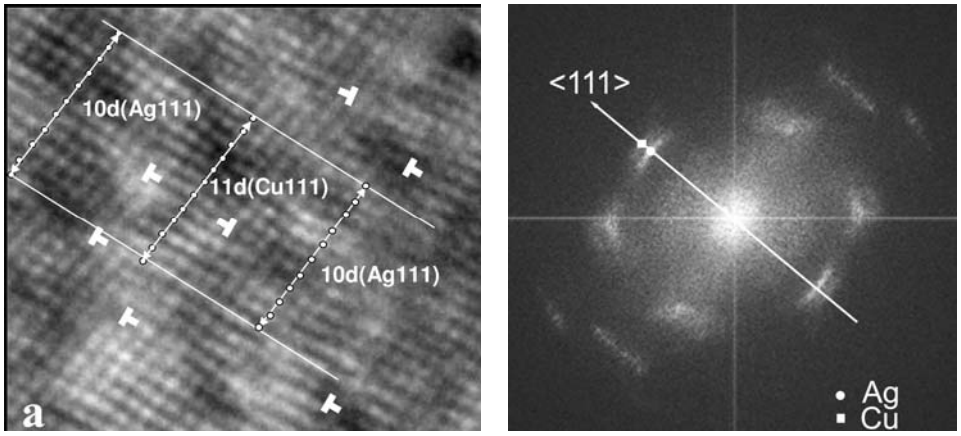

Figure 1 *Cross section high resolution TEM image and FFT diffraction pattern of Cu-Ag epitaxial nanocomposite film*

The zones are epitaxial to each other; their boundaries are semicoherent and provide a smooth compositional transition from Cu to Ag rich zones. As a result, each column can be described as a 3 dimensional nanocomposite of epitaxial crystallites.
Understanding the morphology and texture in the films we concluded, that phase separation should take place in two steps during growth. The first step occurs by crystallization from liquid phase during liquid like coalescence and then a second separation process takes place by spinodal decomposition of solid solution grains during the growth of columnar crystals. The competing growth of the columnar (single phase alloy) crystals brings about the <111> texture.

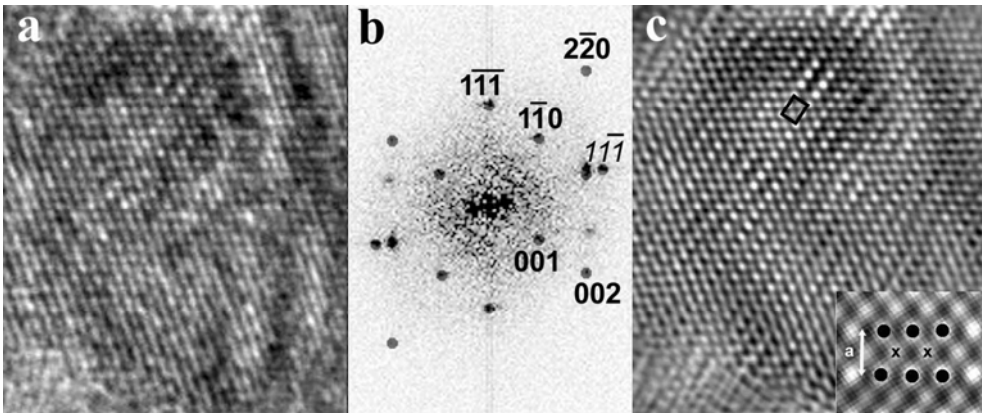

Figure 2 *High resolution image of a Ag domain (a) showing superlattice reflections of (001) and (1-10) type in the FFT pattern indicating the presence of an ordered solid solution in the Cu-Ag alloy (b). The index (1-11) printed in italic in (b) is common for Cu and Ag reflections. The filtered version of the image in (a) indicating the position of the unit cell and the simulated image of the ordered structure in the insert is shown in (c).* ● *stands for only Ag positions, x stands for common positions of Ag and Cu.*

HREM analysis and image simulation discovered the existence of zones with ordered solid solution in the structure (fig. 2). Lattice fringe image of an Ag domain is shown in Fig. 2a. The FFT corresponding to the image is presented in Fig. 2b. The occurrence of 100 and 110 type forbidden reflections proves that the Cu-Ag solid solutions could arrange into ordered solid solution during the structure evolution of the film. The structure of this ordered solid solution is demonstrated in Fig. 2c obtained by Fourier filtering of Fig. 2a. These results suggest that the phase separation occurring during film growth could start by ordering processes. Ordering in solid solution can be one of the routes through the metastable states occurring between supersaturated random solid solutions and phase separated Ag and Cu grains as a final equilibrium state.

Structure and Property Relations in Carbon-Metal Nanocomposites

(OTKA 048699)

Radnóczi G, Balázsi K, Rédeiné Szerencsi M, Grasin R, Jakab A, Kovács A
Sylvestre A (CNRS), Pauleau Y (CNRS) Kukielka S (UTK), Gulbinsky W (UTK)

One step processes of phase separation and layered structure formation are of high interest in growth of two phase nanomorphologies for creating self adapting structures to different applications. Co-deposition of C and metal species can lead to the formation of self organized layered structures.

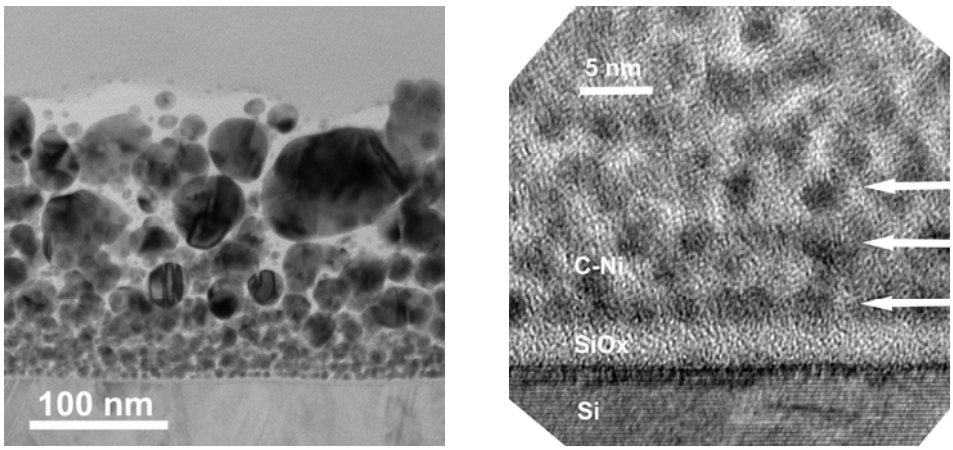

Figure 1 *TEM cross section images of Ag-C (a) and Ni-C (b) films grown by PECVD process. A self-organised morphological gradient and layered structure forms in the film.*

Ag, Ni, Cu and Ti were used as metal components. In the films presented here Ag-C and Ti-C composites were grown at ambient temperature by plasma assisted CVD combined with magnetron sputtering. C was deposited by decomposing CH_4 in RF plasma while the metal component was added by sputtering. Ag-C nanocomposites show layered growth at the initial stages of film development (fig. 1). As the amount of metal and probably the temperature of growth increase an intensive liquid like coalescence of Ag islands starts and full phase separation occurs while large Ag grains develop.

Films having self-organized layered structures and gradient morphologies along their thickness can be created in this way (Fig. 1) depending on chemical interaction and deposition parameters of the two components. Mechanical and tribological properties of the films are compared for different metal-carbon interaction pairs, different carbon phases and metal/carbon ratios.

FOREMOST, Fullerene Based Opportunities for Robust Engineering: Making Optimal Surfaces for Tribology

(EU FP6, integrated project IP-FP6-515840)

Radnóczi G, Balázsi K, Czigány Zs, Misják F, Geszti O, Kovács A, Jakab A

The project arrived to the stage when selection of the coatings for possible industrial application has to be made. To achieve this goal a three day meeting in Budapest has been organized where more than 30 foreign representatives of project partners were participating. The organization and hosting of the meeting was carried out successfully.

Characteristic coatings for applications in tribology and containing fullerene like layered nanostructures are the C-metal nanocomposites and nitride or plastic coatings containing embedded fullerene-like particles, mainly WS_2 as well as CBN based coatings. Different deposition techniques were used for the preparation of the experimental coatings, including advanced deposition processes, such as ion beam deposition and magnetron sputtering as well as more conventional techniques, such as electrodeposition and sol-gel processing.

The structural characterization of the coatings by transmission electron microscopy is carried out partly in Budapest at MFA. Two characteristic structures are shown in figures 1 and 2.

Figure 1 shows an embedded WS_2 nanoparticle in CrN matrix grown by arc evaporative PVD (IonBond, Durham, UK). The particle is almost fully connected to the matrix, however, a small low density region in the shadowed volume below the particle is revealed. The particle has irregular WS_2 layers, the surrounding CrN is of columnar morphology. The expected role of the particles in the structure is to ensure low friction by continuously feeding WS_2 to the working surface, thereby making the coating self-adapting to the tribological needs.

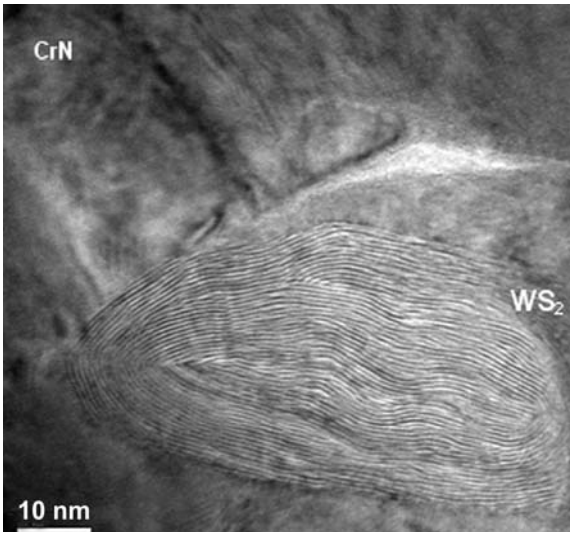

Figure 1
Cross section HREM image of IFLM nanoparticle – WS_2 in CrN matrix. The size of nanoparticle is ~ 60 nm.
The layered structure of the particle is clearly visible.

Figure 2 shows the cross section image of a BCN-C multilayer coating grown on Si for experimental purposes (elaborated at CEA/LITEN in France). The layer is fully amorphous, no sharp interface between BCN and C layers is detectable. The dark and bright layers are the BCN and C layers, respectively. The layer thicknesses differ from the nominal thickness: the multilayer structure is 8x[~15nm BCN + ~70nm C]. The layers show weak contrast (so called mass contrast). Taking into account that the average atomic number of the layers is not significantly different, the origin of the density difference is most probably due to different short range order. The layers are smooth at the substrate but interface waviness increases with film thickness.

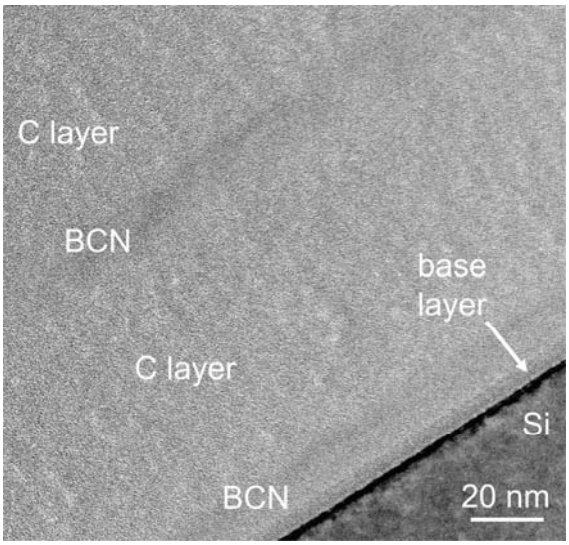

Figure 2
TEM image of BCN/C multilayer. A bit darker contrast of a ~5nm thick layer can be distinguished at the bottom marked as "base layer"

The overall objective of the project is to provide industry with a new generation of composite coating systems and surface engineering solutions, based on the incorporation of inorganic fullerene-like nanoparticles into coatings and lubricants, to significantly reduce and control friction and wear in rolling and sliding contacts in order to extend operational life, reduce maintenance requirements and reduce the environmental impact of a wide range of mechanical systems.

The final application of the coatings is foreseen in industries like aerospace, automotive, machine tools, etc. Reducing friction benefits the environment by reducing energy requirements with a consequential drop in CO_2 emission (http://www.foremost-project.org/home.asp).

Structure formation in co-deposited $Cr_{1-x}Al_xN$ thin films in the $0 < x < 1$ composition range

OTKA T048699; EU FP6 project, NMP3-CT-2005-515844: INNOVATIAL

P.B. Barna PB, Lestyán Gy, Lábár JL, Székely L, Geszti O, Sáfrán Gy, Biró D (Sapientia U)

$Cr_{1-x}Al_xN$ as a ternary nitride has become increasingly important in a wide range of applications. The Al content controls both the structure, including the phase composition (hexagonal and cubic) and the properties of the coatings. Experiments proved a broad range for the solubility of AlN in the fcc CrN ($0,5<x<0.75$), while the theoretical calculations predicted a limit at x= 0,77-0.95. The strong dependence of the maximum possible AlN concentration in the fcc-$Cr_{1-x}Al_xN$ on the deposition parameters is not understood. The aim of our investigations was to investigate the effect of the N_2 pressure on the solubility of AlN in fcc-CrN.

In our experiments the structure formation was studied by the micro-combinatorial experimental method at the co-deposition of Cr and Al. This made possible to prepare films in the composition range of $0 < x < 1$ over the area of a transmission electron microscopic microgrid and to investigate selected areas of well-defined composition. The films were prepared by unbalanced magnetron sputtering at a substrate temperature of 550 ^{0}C on a-C layer supported by the microgrid. The working gas was Ar+N_2 mixture at 1 x 10^{-1} and 2,5 x 10^{-1} Pa N_2 pressure, while the total pressure was 2,5 x 10^{-1} and 5 x 10^{-1} Pa respectively. The thickness of the samples was between 30 and 70 nm. The structure of the films was investigated by conventional and high resolution TEM, selected area electron diffraction (SAED), while the composition of the investigated area was determined by EDX and EELS analysis. The ProcessDiffraction program was applied for the quantitative evaluation of the electron diffraction patters. This made possible to determine the volume fraction of phases as well as that of their textures.

Figure 1 *Selected area electron diffraction patterns and the volume fraction of phases and textures of thin CrAlN films determined by ProcessDiffraction evaluation of the diffraction patterns. The films were deposited at* $P_{Ar+N2}=2{,}5x10^{-1}Pa$, *and* $P_{N2}=1x10^{-1}Pa$.

Figure 2 *Selected area electron diffraction patterns and the volume fraction of phases and textures of thin CrAlN films determined by ProcessDiffraction evaluation of the diffraction patterns. The films were deposited at* $P_{Ar+N2}=5x10^{-1}Pa$, *and* $P_{N2}=2{,}5x10^{-1}Pa$.

The experiments have clearly shown that the N_2 pressure has a dramatic effect on the solubility of AlN in the fcc-$Cr_{1-x}Al_xN$ (Figs. 1 and 2). At high N2 pressure the solubility of AlN in the c-Cr1-xAlxN lattice is increased from 54 mol% to 73 mol% and the composition range, in which the fcc and hcp phases coexist is very narrow ($0{,}73 < x < 0{,}84$). This could indicate that the high N2 pressure promotes the mechanisms of structure formation which support the development of the C#3 configuration of Al distribution in the $Cr_{1-x}Al_xN$ lattice suggested by Mayrhofer et al. [P.H. Mayrhofer, et al., Acta Materialia 56(2008)2469]. The development of the structure with coexisting fcc and hcp phases in the transition composition range can be explained on one hand by the segregation of excessive Al species developing nuclei of hcp-$Al_{1-x}Cr_xN$, on the other hand by the simultaneous nucleation of fcc and hcp phases.

Interrelation between chemical composition, phases, texture and morphology in TiAlYN films

(OTKA T048699, EU FP6 project, INNOVATIAL NMP3-CT-2005-515844)

Moser M (MU), Mayrhofer PH (MU) Székely L, Sáfrán G, Barna PB

Single-phase cubic $Ti_{1-x}Al_xN$ thin films with high Al content are preferred in industrial applications as they combine superior mechanical properties with good oxidation protection. However it was observed, that some additives and specific experimental parameters could promote the formation of a second phase, which is generally the hcp AlN. For example already the addition of 1 at.% Y could promote the hexagonal phase formation at low Ti/Al ratio.

Aim of the peresent work is to collect further information on the correlation between elemental composition, structure and mechanical properties of the coatings and the modified discharge, plasma and target conditions in the case of various sputtering methods.

In recent experiments composition the Ti/Al ratio was varied in the range of 0.72 - 1.18 where the fcc and hcp phases coexist.The variaton of Ti/Al ratio was realized by two kind of methods. The first method was the DC magnetron sputtering with various target composition. In that case the composition could be varied in relatively large steps. The other method was the pulsed DC magnetron sputtering with the same target composition, but with different in pulse duration. By this method the composition could be varied in fine steps.

In these experiments four separate groups of structures could be distinguished as a function of the Ti/Al ratio (Figs.1 and 2)

1) Ti/Al=0.72 (Figs.1a and 2.a). The coating is composed of two layers. Both layers are columnar and the poorly developed columns are composed of nanocrystals. In the first layer the columns are perpendicular to the substrate and the columnar structure corresponds to Zone T. The columns of the second layer are tilted to the substrate normal. In the near-substrate layer the fcc phase is identified with <200> texture as the majority phase. The texture axis is perpendicular to the substrate plane. The hcp is the minority phase with <002> texture and the texture axis is tilted. In the second layer the hcp is the majority phase with <002> texture. The texture of the minority fcc phase is changed to <111>. The fcc and hcp phases have epitaxial relationship.

2) Ti/Al=0.81(Figs.1b and 2b.). At this composition the hcp and fcc phases coexist with hcp <002> and fcc<111>textures in the whole thickness of the film. The phases have epitaxial relationship. Both the columns and texture axes are tilted.

3) Ti/Al=0.88 (Figs.1c and 2c.). Two layers can be distinguished. In the substrate near layer the hcp phase is hardly detectable. The fcc phase has <200> texture with its axis perpendicular to the substrate plan. In the second layer the fcc phase with <200> texture is the majority phase, but the hcp phase can be also detected with <002> texture. The fcc texture is perpendicular while the hcp is tilted. No columnar structure could be detected in any of the layers.

4) Ti/Al ≥1 The structure is composed of well developed V-shaped columns. The fcc phase can be detected in the whole thickness of the film with <200> texture. The texture axis is perpendicular to the substrate plane.

The present results indicate that when the hcp phase starts to dominate the structure evolution the <200> texture of the fcc phase is changing to <111> and the direction of texture axis is changing from perpendicular to tilted one. The detailed analysis of the columnar structure composed of epitaxially grown fcc and hcp nanocrystals is in progress.

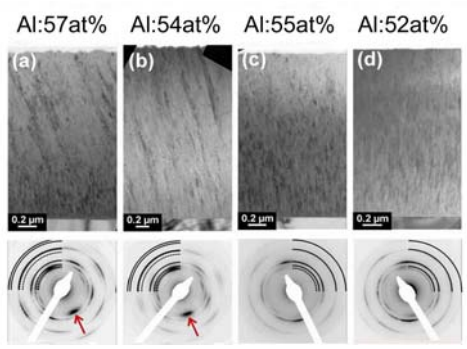

Figure 1 *Bright-field XTEM images of $(Ti_{1-x}\ Al_x)_{1-y}Y_y$ N coatings prepared with pulsed DC-MS using a frequency of 80 kHz and trev of 496 ns (a), 1616 ns (b), 3056 ns (c) and 4976 ns (d). At the bottom the respective SAED patterns are given with standard diffraction rings for cubic- (solid) and wurtzite type $Ti_{0.5}Al_{0.5}N$ (dashed).*

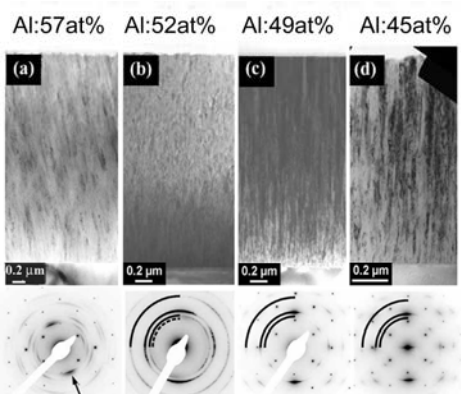

Figure 2 *Bright-field XTEM images of films with Ti/Al ratios of (a)0.72 (b) 0.88, (c) 1.0, and (d) 1.18 DC-MS from $Ti_{0.49}Al_{0.49}Y_{0.02}$ targets with added Ti platelets covering 0.74,1.48, and 2.15% of the target surface. At the bottom the respective SAED patterns are given with standard diffraction rings for cubic- (solid) and wurtzite type $Ti_{0.5}Al_{0.5}N$ (dashed).*

Metanano: „Development of noble metal based innovative products for applications in environment protection, cosmetics, sensors and catalysers”

(NKFP07-A2)

Lábár JL, Geszti O, Jakab A, Pető G, Csanády A (BayATI), Hargitai H (BayATI)
Bajáki Á (Metal Art), Bánki S (Metal Art)

General aim of the application oriented development project is to bring innovation into the Hungarian nanotechnological metal industry. The specific aim of the project is to develop high quality products: dry powders, layers, suspensions and these on

solid substrates for pharmaceutical, cosmetic, sensor and catalyst applications. Both public and military applications are targeted.

The task of MFA is complex structural characterization of both raw material and half-products and products at the nano- and at the atomic level.

In the first year, further development of the technology resulted in reliable production of the noble metal nanoparticles in the size-interval and form needed for several of the targeted applications, as documented by the submission of two patents.

Size distribution of nanoparticles can only be reliably determined by a combination of several methods. Although larger particles are successfully measured by both a Zeta-sizer and by SEM, the size and shape of the sub-ten-nanometer particle fractions can only be determined reliably with a high resolution transmission electron microscope (HRTEM).

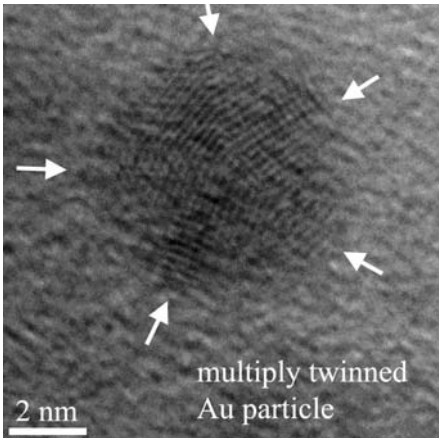

Figure 1 *Identification of a multiply twinned Au nanoparticle prepared by the dropping technique from a Au-sol.*

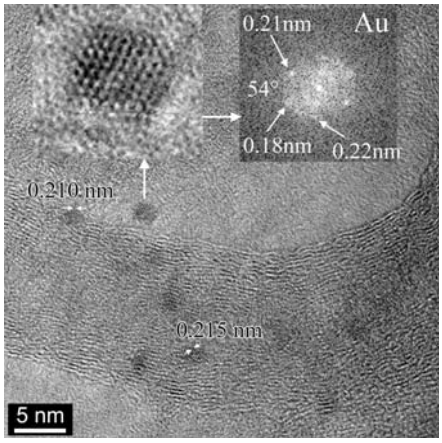

Figure 2 *Au nanoparticles attached to a multiple walled carbon nanotube (MWCNT).*

TEM and EELS study of Pd shell–Au core/SiO_2 catalyst nanocrystals

(Informal co-operation with the Institute of Isotopes, Budapest)

Sárkány A (IKI),Geszti O, Sáfrán G

Pd shells were synthesized on preformed 5 nm size Au particles by seeded growth technique (15–80 at% Pd) using sodium citrate and tannic acid. The Pd overlayer grows pseudomorphically over the Au core causing 5% lattice expansion in the Pd shell. In a Pd(41)–Au/SiO_2 sample XRD showed homogenization of the particles in hydrogen atmosphere above 423 K. The hydrogenation activity of the Pd/Au shell/core particles decreased with increasing thickness of the Pd shell. The

investigations on the hydrogenation activity as a function of the temperature confirm the thermal instability of the Au/Pd core/shell particles. As a consequence of alloying the homogenized Pd(80)–Au/SiO_2 showed higher activity and selectivity than the 1.5 nm thick Pd shell.

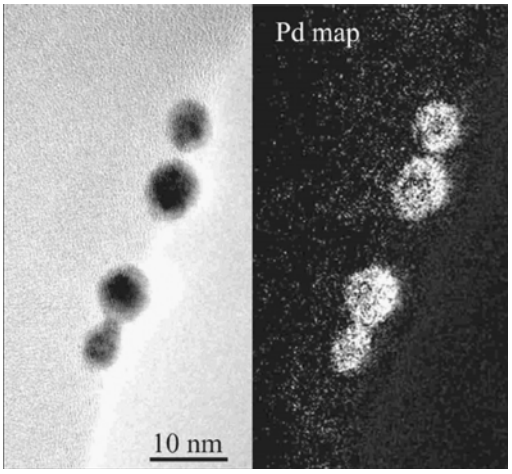

Figure 1 *Au/Pd core/shell nanoparticles; TEM and EELS map*

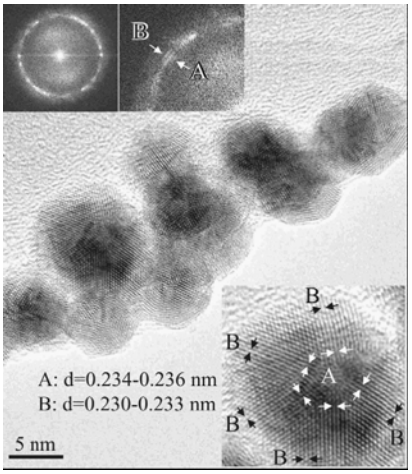

Figure 2 *HRTEM of Pd(80)–Au nanoparticles.*

Corrosion protection with perfect atomic layers, CORRAL

(EU-FP7- 213996) 2008-2011

Pécz B, Tóth L, Barna Á, Kovács I

The project is focused on a special case of corrosion protection: ***sealing***. Sealing is a protection of material against corrosion by application of an extremely dense defect-free layer (sealant), which stops any ion exchange between the material and a corrosive medium. Very thin coatings are essential for precision parts, where the dimensional accuracy of the parts is required. Perfect sealing is essential for many medical, food and pharmaceutical applications as well as reference material containers, where zero release is required. Three different deposition techniques (filtered cathodic arc deposition, high power impulse magnetron sputtering and plasma enhanced atomic layer deposition) will be applied and layers will be deposited on standard steel and aluminum substrates.

MFA performs characterization of the surface morphology and defects on the substrates, as well as of the deposited sealing layers including films deposited onto complex-shape 3D engineering parts.

Diffusion of dopants in Nickel-silicides

(Tét: F36/2006)

Lábár JL, Jakab A, Blum I, D Mangelinck D (PCU, Marseille)

Silicides are used in microelectronics to form contacts between the active components and the metallic interconnections. According to the self aligned silicide (salicide) process, silicides are formed via the reaction between a metallic film and the Si substrate. During this reaction, the dopants that are present initially in the substrate are redistributed both in the Si and in the silicide. This redistribution has an effect on the electrical properties of the silicide /silicon interface. For example, dopant segregation at this interface is known to reduce the Schottky barrier and to improve the conductivity of the device. It was also shown, that in fully-silicided gates (FUSI), dopant accumulation located at the interface between the silicide and the gate oxide allows to modulate the gate work function. It is therefore essential for technological applications to understand and to control the dopant redistribution at silicide/Si interfaces. Few data of dopant solubility and diffusion in silicides are available in the literature and they have been determined mainly in thin polycrystalline silicide films where grain boundaries play an important role.

Behavior of As and B, as dopants was examined in the current study.

As was implanted in Ni2Si layers prepared via the reaction between bilayers of Si and Ni imprisoned between two SiO2 layers on (100) Si substrate. The As concentration profiles in the samples were measured using secondary ion mass spectroscopy before and after annealing (400-700°C). Diffusion coefficients for both volume and grain boundary (GB) diffusion have been determined relying on simulations and using the information about grain structure from TEM measurement.

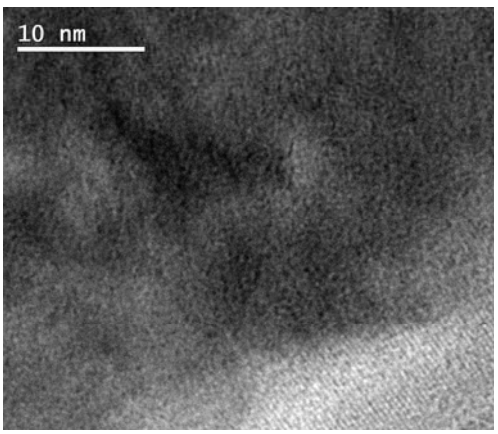

Figure 1 *TEM BF image showing crystalline structure of the Boron-rich layer in NiSi sample annealed at 800℃.*

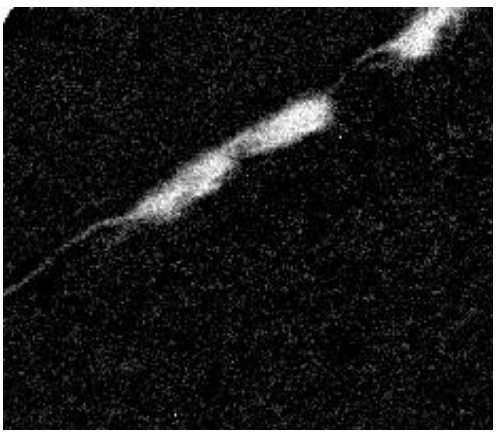

Figure 2 *Elemental Boron map, recorded by energy filtered TEM (EFTEM) from NiSi sample annealed at 800℃.*

Boron / silicide samples were prepared in order to perform Boron diffusion measurements in the Nickel silicides: NiSi and Ni_2Si. Diffusion measurements require the absence of reaction between the different layers. The objective of the TEM study (during a two-month stay of Ivan Blum at MFA) was to determine if the expected structures could be formed (by 400°C anneal) and if they are stable during high temperature anneals (800°C). In sputter deposited samples, the silicide has a porous structure. Obviously, this porosity is due to the fiber-like structure of the Si deposited by sputtering at room temperature. This structure was also observed for the B layer. Although these samples could not be used directly for diffusion measurements, important experimental facts were collected. Formation of the respective silicide phases was corroborated by both EDS and EELS and electron diffraction. No reaction between the silicide and the B layer was observed when the sample was annealed at low temperature. Formation of an additional surface layer is observed for the silicide / B samples after high temperature annealing. This layer is not uniform, some parts of the sample are not covered. Elemental maps indicate that the layer has a high concentration in B, but it is not possible from the elemental maps to determine if the layer contains another element with low concentration. High resolution images of the NiSi / B sample show that the layer is crystalline. The observed lattice spacing and angle values match either the tetragonal B phase or the SiB_6 phase. Conclusive identification needs further study.

Structural and electrical properties of Au and Ti/Au contacts to n-type GaN

Dobos L, Pécz B, Tóth L, Horváth ZsJ, Horváth ZE

The nanostructure and electrical properties of metal contacts to n-GaN layers grown by MOCVD onto sapphire substrates are the subjects of the present work.

The achieved results are the following: samples annealed at 400 and 700 °C did not show any substantial change in their microstructure. However, in the case of Au/Ti metallisation annealed at 900 °C, elongated grains of a new phase (Au_2Ga) were formed between the GaN and the Ti layer with boundaries lying parallel with the interface (Fig. 1).

High resolution study of the interface revealed some further phases, like Ti_2N and TiN (observed in a twin configuration) (Fig. 2).

The as-deposited Au and Ti/Au contacts exhibited nonlinear I-V characteristics. As a common effect, annealing decreased the barrier height. The contacts remained rectifying until annealing at 700 °C. After 900 ^{o}C the Au/GaN contact degraded, while the Ti/Au/GaN contact became ohmic.

High ideality factors indicated that the dominating current mechanism was the thermionic-field emission.

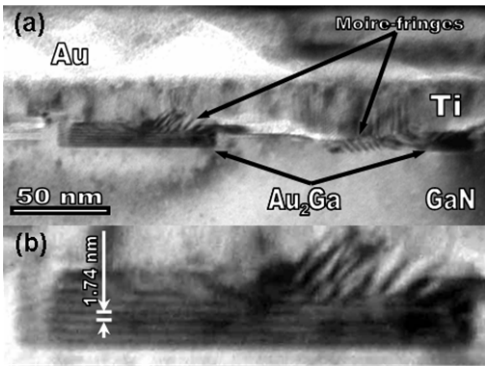

Figure 1 *XTEM micrograph of the interface of n-GaN/Ti/Au contact heated in vacuum at 900 °C for 10 min.* ***a:*** *Grains of the Au_2Ga phases and Moirè-fringes have been revealed in cross section.* ***b:*** *An enlarged image of the Au_2Ga phase grain.*

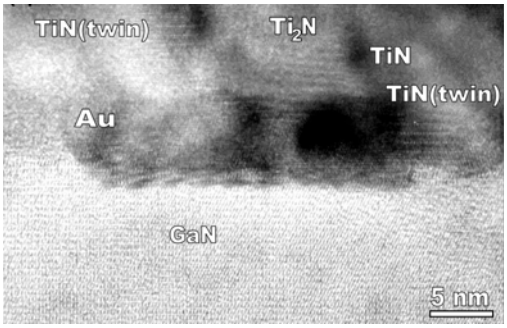

Figure 2 *High resolution image of the n-GaN/Ti/Au interface after annealing at 900 °C. HRTEM micrograph with the formed phases.*

The changes discussed above are responsible for decreasing barrier height and increasing resistivity of Au/Ti/GaN contacts during the last annealing step. The structural studies revealed that obtaining a low Schottky barrier in these contacts requires the penetration of Au through the Ti layer to reach the GaN surface and diffusion into the topmost part of epi GaN layer in addition to N outdiffusing from the GaN surface into the metal layers.

Hybrid Substrates for Mass Production of High Frequency Electronics, HYPHEN

(EU-FP6 IST 027455)

Pécz B, Tóth L, Dobos L, Radnóczi GZ, Riesz F, Bove P (PICOGIGA), Langer R (PICOGIGA), Lahrèche H (PICOGIGA) di Forte Poisson MA (ALCATEL-THALES)

The goal of the project is the development of hybrid substrates for growth of GaN layers. The starting wafer is polycrystalline SiC, which is available in large diameter as well. About 500 nm thick single crystalline Si, or SiC layer is transferred onto the starting wafer by the Smart Cut™ process of SOITEC. Thermal conductivity two times higher than Si is expected on these new type composite substrates.

MFA performs characterization of the wafers and layers grown both by molecular beam epitaxy (MBE) and chemical vapour deposition (CVD). The non-destructive Makyoh topography is used to determine the bow of whole wafers. Transmission electron microscopy (TEM) is used for the characterization of layers, interfaces and for the determination of dislocation density.

The obtained results are the following: We have found that the polycrystalline SiC wafer has a columnar structure and the characteristic sizes (of the columnar grains) were also determined. The smart-cut transferred Si and SiC single crystalline layers are free of defects, but the top surface of the composite template is a little bit wavy. The surface roughness in the case of Si can reach an rms=5 nm, but it was demonstrated in this project, that the rms can be decreased below 1 nm by special methods. In the case of the SiCopSiC (single crystalline SiC on polycrystalline SiC wafer) substrates, the top surface of the bonded SiC stripe has an rms value of about 3 nm. Our investigations showed, that the top surfaces of the grown nitride layers are also very flat in that case. Orientational relationships are the same as in the case of GaN grown on thick, single crystalline Si, or SiC reference wafers.

Dislocation density values were measured on TEM images taken on plan view samples. For reference purposes similar GaN layers were used grown on bulk Si and on whole single crystalline SiC wafers. In all cases the dislocation density values measured on the layers grown onto composite substrates were in the same range like on references samples. For example the dislocation density is $1x10^{-9}$ cm^{-2} for the case of MOCVD grown layers on SiCopSiC substrates, while the appropriate values for MBE grown layers are a little bit higher ($4\text{-}5x10^{-9}$ cm^{-2}).

An example for a HEMT (High Electron Mobility Transistor) structure is shown in Fig. 1 showing a sample grown by MBE.

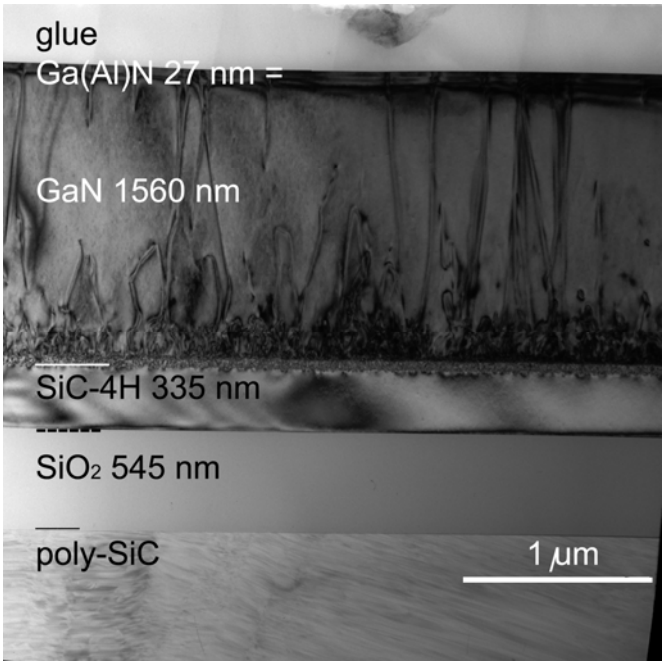

Figure 1
Overview of an MBE grown layer structure.

A 335 nm thick region of the seed hexagonal SiC substrate is transferred onto the above SiCopSiC substrate, what means, that the remaining wafer can be used again for the same process. The 1560 nm thick GaN layer contains high number of

threading dislocations, however, their number is decreased in the near surface region. The processed wafers resulted in working transistors.

Composite substrates have been successfully prepared and then nitride layers were grown on them with very high quality epitaxy. Defect density values in the grown layers are in the expected range.

HIGH-EF: „Large grained, low stress multi-crystalline silicon thin film solar cells on glass by a novel combined diode laser and solid phase crystallization process"

(FP7-ENERGY-2007-1-RTD)

Lábár JL, G Sáfrán G, Pécz B, Jakab A, Andrä G (IPHT), Gimpel T(IPHT), Gawlik A (IPHT), Ose E(IPHT), Bochmann A(IPHT), Falk F(IPHT), Christiansen S (IPHT) Schneider J (CSG Solar)

Crystalline silicon thin film solar cells on glass substrates are a low cost alternative to silicon wafer cells. HIGH-EF will provide the silicon thin film photovoltaic (PV) industry with a unique process allowing for high solar cell efficiencies (potential for >10%) by large, low defective grains and low stress levels in the material at competitive production costs. This process is based on a combination of melt-mediated crystallization of an amorphous silicon (a-Si) seed layer (<500 nm thickness) and epitaxial thickening (to >2 μm) of the seed layer by a solid phase epitaxy (ESPC) process.

The main contribution of MFA is TEM based defect structure and population analysis. Main results in the first year: a-Si layers deposited by electron beam evaporation on top of multicrystalline seed layers on glass were crystallized epitaxially up to a thickness of 1.1 μm. In this way we succeeded in preparing a layer system as required for multicrystalline silicon thin film solar cells on glass with grains in the 100 μm range. Success depends on the speed of epitaxial growth as compared to the time-lag needed for homogeneous nucleation, both depending on the deposition rate. An appreciable reduction in the processing time can be achieved at an elevated annealing temperature. Fig. 1 shows the structure of a 500 nm thick a-Si layer crystallized by ESPC at 650°C on a crystalline seed. It is seen that not all grains of the seed continue to the surface. The TEM cross section image of Fig 1 shows that on top of the seed (Si1) about 100 nm of the deposited a-Si crystallized epitaxially (Si2) but the remaining a-Si on top was converted to fine grained material (Si3). Apparently a competing nucleation process took place in the near-surface region. At a reduced temperature of 600°C there is no time lag in epitaxial growth, as observed during EPSC of an a-Si layer deposited at a rate of 100 nm/min on top of a laser crystallized seed layer on glass. After 7 h the crystallization is complete. The complete transformation to large grains up to the surface is confirmed by Fig. 2 that shows a corresponding TEM cross section image of a 550 nm thick ESPC layer on a seed layer demonstrating that perfect epitaxy occurred. For perfect epitaxy a perfectly clean surface of the seed prior to a-Si deposition is crucial.

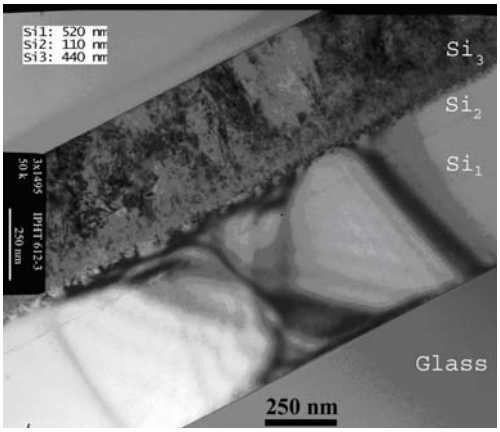

Figure 1 *TEM cross section image of an ESPC layer on seed (Si1) annealed at 650°C for 6 h showing an epitaxially crystallized layer (Si2) and a fine grained layer (Si3)*

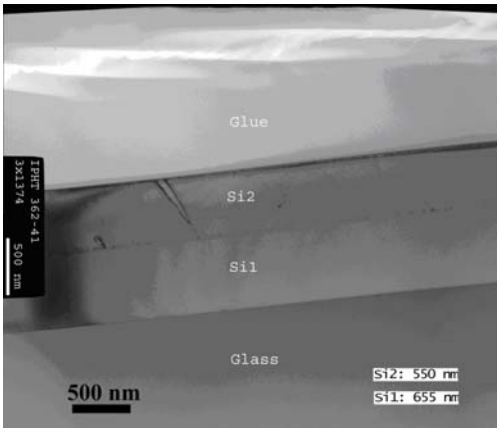

Figure 2 *TEM cross section image of a layer system consisting of ESPC layer (Si2) on seed (Si1) after annealing for only 7 h at 600°C*

First observations give hints, that doped a-Si grows faster so that thicker films can be crystallized in even shorter time. In the next steps the consortium will prepare complete solar cells in ESPC silicon layers.

Materials for Robust Gallium Nitride, MORGaN

(EU-FP7-NMP- 214610) 2008-2011

Pécz B, Tóth L, Dobos L, Radnóczi GZ

The MORGAN team will develop GaN-based devices for power electronics with the coordination of THALES. Nitride layers will be grown on diamond, and polycrystalline diamond will be also used for the passivation of nitride devices.

This project will therefore try to demonstrate the advantage of innovative **composite substrates** and devices for use in extreme environments both in terms of electric field and thermal dissipation**.** MORGaN will combine the excellent thermal behavior of polycrystalline diamond to the electrical efficiency of GaN compounds. The full potential of GaN without being limited by the thermal conductivity of SiC will be realized by the end of the project. Another goal of the project is to develop novel technologies and GaN based devices (for example sensors operating up to 1000^{o}C) working in harsh environment. MFA performs characterization of the wafers and layers by transmission electron microscopy. Diamond substrates, layers grown onto them directly, as well as novel metallization techniques will be characterized in this project started in November 2008.

Ion implantation enhanced formation of 3C-SiC grains at the SiO_2/Si interface after annealing in CO gas

(OTKA- K75735 and RITA - Research Infrastructures Transnational Access Contract Number 025646t)

Pécz B, Dobos L, Pongrácz A, Battistig G Stoemenos J (AU) Voelskow M (FZD), Skorupa W (FZD)

Silicon carbide with its hexagonal and cubic polytypes is one of the wide band-gap semiconductors used for high temperature applications. Obviously the growth of cubic SiC on Si would be very advantageous, because very large, high quality substrates would then be available at relatively low cost. However, beside the problem of the large misfit, another general problem in that is the formation of voids inside the substrate.

Earlier experiments showed, that SiC grains can be grown at the SiO_2/Si interface without voids using a simple method, i.e. annealing in CO gas. Full SiC coverage of silicon surface can not be achieved due to the limits of that method. However, nanocrystals were prepared and also separated later from the Si substrate.

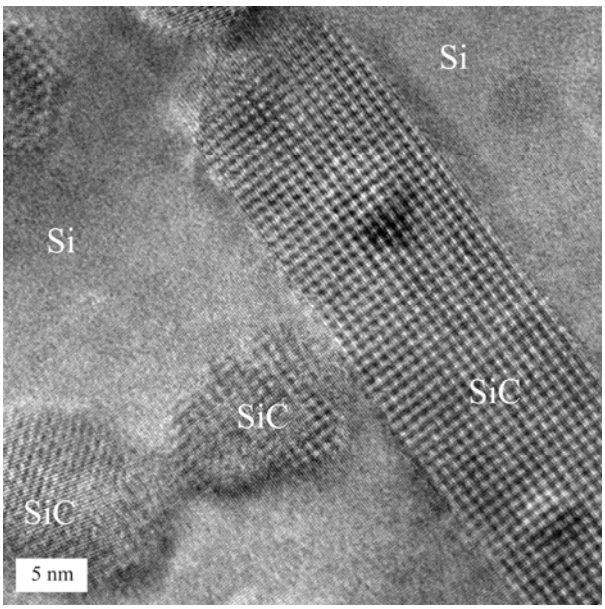

Figure 1
High resolution TEM image showing the SiC crystallites revealed by the moiré pattern of the overlapping Si and SiC lattice.

The present experiments aim to create nucleation centers for the SiC crystallite growth by carbon ion implantation. The formation of the nucleation clusters as well as the morphology, the size and the density of the nanocrystals were systematically studied by conventional and high resolution Transmission Electron Microscopy (TEM). Accordingly the nanocrystallites are formed following two different modes of growth: In the first mode facets develop along the <100> crystallographic direction giving tetragonal grains, but in the second mode facets are growing along the <110> direction,

what results in elongated nanocrystallites. Both of them are shown on the TEM image taken on a plan view sample at high resolution. The sample was prepared in the following way: At first 150 nm thick SiO_2 layers were grown at 1050°C in dry oxygen on the (100) Si wafers. Afterwards, these wafers were implanted at 550°C with carbon ions at doses of $4x10^{15}cm^{-2}$ and at energy of 40 keV. Then, the implanted wafers (together with reference samples) were annealed in CO at 1080°C for 130 min. On the plan view image the (220) silicon lattice planes of are resolved, while the SiC grains show a very regular Moiré pattern due to the overlapping of the two crystal lattices. The mean size of the SiC crystallites amounts to 11 nm whereas they cover about 31% of the surface area.

In a systematic study it could be shown that combined low dose carbon implantation and subsequent high temperature annealing in CO leads to a substantial increase of the coverage of the Si surface by high quality 3C-SiC nanocrystallites.

Fabrication and study of new nano-structures in sapphire implanted with light ions

(Co-operation with the Inst. Technol. e Nuclear Sacavém, Portugal)

Sáfrán G, Alves E (INS), Marques C(INS), McHargue CJ (INS)

The physics of formation and stability of ion beam modified structures is far from being well-understood. We have studied the defect behaviour of sapphire implanted with carbon and nitrogen with 1×10^{16} to 1×10^{17} cm^{-2} fluences at 150 keV. The implantation occured at RT, 500 ˚C and 1000 ˚C. RBS-channeling revealed a surface region with low residual disorder in the Al-sublattice. Near the end of range the channeled spectrum almost reaches the random level, indicating a high damage level for high fluences

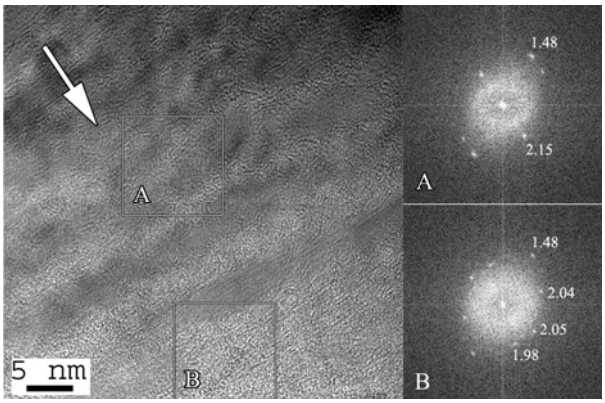

Figure 1 *HRTEM of sample implanted with 1×1017 C+/cm2 and annealed at 1000 ºC. Inset A: FFT of the damaged area. Additional reflections in inset B: graphite nanocrystals in the amorphous region.*

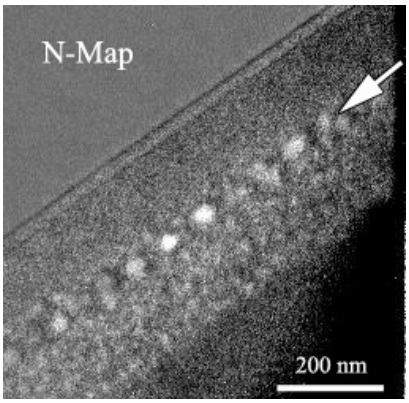

Figure 2 *EELS N-Map representing high N concentration in the bubbles lined up along the c-plane.*

HRTEM showed layered structure for the C implanted sample with embedded nanocrystals in a buried amorphous region. The EELS elemental mapping revealed buried N bubbles along the c-plane of sapphire in the N-implanted sample (1000˚C).

HRTEM investigation of Co-Pt Perpendicular Magnetic Media for Tbit/inch^2 Recording Densities

(Co-operation with the Akita Institute of Advanced Technology AIT))

Ariake J (AIT) Sáfrán G, Geszti O

Perpendicular magnetic recording (PMR) technology provides extreme densities up to Tbit/inch^2 in computer hard disk drives data storage. It applies „single pole" head and storage layers with nano-grains structure of perpendicular anisotropy. In our cooperation Co-Pt-TiO_2 composite storage media were deposited and studied by magnetic measurements and HRTEM. MFM and HRTEM proved that TiO_2 addition effectively decouples the grains and magnetic domains of the films and so reduces media noise. Such a medium on Ru seedlayer is illustrated in Fig. 1. According to new results, however, optimized media require a certain coupling of the magnetic nanocrystals. This can be realized by "stacked structure" or "continuous-granular composite (CGC)", which are the subject of our further studies.

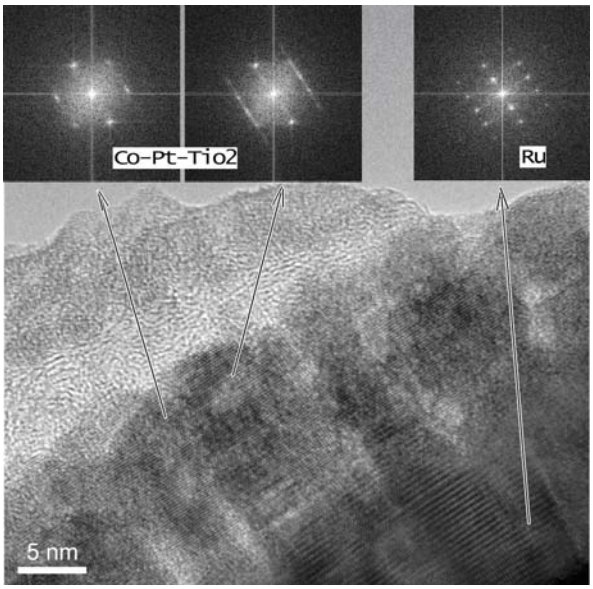

Figure 1 *HRTEM of a Co-Pt-TiO_2 PMR layer deposited onto Ru seedlayer. The FFT-s show the strict c-axis orientation of the columns (5~8nm dia) separated by the TiO_2*

Monte Carlo calculation of backscattering factor for complex structure

(PL-15 Project between the Polish and Hungarian Academy of Sciences)

Kotis L, Menyhárd M, Zommer L (IPC), Jablonski A (IPC)

Zommer and Jablonski were the first to develop a MC model for calculations of the backscattering factor (BF) for multilayered systems. These theoretical results were compared to experimental ones in this work.

A multilayer structure of 3X(41 nm Ni/ 28 nm C) on top of Si substrate was AES depth profiled and the intensities of the Auger lines of Ni_{MVV} (61eV), C_{KLL} (272 eV), and Ni_{LMM} (848 eV) were measured. Note that the intensities measured are not constant (Fig. 1) in the pure regions of the material where only one element is present. The intensities for the two different Auger lines of Ni and C are different. Fig. 2 shows the measured and calculated normalized intensities in the case of the Ni_{LMM} (848 eV) Auger line.

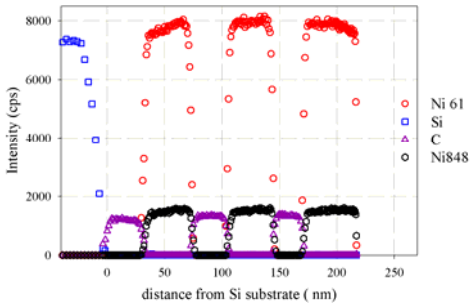

Figure 1 *The as recorded AES depth profil.*

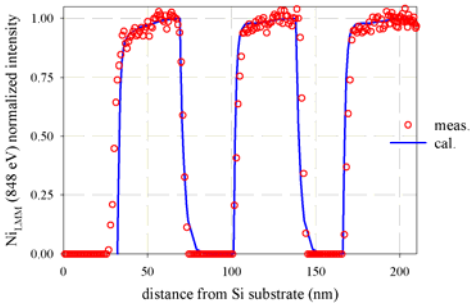

Figure 2 *The measured and calculated normalized intensities for the Ni_{LMM} (848 eV) Auger line.*

The agreement is astonishingly good. It should be also emphasized that the backscattering factor changes even in a depth of 200 nm, and is different in all Ni layers. Thus it is very unlikely that simple analytical model can account for these changes.

FIB mixing

(SLO 7/05 Bilateral contact between Slovenia and Hungary)

Barna Á, Kotis L, Lábár JL, Sulyok A, Menyhárd M, Osvath Z, Tóth AL Zalar A (JSI), Panjan P (JSI)

XTEM studies show (in good agreement with the previous AES results) that the interface mixing of the C/Ni system due to FIB irradiation results in Ni_3C. Ni_3C is a metastable compound. The cross sectional XTEM images, shown in Fig. 1, verified that the C/ Ni_3C interface is really sharp. By the help of the AES depth profiling we could determine (shown in Fig.2) that the number of created Ni_3C molecules depends on the 0.6 power of the fluence. This dependence is similar to that which is expected if the layer forms by usual diffusion or ion mixing.

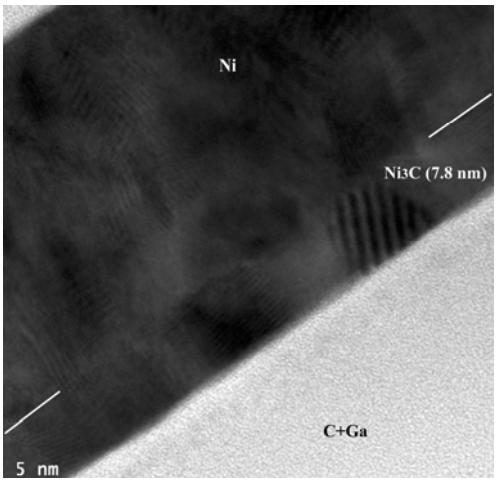

Figure 1 *The XTEM image of the C/Ni sample irradiated by fluence of 400 Ga^+/nm^2.*

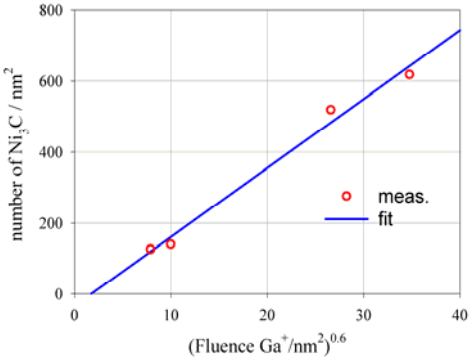

Figure 2 *The amount of Ni_3C formed as a function of Ga+ irradiation.*

Experimental determination of the Surface Excitation Parameter (SEP) by EPES

(PL-15 Project between the Polish and Hungarian Academy of Sciences)

Gergely G, Gurbán S, Menyhárd M, Jablonski A (IPC)

The inelastic losses of a medium energy electron are different in the surface region with respect to the bulk. The $P_{se}(E,\theta)$ surface excitation parameter (SEP) is defined to describe the enhanced energy losses in the surface region. P_{se} might be calculated

theoretically applying various material parameters and formulae derived by various assumptions. We have proposed the derivation of SEP from experimental data using the ratio of the measured and calculated (EPESWIN) elastic peak intensities, since the influences of SEP appear in the elastic current as well. The evaluation presented here uses Goto's experimental data for Si, Ni, Ag, Au and Cu. The best fit of measured and calculated data was utilized for determining the material parameters contained by SEP. Our SEP material parameter results have been published. The SEP corrected IMFP data showed better agreement with calculated TPP-2M. A new procedure, based of utilization of Goto's EPES data was elaborated for quantifying experimental AREPES spectra of Zemek, published in arbitrary units. Reasonable agreement was achieved between measured, SEP corrected and calculated AREPES spectra for Si and Ni.

Nanopatterning on striped Si: the molecular dynamics simulations of ripples

(DAAD-MÖB and OTKA K-68312)

Süle P, Odor G Liedke B (FZD), Heinig K-H (FZD)

The controlled way of surface nanofabrication is still a great challenge of nanoscience although a great deal of efforts have been done in the last decades towards the understanding of processes responsible for the formation of regular patterns.

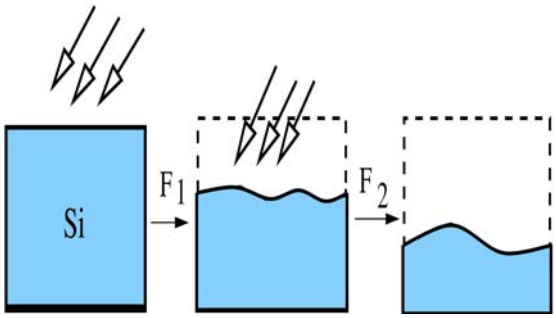

Figure 1 *The schematics of the sputtering induced surface patterning process First few nms of top layers are eroded and sputtered with ion fluence F_1. During this process the surface becomes somewhat roughened and wavy, although smoothening effects are strong. In the next step, ripples develop under the effect of fluence F_2. The assumption $F_1 >> F_2$ allows the simplification of simulated sputtering. The total fluence is F_1+F_2.*

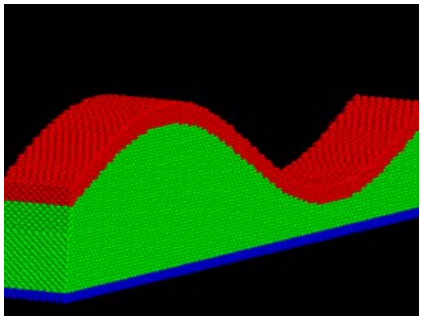

Figure 2 *The snapshot of a prepatterned wavy surface of striped Si(110) with 200 nm wavelength before ion-bombardments. The colored picture is shown with the fixed bottoms and surface region for a steeper wavy system (amplitude h_0= 5 nm).*

Ion-sputtering induced self-organized surface nanopatterning is a hot topic of the last decades because of possible potential application field. Periodic ripple formation on surfaces has been the subject of numerous experimental and theoretical works. The formation of ripples on Si has also been reported. In general, the fundamental understanding of the occurrence of periodic surface features is still lacking. Atomistic computer simulations could be an important ingredient of further modelling of nanopatterning.

One can introduce few simplifications which could help reducing the required simulation effort. Firstly, the large part of ion impacts during ion-sputtering leads to the ion-erosion of the surface. These experiments take a long time (few hours) due to the slow process of the ion-milling depending on the applied fluxes and ion impact angle. Hence, the patterning of the surface is taking place after the erosion of few nm surface layer. Simulations can be started right after this process with some prepatterned surfaces. The preparation of such prepatterned areas could help boosting simulations (see also Fig. 1). After the ion-erosion process with some F_1 fluence, the system surface becomes weakly rough and the topmost layers are amorphized and saturated by vacancies and/or by noble gas atoms. At a certain point the system could go through a phase transition into the ripple phase due to the instability of the ion-frustrated system. This model does not support the occurrence of progressive ripple development during ion-erosion.

Anisotropy driven nanocluster burrowing obtained by molecular dynamics simulations

(OTKA K-68312)

P. Süle

We explore the occurrence of transient nanocluster penetration (burrowing) in various substrates using atomistic simulations at low energy cluster impacts (few eV/atom). We point out that the cluster to substrate atomic mass and size anisotropy plays a significant role in the mass transport: clusters with heavier and smaller atoms burrow into a substrate composed of lighter and larger atoms.

The transient burrowing process is largely insensitive to the strength of cross-interaction (that is proportional to the heat of mixing) and is driven by the atomic mass ratio and lattice mismatch instead of chemical forces. These findings suggest that an anomalous mechanism governs ultrafast cluster sinking. The deep penetration of metallic clusters into metallic substrates could allow the preparation of metallic inclusions and buried nanostructures implanted into the substrate. Beyond the possible technological application of cluster burrowing, the explored new phenomenon could also be interesting in a theoretical point of view. In particular, the understanding of transient cluster mobility in the bulk could contribute to the advance of the emerging new field of anomalous diffusion.

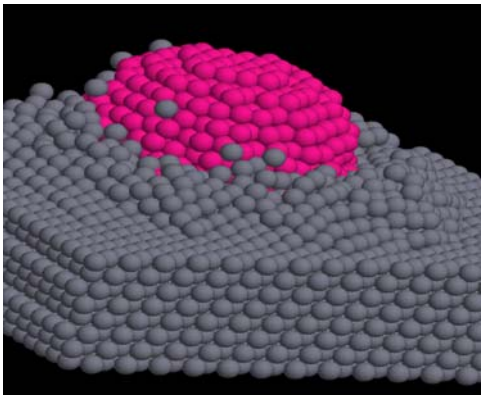

Figure 1 *The snapshot of the simulation cell of the partly burrowed spherical Pt nanocluster in Al at 1.5 ps (1 eV/atom impact energy, ~1000 m/s impact speed).*

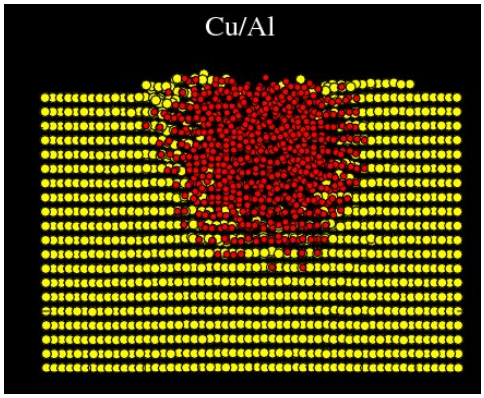

Figure 2 *The cross-sectional view of various deposited burrowing cluster/substrate systems Cu/Al at low impact energy.*

These peculiar results provide new evidences to the new concept that atomic transport could become anomalous in the nanoscale under not yet clearly established conditions. In some of these processes common features are the athermal characteristics (non-Arrhenius atomic transport) on one hand and that the deposit-surface interaction is largely independent of chemical forces on the other hand.

Ceramics and Nanocomposites Department

Head: Csaba Balázsi, Ph.D.,

Research Staff

János Volk, Ph.D.,
Deputy Head of Department

Péter Arató DSc.,
László Bartha, DSc., Professor Emeritus
András Deák, Ph.D.,
István Gaál, CSc.,
Gréta Gergely, Ph.D.,
Ngyuyen Quoc Khanh, Ph.D.,
Sándor Kurunczi, Ph.D.,
István Endre Lukács, Ph.D.,
Judit Pfeifer, CSc.,
Attila L. Tóth, Ph.D.,
László Uray, CSc.,

Technical Staff

János Chalupa, technician
Mihály Hubai, technician
Levente Illés, BSc., engineer
Ferenc Wéber, MSc., engineer

Ph.D. students / Diploma workers

Balázs Fényi, Ph. D. student
Orsolya Koszor, Ph. D. student
Anett Sebestyén, Ph.D student

Gábor Galántai, Diploma worker
Viktória Halász, Diploma worker
Viktória Konrád, Diploma worker
Áron Nagy, Diploma worker
Zoltán Szabó, Diploma worker
Valentin Sóti, Diploma worker
Ádám Wágner, Diploma worker

Silicon Nitride-Based Ceramics and Nanocomposites

(Supported by SVEDNANO, OTKA K63609, MTA-NEI, TéT and János Bolyai Postdoctoral Grant)

Cs. Balázsi, G. Gergely, O. Koszor, B. Fényi, J. Pfeifer, F. Wéber, P. Arató

The range of interest on ceramic nanocomposites is continuously rising, high level of synergism of mechanical, thermal and physical properties is foreseen. In spite of good perspectives their large scale production has not been started till now. This discrepancy is caused by the relative high costs of necessary equipment and by the difficulties of controlling nanotechnologies. Our team elaborated firstly a processing method for composites with silicon nitride matrix and carbon nanotube (CNT) reinforcing phase.

In this year we continued the investigation of relationships between processing parameters, micro and nanostructures and properties of CNT/silicon nitride composites. Experiments also were done where silicon carbide alone or in a combination with CNT served as reinforcing phase. The CNT content varied between 1 and 10 m%, gas pressure sintering or hot isostatic pressing were applied, several heat treatments were tried before or after the sintering. The dependence of phase composition on the atmosphere was highlighted. The study of silicon carbide based composites began, both commercial powders and nanopowders prepared by reaction sintering n in the Institute of Materials and Environmental Chemistry CRC HAS were involved.

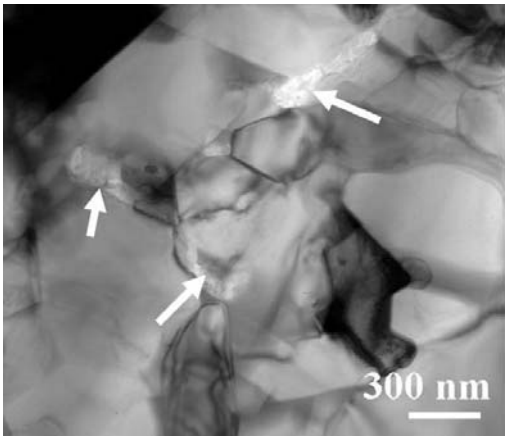

Figure 1 *Cross-section bright field TEM image shows the CNTs located into porosities between β-Si_3N_4 grains.*

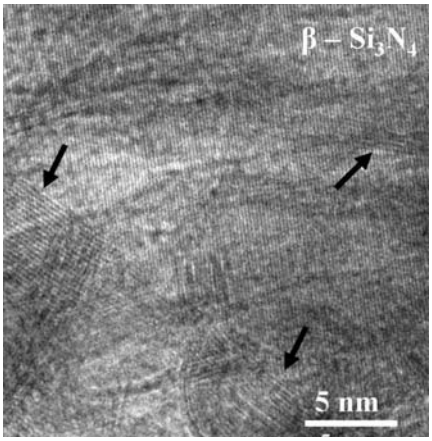

Figure 2 *HREM image shows the silicon nitride-CNTs interfaces.*

Our team worked hard in investigating the spatial distribution of different phases. A large amount of direct observation was carried out by scanning electron microscope (SEM) and transmission electron microscope (TEM). A method was elaborated for

chemical etching the glassy phases revealing the geometry of skeleton. Cross-section bright field TEM and HREM image shows the CNTs located into porosities between β-Si_3N_4 grains and the silicon nitride-CNTs interfaces (Figure 1 and 2).

Characterizing the dispersion of CNTs in ceramic composites by global methods is mandatory in order to understand in detail the structure of these composites. The dispersion of nanotubes in ceramic matrices is usually investigated by scanning electron microscopy of fracture surfaces or transmission electron microscopy of thin slices from the composite. Although these methods are able to give some estimates about the dispersion grade of nanotubes and the typical size of the aggregates the provided information is local and partial. We have chosen small angle neutron scattering (SANS) experiments to observe the global dispersion of CNTs in silicon nitride. The SANS measurements were performed at the cold neutron research facility of the Budapest Neutron Centre.

As can be seen in (Figure 3) two lines with different inclinations can be fitted to the experimental data, the scattering intensities following a power law behaviour in both regions, although with different exponents. For small wave vectors a slope value of -3.8 is found, while for larger wave vector scattering the power law exponent is -3.2.

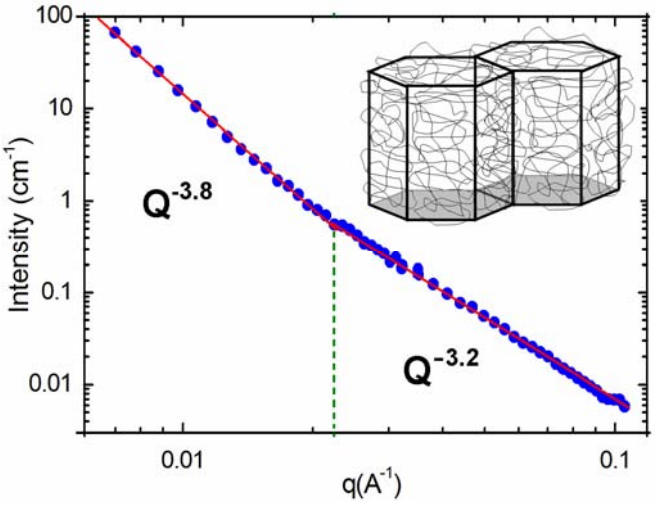

Figure 3
Small angle neutron scattering spectra of Si_3N_4/SWCNT nanocomposite revealing the power law behaviour with decay rates indicating the surface fractal behaviour of the nanotubes dispersed in the ceramic matrix. Inset: schematic structural model of Si_3N_4/SWCNT nanocomposite constructed based on SANS data. The hexahedrons represent the Si_3N_4 crystallites while the entangled curves the nanotubes surrounding them.

These values not only indicate a quantitative difference but also a qualitative one, since they correspond no longer to mass fractals but rather to surface fractals. A natural interpretation of this surface fractal behaviour is that carbon nanotubes are surrounding the β silicon nitride crystallites of the matrix forming entangled networks on the surface of the grain boundaries.

Ceramic composites are frequently characterized by such quantities as phase composition or porosity, which concern the whole body. It is important to emphasize that the value of macroscopic parameters are determined by the micro and nano structure, the mechanical and physical properties can be controlled only by regulating all elements of structure.

The density – four point bending strength curve for samples made with carbon nanotube additives is shown in Figure 4. It is clear that the rate of densification decreased with increasing additive content as in the case of carbon black, graphite and CNT additions. The linear tendency of density-strength relation suggested that the mechanism of densification did not change during sintering because the bond between ceramic phases and CNTs was strong. It is worth to mention that these averaged four point strength values have been obtained for samples realised by gas pressure sintering (GPS). While the mechanical properties are determined by the bonds between neighbouring ceramic particles, electrical conductivity is controlled by the distribution of CNTs. The second stage of HIP treatment increased the density, increased the modulus of elasticity and the strength, at the same time radically decreased the conductivity.

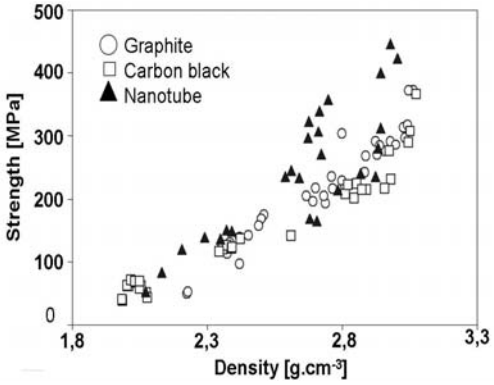

Figure 4 *Mechanical properties of Si_3N_4 based nanocomposites with different carbon addition.*

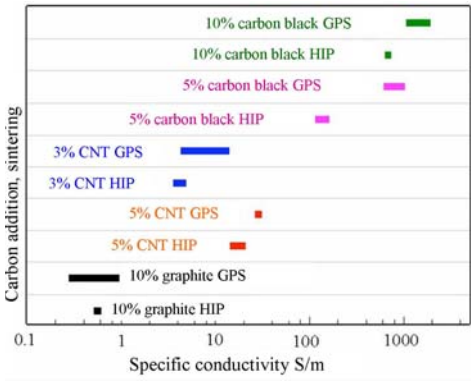

Figure 5 *Electrical properties of Si_3N_4 based nanocomposites with different carbon addition.*

The DC specific conductivity was determined in co-operation with Miskolc University. It was found that 3 wt% CNT is sufficient to alter the transport properties of the HIPed composites. The order of magnitude of electrical conductivity of silicon nitride ceramics is 10^{-11} - 10^{-12} Sm^{-1} while its value in the composite realized by GPS and HIP was as high as 18 Sm^{-1} in the case of CNT additions, at the same time the difference between mechanical properties of ceramic and composite was less than 50%. These data mean that the percolation trough the CNTs network providing the conductivity, while the ceramics are bonded each to the neighbouring particles providing the mechanical strength. In the case of carbon black addition electrical conductivity of 1000 Sm^{-1} have been obtained (Figure 5). It is sure that a composite which is wear resistant, refractory and conductive will be used in a wide region.

Nano hydoxyapatite and polymer based bio-compatible nanocomposites

(Supported by OTKA BIOCER, OTKA-NSF-MTA)

Cs. Balázsi, F. Wéber, G. Gergely, O. Koszor, K. Balázsi, I. E. Lukács, E. Horváth, S. Kurunczi, L. Handa

Over the last several decades, bioceramics have helped improve the quality of life for millions of people. These specially designed materials - polycrystalline aluminum oxide, hydroxyapatite (a mineral of calcium phosphate that is also the major component of vertebrate bone), partially stabilized zirconium oxide, bioactive glass or glass-ceramics, and polyethylene-hydroxyapatite composites - have been successfully used for the repair, reconstruction, and replacement of diseased or damaged parts of the body, especially bone. Hydroxyapatite (HAP) is chemically similar to the mineral component of bones and hard tissues in mammals. It is one of few materials that are classed as bioactive, meaning that it will support bone ingrowth and osseointegration when used in orthopaedic, dental and maxillofacial applications.

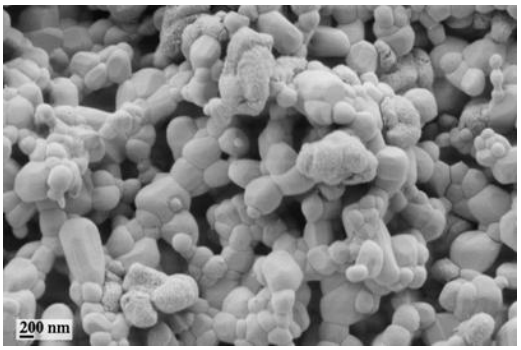

Figure 1 *SEM image of HAP powder*

Hydroxyapatite may be employed in forms such as powders, porous blocks or beads to fill bone defects or voids. These may arise when large sections of bone have had to be removed (e.g. bone cancers) or when bone augmentations are required (e.g maxillofacial reconstructions or dental applications). The bone filler will provide a scaffold and encourage the rapid filling of the void by naturally forming bone and provides an alternative to bone grafts. It will also become part of the bone structure and will reduce healing times compared to the situation, if no bone filler was used. Coatings of hydroxyapatite are often applied to metallic implants (most commonly titanium/titanium alloys and stainless steels) to alter the surface properties. In this manner the body sees hydroxyapatite-type material which it is happy to accept. Without the coating the body would see a foreign body and work in such a way as to isolate it from surrounding tissues. Hydroxyapatite was successfully produced by using recycled eggshell/seashell and phosphoric acid.

Elaboration processes of the HAP has been developed and applications by electrospinning. Our laboratory started to study various kind of ceramic-polymer composites with the new set up purchased by Ceramics and Nanocomposites Department. Electrospinning gave a three dimensional arrangement of polymer micron and nanofibers. In composites prepared in our laboratory HAP nanoparticles were dispersed in a polymer matrix (Figure 2 and 3).

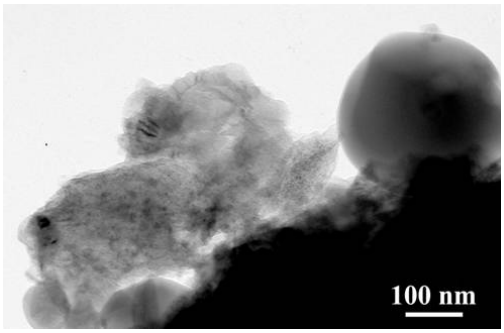

Figure 2 *Nanocystalline bi-modal hydroxyapatite from eggshell.*

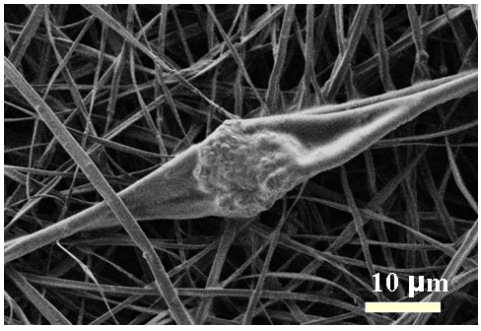

Figure 3 *Fibrous structure of hydroxyapatite-polymer composite.*

Figure 4 *Porous body implant realized by rapid prototyping.*

Figure *5 Replacement of diseased or damaged parts of the bone by using polymer bone fillers together with drugs.*

This structure has high porosity and large specific surface, consequently provides good conditions for biodegradation. In composites prepared in our laboratories hydroxyapatite nanoparticles were dispersed in a polymer matrix (Figure 4 and 5). It is thought that the nanograins may be particular places for the regeneration of bone tissue. Our experiments on the interaction between composite and tissues are continued.

In co-operation with Pannon University we realized body implants e.g. porous blocks as bone fillers for targeted drug delivery applications. The cancerous bone parts were removed and porous bone fillers together with drugs were introduced for remediation.

Tungsten Oxide Functional Ceramics

(MTA-OTKA-NSF)

C. Balázsi, J. Pfeifer, I. Lukács, Z. E. Horváth, A.L. Tóth

Tungsten oxides and oxide hydrates are among the most used materials in electro-, photo- and gasochromic applications. Lately, tungsten oxides are commonly studied for application as sensing layers for hazardous gas detection as well, however their sensing property has not yet fully explored due to a lack of comprehensive knowledge of sensing mechanisms.

The synthesis and deposition of the sensing layer is the most crucial part in the fabrication of a sensor device. In the present study cheap and simple wet processes and colloid chemistry methods have been used for the production of electrochromic and/or sensing tungsten oxide films. The following scheme describes the preparative route to obtain h-WO_3 powder:

$Na_2WO_4.2H_2O$ *(solution)*$\rightarrow$ $H_2WO_4.H_2O$ *(gel)*$\rightarrow$ $WO_3.1/3H_2O$ *(suspension)*$\rightarrow$ $WO_3.1/3H_2O$ *(powder)*$\rightarrow$ h-WO_3 *(powder)*

Gel samples are prepared by HCl precipitation from sodium tungstate solution. The resulted gels are washed and centrifuged 3-5 times. Suspensions of the washed gels are passed to hydrothermal dehydration at autogenous pressure at 125 ºC ± 5 ºC.

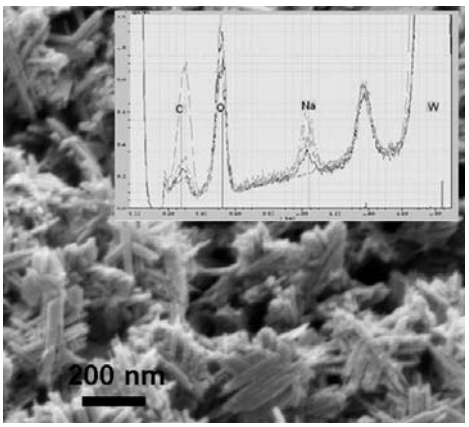

Figure 1 *SEM image of h-WO_3 film, with Na content of the grains determined by EDS in the insert.*

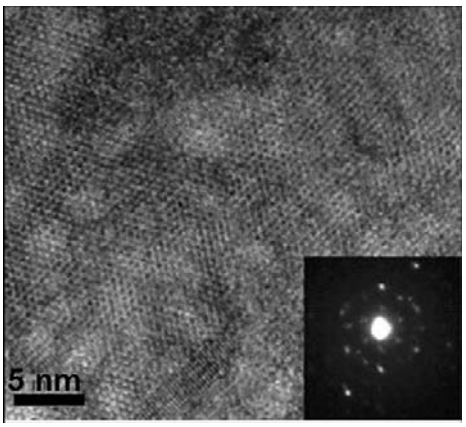

Figure 2 *HREM image (insert: SAED) of h-WO_3 nanorods.*

Products after hydrothermal dehydration are dried at room temperature or used as "as received" suspensions. The crystalline h-WO_3 derivative consists of aggregates (1-2μm) of nanocrystalline rods and platelets with thickness of ~ 20-30 nm.

Responses of the sensors to organic vapors, NH_3 and NO_x gases have been studied by Professor Gouma and Lisheng Wang at the Department of Materials Science & Engineering SUNY, Stony Brook.

Results show, that wet processed tungsten oxide sensors have a wide range of application in hazardous gas detection. The sensitivity of h-WO_3 to NO_x gases at sensing temperature of as low as 150° C is outstanding.

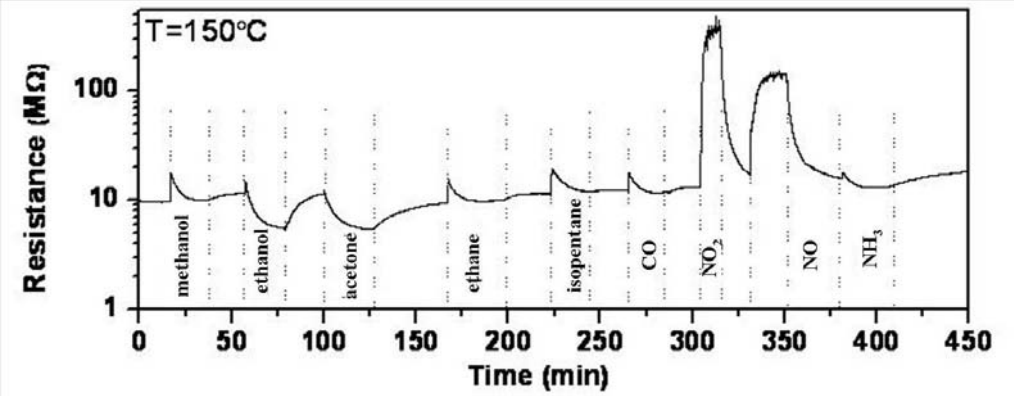

Figure 3 *Responses of h-WO_3 to 1 ppm of different gases at 150 °C.*

150° C as working temperature is promising for the point of view of the application of polymer based targets (polymer micro and nano fibers). Very recently we have been able to incorporate tungstic acid particles into electrospinned polymer fibers, which can be used as fillers in sensing tubes.

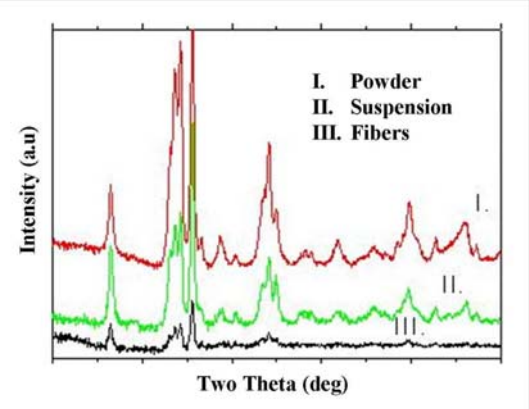

Figure 4 *XRD patterns of tungstic acid in powder, H_2O/acetone/cellulose acetat suspension and fibers produced by electrospinning the suspension*

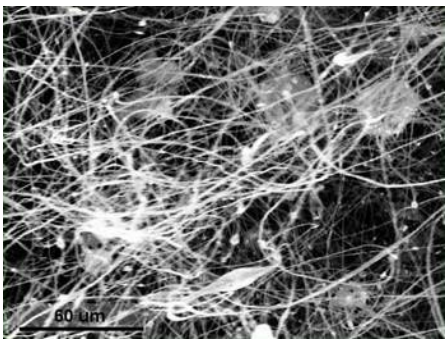

Figure 5 *SEM image of polymer fibers electrospinned from H_2WO_4/H_2O/acetone/CA suspension*

A new approach was introduced when room temperatures detection of hazardous gases is desired, consisting in embedding a low amount of metal decorated (Ag, Au)

carbon nanotubes into the hex-WO_3 matrix (Figure 6). Indeed, the new fabricated hybrid material composites were able to detect as low as 100 ppb of NO_2, with no need to heat the sensors substrates during operation (Figure 7).

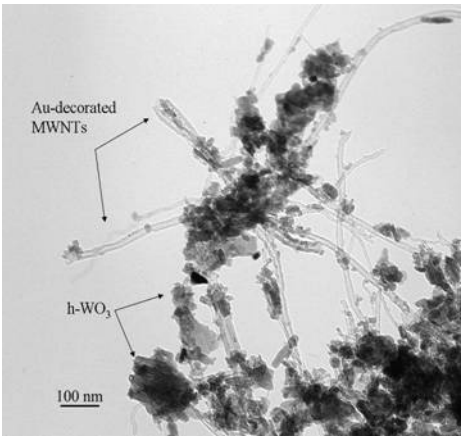

Figure 6 *TEM images of hexagonal WO_3 with Au decorated MWCNTs.*

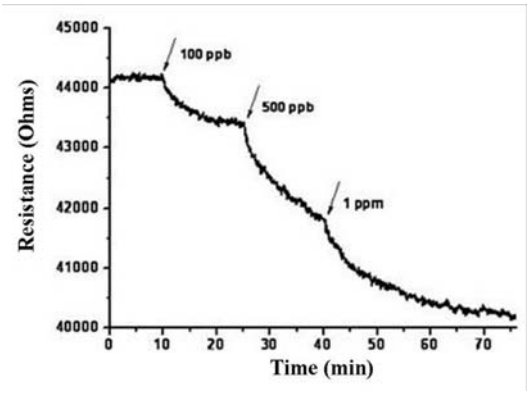

Figure 7 *Resistance of Au-MWCNTs/hex-WO_3 (1/500 wt%) film operated at room temperature.*

The detected concentration level (100 ppb) is very close to the ambient air quality standard for nitrogen dioxide established by the Department of Environment and Natural Resources, USA (i.e. 53 ppb, http://daq.state.nc.us/rules/rules/D0407.pdf), and we think it can be attributed beyond to the nanosize structure to the open channels in the crystals.

Electromechanical characterization of vertically grown ZnO nanorods

(In cooperation with PPKE, Bay-Nano, and NIMS)

J. Volk, G. Galántai, I. E. Lukács, A. L. Tóth

Although the piezoelectric property of ZnO thin films has been exploiting in several applications since the early 1970s, piezoelectric ZnO nanowires came into the focus of interest only recently when Wang et al. demonstrated energy harvesting by ZnO nanowire arrays. The origin of the operation is the internal electric field which is built up between the compressed and tensed side of the bent piezoelectric nanowire (Figure 1). Although the piezoelectric nature of the wires has been demonstrated in nanogenerators as well as in force sensor FET, the mechanism and the attainable efficiency are under debate. In addition, the mechanical quantities published in the literature strongly scatter (Young's modulus in the range of 58-150 GPa) and the size effect is also controversial.

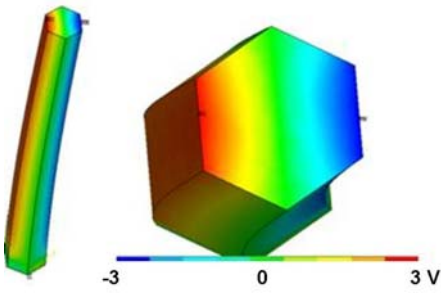

Figure 1 *Electric potential distribution in a curved ZnO nanowire calculated by finite element analysis*

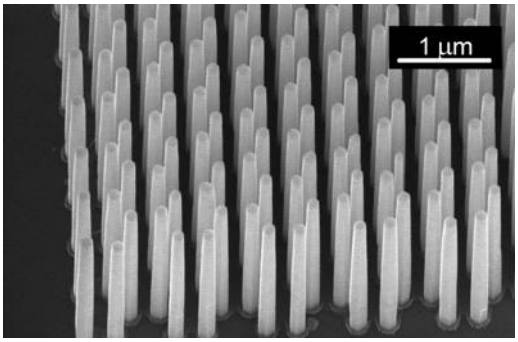

Figure 2 *Scanning electron micrograph on highly ordered ZnO nanowire array*

In our work highly ordered vertical ZnO nanorods were grown by a novel synthesis route using direct writing lithographic method and low temperature (T=80 °C) aqueous chemical growth (Figure 2). The mechanical test, which was carried out by a micromanipulator arm mounted in a scanning electron microscope revealed that the epitaxial nanorods are surprisingly robust (Figure 3).

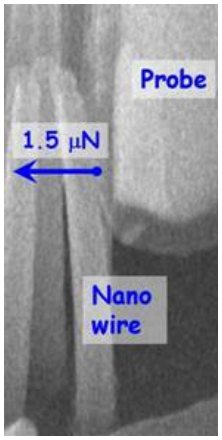

Figure 3 *Mechanical testing of a vertical ZnO nanowire by a micromanipulator tip*

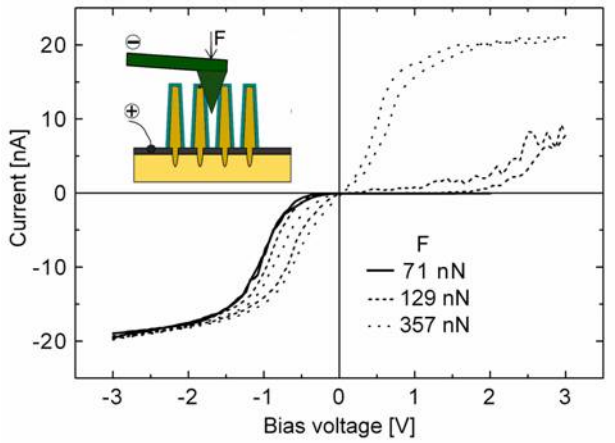

Figure 4 *Current-voltage curves taken by a conductive AFM tip at different bending force values*

In order to determine the bending modulus, at first the spring constant of the manipulator probe was calculated by using finite element calculation (k=1.51 N/m). From the geometry of the nanorod and from the deflection of the probe tip and of the nanorod the bending (Young) modulus can be calculated (Y=202±60 GPa).The effect of the bending condition on the electrical behavior was also investigated by

conductive AFM technique. The experiment was done in Bay-Nano Institute in Miskolc, Hungary by Dr. N. Hegman and Dr. A. Sytcheva. Here, a vertically moving Pt coated AFM tip buckled six neighboring nanorods and current-voltage (I-V) characteristics were taken at different force values. The results showed that the I-V curve drastically changes when the applied force is increased (Figure 4) which can be advantageous for force sensor application. However, in order to describe the behavior correctly and separate the contributions of the different effects such as contact resistance, internal resistance of the nanorod, and piezoelectricity induced Schottky barrier height change, a further systematic investigation is required in the future.

Accurate light wave manipulation by fully engineered zinc oxide nanopillar arrays

J. Volk

Zinc oxide as a wide band gap semiconductor (3.37 eV) having large exciton binding energy (~60 meV) is predestinated to be a key material of the future nano-photonic devices operating in the visible and in the near ultraviolet wavelength region. The enormous progress makes us envision the emergence of all-ZnO integrated devices; however, the essential inter- and intra-chip connections have been still missing.

In our project, we propose an innovative concept in which a vertical ZnO nanopillar array is used for the manipulation of the light wave propagating parallel to the surface in free space. The solution is based on the scattering optical element (SOE) concept which can be regarded as the three dimensional extension of the diffractive optical elements (DOE). However, instead of using a single layer of phase-controlling component, SOEs are based on multiple scattering by a few layers of individual scatterers. The positions of the scatterers are optimized by a powerful combination of

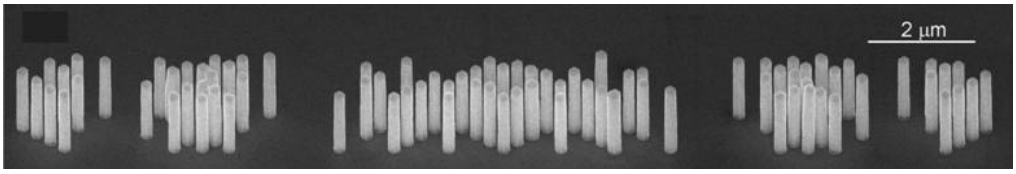

Figure 1 *Perspective view SEM images taken on the homoepitaxial ZnO nanopillar array. The highly uniform prism-shaped vertical nanocrytals are collectively aligned according to the crystal orientation of the wurtzite type ZnO substrate.*

two-dimensional (2D) multiple scattering theory and genetic algorithm. According to the simulations, the inverse designed SOE structures can fulfill different functions such as light focusing, directional light emission, wavelength demultiplexing etc.

In our work which was done in collaboration with Dr. A. Hakansson and Dr. H. T. Miyazaki at NIMS in Japan we demonstrated a nanopillar lens (Figure 1) with a focal distance of 28 μm (Figure 3 and 4) but according to our calculation by using a

different scatterer arrangement a much shorter focal distance (~10 μm) can be easily reached. We believe that the ZnO nanopillar lens can be a promising tool for focusing the light coming from an external source into a specific volume on the chip, which can be either a rectangular or photonic waveguide as well as a ZnO nanowire based photodetector. However, we also expect that the real potential of the method will be utilized when the scatterers not only modulate but also emit the light enabling directionally emitting devices.

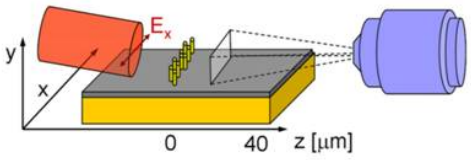

Figure 2 *Schematic illustration of the optical characterization set-up. The laser light coming from left is modulated by the nanorod array and is collected by a moving objective lens at the right side.*

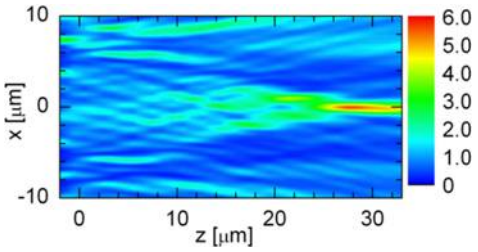

Figure 3 *The y-averaged x-z intensity gain map shows the desired focusing effect at z = 28 μm*

Opening up and X-ray analysis of ultrafine buried BN inclusions in hot rolled steel by combination of FEG-SEM, FIB, and EDX methods

A.L.Tóth [MTA MFA] and E. Dénes [Dunaferr]

Although integral analysis of boron concentration in steel is well established, and even the distribution of the average boron content between solved and precipitated state is also possible, in order to clear the role of boron as hidrogene trap, it is important to develop methods for characterization the structure of the inclusions containg boron.

The TEM based methods are expensive and analyse only a small fraction of the sample, while the conventional SEM analyses the larger precipitations only (due to its rough beam at low energies optimal for light element analysis).

Combining the electropolishing followed by electrolithic thinning (generally used for TEM preparation) and capabilities of the GEMINI column of our LEO1540XB system (100.000x magnification with 1,5 keV electrons, having 50 nm penetration depth) the precipitations could be analysed, but only those which had been stripped off to the surface during polishing (Figure 1)

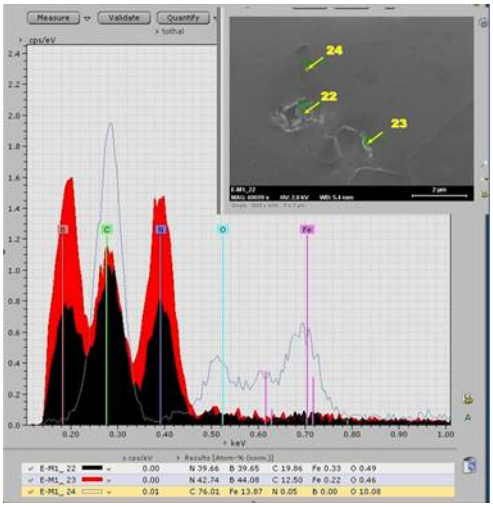

Figure 1 *Nitride and carbide inclusions in cold rolled steel*

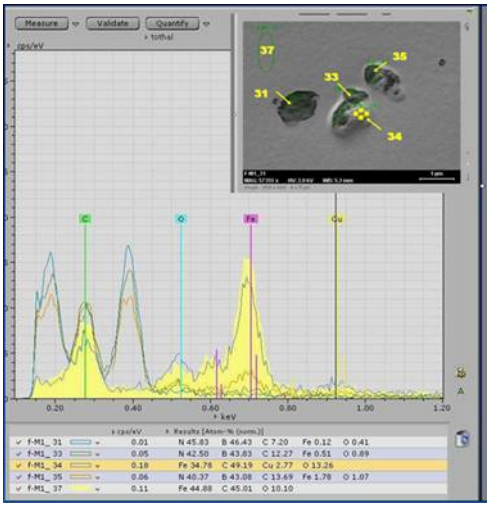

Figure 2 *Nitride and carbide inclusions in hot rolled steel*

In some cases BN precipitates were observed in a shell containing Fe, C and frequently Cu (Figure 2) , but it had to be proven, that it is their native place.

Using the controlled local FIB material removal (Figure 3) from the top of the carbide hills buried nitride inclusions it has been proved, that the boron nitride inclusions are surrounded by carbide shell (Figure 4). During subsequent cold rolling these shells are boken up,and the boron inclusion can act as hidrogen trap.

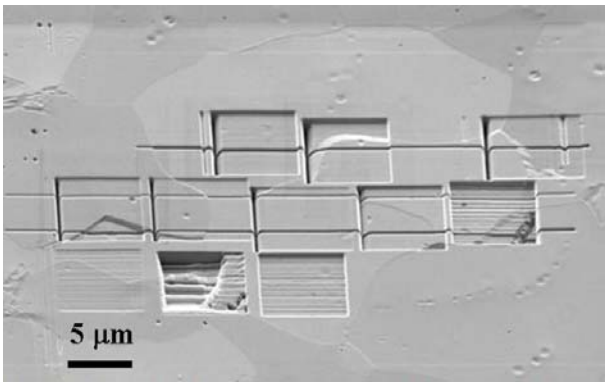

Figure 3 *FIB sputtering from steel grains with different orientation. The sputtering speed is 1,5-5-5 nm/s (rate values: 0.06-0.18 um^3/nC) depending on orientation*

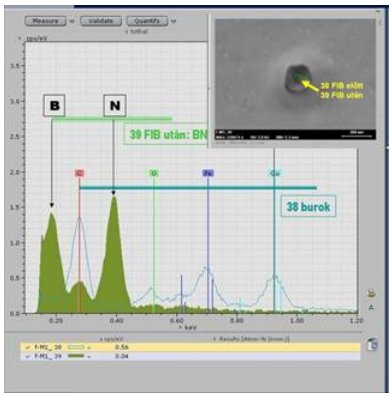

Figure 4 *X ray spectra from the carbide shell and the nitride core of the same inclusion*

The field emission SEM providing high resulution at low energies together with an appropriate EDS system can be used for analysis of ultrafine boride and carbide inclusions in steel, but in order to reveal the complex {nitride core–carbide shell} structures controlled use of extrafine local FIB etching is necessary.

Nanoparticulate LB-films

András Deák

In the laboratory we concentrate on the preparation and investigation of thin films prepared from different nanoparticles. Our main purpose is to prepare thin films with special optical, structural and electrooptical properties. We use for the film preparation amorphous silica (Stöber-silica), and semiconductor (CdTe, CdSe, CdS) nanoparticles in a wide size range.

We are closely cooperating with different groups within the Institute, the country, but also with groups from abroad. We develop new ideas and applications, where films prepared from nanoparticles with a well-defined structure are of significant importance. Some examples of our recent activity:

LB-films prepared from silica nanoparticles for nanosphere lithography.

Interaction of particulate masks and ion-irradiation (shape deformation of the particles).

Preparation of Au nanostructures using nanosphere lithography.

ZnO-based nanostructures.

SiC nanopatterns prepared by nanosphere lithography.

Biofunctionalization of SiC nanowires.

SiO_2/Ge photonic structures using LB-films.

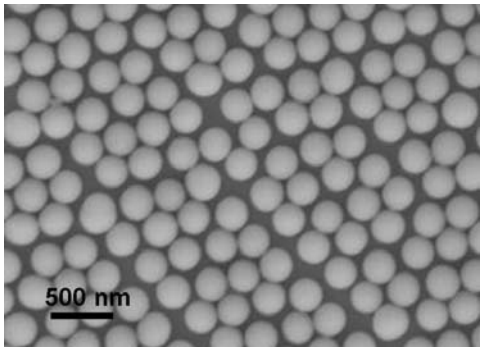

Figure 1 *Langmuir-Blodgett monolayer of ca. 350 nm Stöber-silica nanoparticles.*

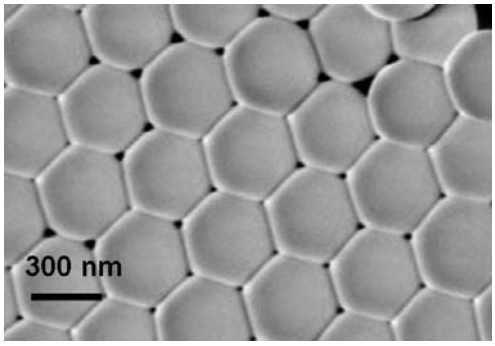

Figure 2 *By post-synthetic modification of the LB-film the openings between the particles can be closed in a controlled way.*

Distinctive test for the delamination propensity of various types grain boundaries and deformation induced boundaries.

I. Gaál , A. L. Tóth, Gy. Radnóczi

Model experiments on bicrystals prove that high and low angle grain boundaries, incidental dislocation boundaries and dense dislocation walls have markedly different delamination propensity. It turned out upon our fractographic studies of lamp grade tungsten (NS tungsten) that the presence of boundaries with different delamination propensity can be also revealed on ultrafine grained tungsten via comparative scanning fractography and transmission electron microscopy.

It is well known that primary recrystallized NS tungsten consists of elongated columnar crystallites lying parallel to the wire axis, and a significant part of the grain boundaries is of low angle type (Figure 1). Longitudinal fracture surfaces reveal on their SEM micrographs (Figure 2) the same type of grain structure, and also the extent of the revealed grain facets are comparable to those on Figure 1, provided that the fracture surfaces were prepared at 77 K by means of the common double notch fracture. Therefore, both high and low angle grain boundaries have similar delaminanation propensity. On the other hand the well known fibrous tensile fracture at the ambient produce delamination contours at the transversal fracture surfaces that are markedly different. Therefore, at the ambient the delamination propensity of the high and low angle grain boundaries should be markedly different in tensile test.

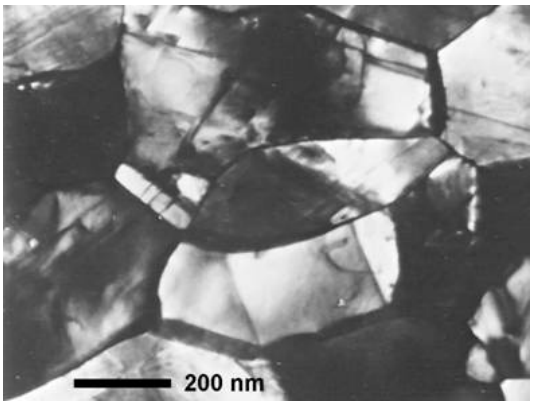

Figure 1 *Transversal transmission electron micrograph taken on primary recrystallized utrafine grained tungsten (sample A)*

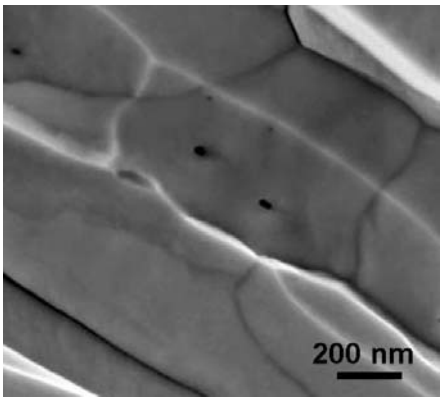

Figure 2 *Longitudinal scanning electron micrograph taken on the suitably prepared longitudinal fracture surface of sample A.*

Modelling of the sintering atmosphere in spark plasma sintering

I. Gaál

Spark plasma sintering (SPS) is a variant of hot pressing applying very rapid heating rates due to heating of graphite die and punch through pulsed low voltage high density direct electric current. Recently, extensive efforts were made towards investigation and development of spark plasma sintering (SPS) as a promising technique for rapid consolidation of a great variety of granular ceramics, semiconductors and metallic systems at relatively low temperatures resulting in nearly full density ultrafine grained or nanocrystalline materials. However, a significant gap exists between the impressive technological and fabrication achievements to the fundamental understanding of the SPS mechanisms. This gap is due to the complexity of the thermal, electrical and mechanical processes that may be involved during the SPS.

The chemistry of the sintering atmosphere inside the graphite die attained surprisingly little attention in the modelling of SPS, although its major effect on the densification is well documented in the conventional consolidation processes of oxide systems. We are aware of only one attempt for the thermochemical modelling of the die atmosphere effects on SPS. The analysed oxide was TiO_2. (Quack D.N. et al J. Am. Ceram. Soc. 91 (2008) 970-974

We modelled the TaC formation in the SPS sintering of Ta (Angerer P. et al. (Int. J. Refr. & Hard Materials 26 (2008) 312-318) by means of the graphite-oxygen-tantalum transport reactions inside the graphite set up by taking into account also the published kinetic data of the oxygen-graphite reactions. The modelling was based on the theoretical frame work of the gas transport reactions in the halogen lamps. (The secondary effect of the vacuum chamber was also analysed.)

First steps toward inexpensive ZnO nanowire based biosensors

N.Q.Khánh, J.Volk, S.Kurunczi, A.Deák, A.Tóth, I.Lukács, and Á.Németh

ZnO as a biocompatible, wide band gap semiconductor is a very promising candidate material for biosensor application. One of its advantages is the ability of ZnO nanostructures to grow by such a simple, low temperature, economical method like a wet chemical technique. The low temperature applied in this method ensures a wide range of substrates can be used including even a plastic one. For the realization of an inexpensive ZnO nanowire based biosensor, work concerning ZnO nanostructures growth by wet chemical technique, as well as immobilization of protein on different ZnO face has been carried out in our laboratory.

From ZnO nanorod to nanowire by wet chemical growth: Because the single crystalline ZnO substrates are rather expensive, Si wafers covered with RF sputtered

ZnO have been used as substrate for growth, which has a textural structure perpendicular to the substrate surface as revealed by X ray diffraction.

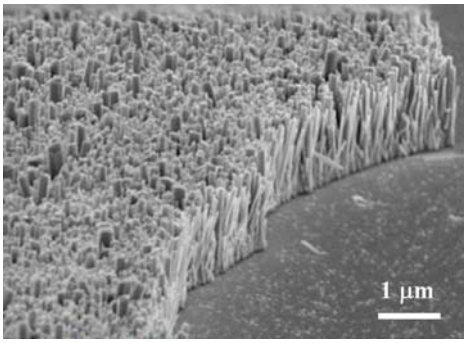

Figure 1 *ZnO nanorods grown on sputtered ZnO substrate in aqueous zinc nitrate/ hexamethylenetetramine (HMT) solution*

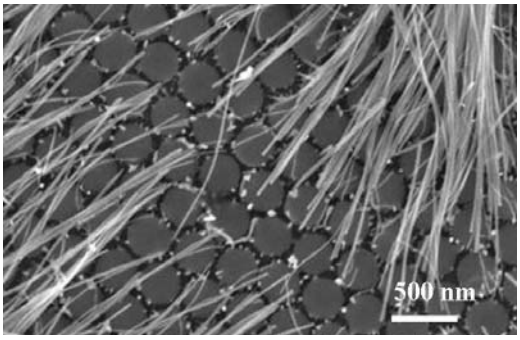

Figure 2 *ZnO nanowires grown on ZnO substrate covered with LB silica colloid film in aqueous zinc nitrate/ hexamethylene-tetramine (HMT) solution*

Growth in aqueous zinc nitrate/ hexamethylenetetramine (HMT) solution produced nanorods with low length/diameter aspect ratio. The thickness of the rods varies widely in 50-200 nm range. Increasing growth time with and without solution freshening both results in longer nanorods (Figure 1). Covering the substrate surface with a LB silica colloid film, very thin (~30 nm) ZnO nanowires with high aspect ratio can be archieved (Figure 2). The role of the surface film in nanowire growth is stil not clear and is to be the target of further investigation.

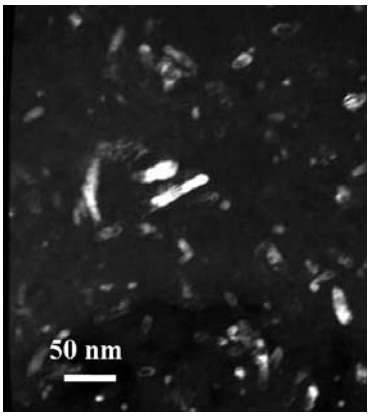

Figure 3 *Dark field TEM image of the nanocrystalline particles synthesized by hydrolysis of zinc acetate.*

Synthesis of ZnO nanocrystalline seeds: For sensors using nanowires in *lateral arrangement* which is technically more desirable, the substrate with sputtered ZnO on top is not suitable, because of the vertical texture structure. Indeed, we could hardly observe any side growth at the edge of the samples. For this reason, the growth of a ZnO nanowire should be performed in two steps: first, growth of free standing nano crystalline ZnO seed, and second, lateral growth of nanowire using these seeds. The ZnO particles available by using aqueous Zinc nitrate/HMT solution are rather thick (about 1 μm) rhombus-like rods. Hydrolyzis of zinc acetate in the presence of potassiumhydroxide gave more aceptable nanocrystalline seeds (see Figure 3). However, the nanocrytalline particles have to be purified from an undesired material, probablly double layered zinc acetate.

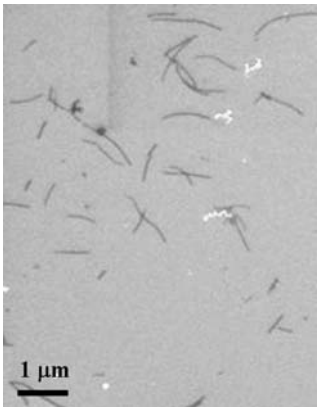

Figure 4 *Proteins bound on (0001) ZnO surface*

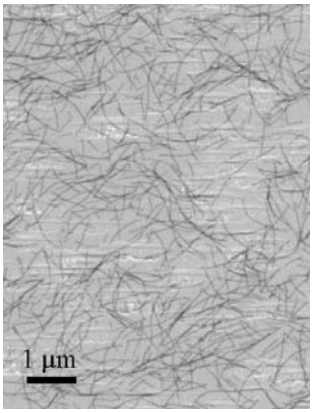

Figure 5 *Protein bound on (0-100) ZnO surface*

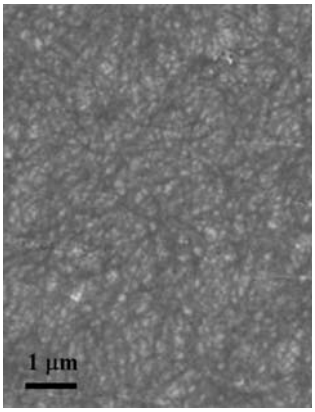

Figure 6 *Protein bound on silanized (0-100) ZnO surface*

Immobilization of proteins on ZnO surface: Though ZnO is known as biocompatible material, we have found that the bonding of the protein to ZnO depends on the face of ZnO crystal and can be greatly affected by the surface treatment. From a point of view of protein immobilization, (11-20) or (1-100) crystal faces are more favourable compared to (0001) face (Figure 4 and 5). Silanization also can enhance significantly the efficiency of the immobilization process (Figure 6).

Biosensors and biocompatible surfaces

S. Kurunczi, P. Petrik, Cs. Balázsi, F. Vonderviszt, I. Bársony

The new field of research has been launched out at the Institute (MFA) with the aim at combining the selectivity of protein receptors and the sensitivity of optical detection. The new “bio-nano-opto” laboratory has been set in order to immobilize the protein receptors on sensing surfaces. Flagella are the locomotive organelles of bacteria. Flagellin, the subunit protein of bacterial flagellar filaments, is a protein polymerizable to form long filaments. The bio-concept in this project is to engineer the central portion of flagellin to give it receptor functionality and/or to give it surface binding functionality (University of Pannonia, Veszprem, Prof. Vonderviszt). These filamentous receptor structures may serve as basic recognition units for biosensors and simple diagnostic kits. Optical sensing methods being developed at the MFA will serve as sensitive readout platforms for biosensors.

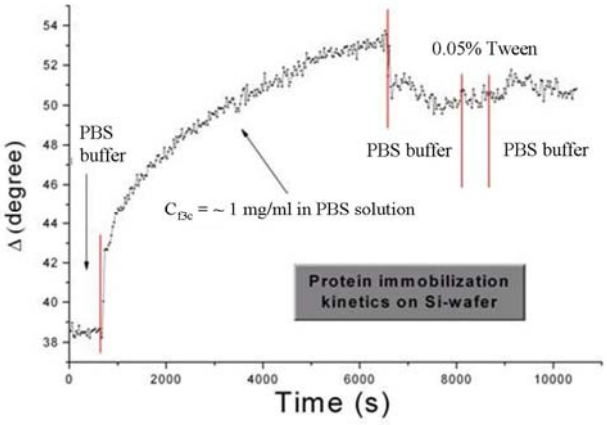

Figure 1
In Situ ellipsometric sensogram taking at 600 nm wavelenght with a 5 ml flow-cell (recorded with the Sopra ESG4 ellipsometer)

In this project we focus on the immobilization of flagellar filaments. Immobilization chemistry is based on silanization and glutaraldehyde cross-linking. The optimization of the procedure is carried out with in situ ellipsometry.

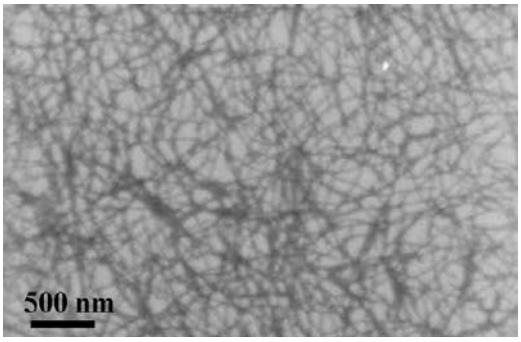

Figure 2 *Scanning electron microscope image from the immobilized protein layer.*

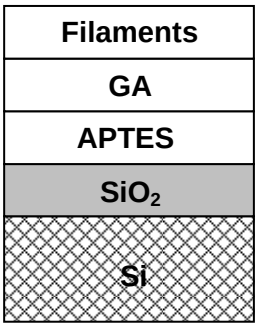

Figure 3 *Structure of the protein layer immobilized on the silicon wafer: Filaments ~ 10nm, GA ~ 1 nm, APTES ~ 1 nm, SiO2 ~ 20 nm*

Improvement of the bio-ellipsometry will be carried out with a new design of flow cell (with smaller volume). The work will be extended to study the biocompatibility of different hydroxyapatite surfaces in situ. Currently we are working on the preparation of thin hydroxyapatite layers which can be further examined in situ bio-ellipsometry.

Complex Systems Department

Head: György SZABÓ, D.Sc., scientific advisor

Research Staff

István BORSOS
Imre EÖRDÖGH
Zoltán JUHÁSZ, Ph.D.
Levente MOLDVAI, engineer
Géza ÓDOR, D.Sc., scientific advisor
Krisztina SZAKOLCZAI
Károly SZÁSZ, engineer
Attila SZOLNOKI, Ph.D.

Ph.D. students / Diploma workers

Jeromos VUKOV, Ph.D. student
Attila ZÖLDE-FEJÉR, Ph.D. student

Technical Staff

Andrea CSALÓTZKYNÉ BOLGÁR, computer programmer

The staff of this department is composed of theoretical physicists, studying different pattern formation phenomena for a wide scale of models, and engineers developing instruments and software based on adapting controls, data and/or image processing. Utilizing the experience in the latter topics we have been studying and comparing the melody structure of folk songs collected for more than 20 nations.

We have a long tradition in the investigation of atomic ordering processes using both analytical and numerical methods. In the last decade the techniques of non-equilibrium statistical physics were adapted to study evolutionary games. This means that instead of many interacting particles we can study communities of players representing a wide scale of biological and economical objects like bacteria, animals, humans, companies, etc.

In the subsequent two sections we detail some interesting results achieved in the field of evolutionary Prisoner's Dilemma games and computer simulations of the formation of nanoscale ripple and dot patterns due to the self-organizing process driven by ion implantation.

Self-organization of nanostructures: computer simulations of pattern formation and scaling

(DAAD-MÖB, Grant Nos. D/07/00302, 37-3/2008)

G. Ódor, B. Liedke (FZD), K.-H. Heinig (FZD), P. Süle, N. Satoshi (FZD)

In nanotechnologies like nanoelectronics, nanophotonics, and plasmonics large-area nanopatterns are needed, which can be fabricated today only by expensive techniques, e.g. electron beam lithography or direct writing with electron and ion beams (top-down-approach). Usually large areas of periodically pattern surfaces are needed (as for photonic crystals or optical metamaterials), which can be alternatively synthesized by cost-efficient self-organization processes (bottom-up approach).

In the framework of the DFG-project HE2137/4-1 within the German-wide DFG-researcher-group 845 the German applicant will study from 8/2007 – 7/2010 how large-area-ordered nanoscale ripple and dot pattern can be produced by self-organization driven by ion irradiation. This self-organization process is fully compatible with standard microelectronics technologies, it is cost-efficient and it can lead to very long-range order in the surface pattern. On the other hand, the evolution of the surface pattern (ripples, dots, alignment of the ripples and the 2D lattice structure of the nanodots) depends sensitive on the process parameter like angle of the ion impact and temperature of the sample. With respect of the parameters listed above "phase diagrams of ordering states" with sharp "phase transitions" have been found experimentally.

Furthermore, for the ordering states a scaling of the surface undulation height and its wavelength as a function of time or irradiation flux have been discovered. Although many sophisticated models (Bradley-Harper with extensions) have been developed, the description and understanding of the "ordering phase diagrams" and scaling behaviour is unsatisfying so far. The first simple atomistic computer simulations are just appearing in international journals.

As the first step in this project we have showed that a 2+1 dimensional discrete surface growth model exhibiting Kardar-Parisi-Zhang (KPZ) equation scaling can be mapped onto two dimensional reaction-diffusion model of directed dimers (Fig. 1). In case of KPZ height anisotropy the dimers follow driven diffusive motion.

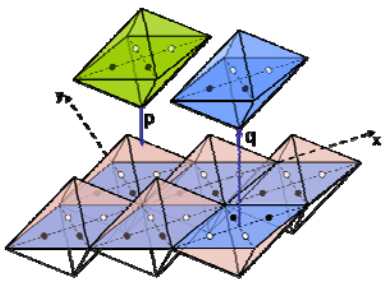

Figure 1
*Mapping of the 2+1 dimensional surface growth onto the 2d particle model (**bullets**). Surface attachment (with probability p) and detachment (with probability q) corresponds to Kawasaki exchanges of particles, or to anisotropic **diffusion of dimers** in the bisectrix direction of the x and y axes. The crossing points of dashed lines show the base sub-lattice to be updated.*

We have confirmed by numerical simulations that the scaling exponents of the dimer model are in agreement with those of the 2+1 dimensional KPZ class. The straight line motion of dimers in the two dimensional space is very similar to the motion of particles of the asymmetric exclusion (ASEP) process. The difference is that since the dimers are extended objects, their motion is slowed down by the dimer particle exclusion and the sub-lattice update as compared to the single particles of the ASEP. As a consequence their motion is described by somewhat larger dynamical exponent ($z \cong 1.64$) than that of the ASEP ($z = 3/2$), so the change of z(d) seems to be a purely topological phenomena in KPZ. This provides a better understanding of the relation of universality classes of surface classes to those of the reaction-diffusion models.

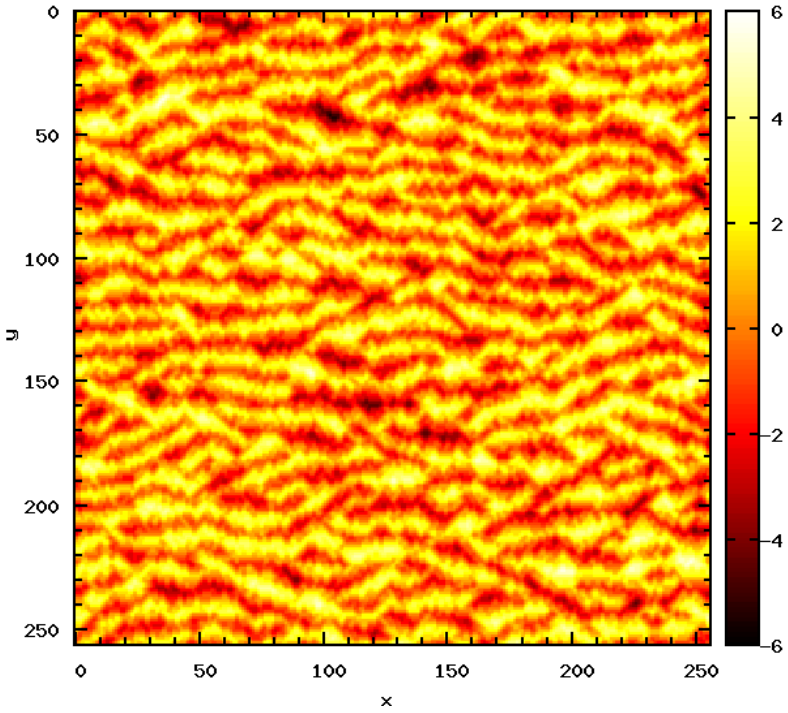

Figure 2 *Ripples (see height scale) generated by a competing smoothening KPZ and a roughening, anisotropic Mullins type of surface diffusion at 10 KMCS. The simulations are performed by the Octahedron/dimer model. The pattern exhibits roughening as time evolves such that the wavelength increases. This corresponds to stripe roughening in the underlying driven diffusive dimer model.*

Interestingly the x/y symmetric surface dynamics maps onto a strongly anisotropic reaction-diffusion model. This mapping opens up the possibility of analysing the KPZ class via reaction-diffusion models and effective simulations. Furthermore, by adding competing, surface diffusion to the KPZ dot and ripple formation is also possible (Fig. 2).

ACTIVITIES

MFA Seminar Talks

06 February 2008	**Dr. Ádám Gali** (Budapest University of Technology and Economics, Budapest, Hungary) *Biological sensing with semiconductor surfaces and nanostructures (in Hungarian)*
13 February 2008	**Dr. Péter Petrik** (MTA MFA, Budapest, Hungary) *Investigation of nanocrystalline, biological, photonic, and ion implanted structures with ellipsometry (in Hungarian)*
19 March 2008	**Dr. Róbert Horváth** (University of Cranfield, Cranfield, UK) *Optical waveguide sensors and their application in nanotechnology (in Hungarian)*
26 March 2008	**Dr. Gábor Kósa** (Swiss Federal Institute of Technology, ETH, Zurich, Switzerland) *Swimming micro robots for medical applications*
04 April 2008	**Dr. Zsolt Czigány** (MTA MFA, Budapest, Hungary) *The formation and properties of fullerene-like CN_x structures (in Hungarian)*
16 April 2008	**Prof. Judit Budai** (University of Szeged, Szeged, Hungary) *Preparation of carbon layers with laser deposition and their investigation with ellipsometry (in Hungarian)*
23 April 2008	**Anita Pongrácz** (MTA MFA, Budapest, Hungary) *A report on the activity at the Microelectronics Laboratory of the University of California, Berkeley (in Hungarian)*
30 April 2008	**Krisztián Kordás** (University of Oulu, Oulu, Finland) *Synthesis and selected application of carbon nanotubes*
14 May 2008	**Péter Basa** (MTA MFA, Budapest, Hungary) *Semiconductor nanocrystals in dielectrics for memory purposes (in Hungarian)*

14 May 2008	**Dr. Sándor Kurunczi** (MTA MFA, Budapest, Hungary) *Investigation of the optical properties of protein layers for biosensorics applications (in Hungarian)*
21 May 2008	**Dr. Karl-Heinz Heinig** (Forschungszentrum Dresden-Rossendorf FZD, Germany) *Old physics for modern nanotechnologies – studies of nano-scale ordering by simulations and experiments*
04 June 2008	**Dr. Márta Pardavi** (The George Washington University, Washington DC, USA) *The stability of 2D ordered magnetic nano-systems (in Hungarian)*
11 June 2008	**Dr. László Dobos** (MTA MFA, Budapest, Hungary) *Investigation of contacts formed to III-nitride group semiconductors (in Hungarian)*
18 June 2008	**Dr. Zoltán Juhász** (MTA MFA, Budapest, Hungary) *Analysis of the relationship between Eurasian and Hungarian folk music using self-organizing maps (in Hungarian)*
25 June 2008	**Dr. István E. Lukács** (MTA MFA, Budapest, Hungary) *Electron beam litography at MFA (in Hungarian)*
25 July 2008	**Prof. Mikio Takai** (Osaka University, Osaka, Japan) *Visualization of three dimensional nanostructures by time-of-flight RBS using nuclear nanoprobe*
26 August 2008	**Dr. Bernard Gruzza** (Blaise Pascal University, Clermont-Ferrand, France) *Study of the InN/InP and GaN/GaAs structures by electron spectroscopies*
22 September 2008	**Dr. Joanna R. Groza** (University of California, Davis, USA) *Field Activated Sintering Technique (FAST) – electrical current effects in materials processing (challenges and opportunities)*
05 November 2008	**Dr. Csaba Balázsi** (MTA MFA, Budapest, Hungary) *Electrospinning at MFA (in Hungarian)*

11 November 2008 **Dr. András Vladár**
(National Institute of Standards and Technology, NIST)
The metrologic aspects of scanning electron microscopy on the nanometer range

12 November 2008 **Bartosz Liedke**
(Forschungszentrum Dresden-Rossendorf FZD, Germany)
Ion bombardment of solids – unified simulation of damage formation and thermally activated relaxation

12 November 2008 **Dr. István Gaál**
(MTA MFA, Budapest, Hungary)
Fuel cells (in Hungarian)

13 November 2008 **Prof. Christina Scheu**
(University of Munich, Munich, Germany)
Introduction to electron energy loss spectroscopy
Application of electron energy loss spectroscopy in materials science

14 November 2008 **Dr. Peter Nellist**
(University of Oxford, Oxford, UK)
Atomic resolution and three-dimensional imaging and analysis of materials: The impact of aberration corrected scanning transmission electron microscopy

21 November 2008 **Ivan Blum**
(University of Marseille, Marseille, France)
Diffusion of dopants in nickel silicides for microelectronics applications

26 November 2008 **Csaba Major**
(MTA MFA, Budapest, Hungary)
Investigation of ZnO layers using wide angle ellipsometry (in Hungarian)

05 December 2008 **Dr. András Deák**
(MTA MFA, Budapest, Hungary)
Preparation of nanoparticulate thin film structures with Langmuir-Blodgett technique (in Hungarian)

05 December 2008 **Dr. Zsolt Zolnai**
(MTA MFA, Budapest, Hungary)
Shape transformation of micro and nanostructures induced by ion irradiation (in Hungarian)

R & D partners / International Cooperation

Bálint Zsolt
Natural History Museum, Budapest, Hungary

Bergmann, Erich
HES-SO, Geneva, Switzerland

Berthier, Serge
University Pierre et Marie Curie, Paris, France

Calderon Moreno, Jose
Department of Applied Physics, EPSC and Center for Research in NanoEngineering, Universitat Politècnica de Catalunya, Barcelona, Spain

Christiansen, Silke
Institute of Photonic Technology, Jena, Germany

Dub, Sergey
Institute for Superhard Materials, National Academy of Sciences - Kyiv, Ukraine

Dusza, Ján
Department of Structural Ceramics, Institute of Materials Research, Kosice, Slovakia

Gago, Raul
Center of Microanalysis of Materials of Autonomic University of Madrid, Madrid, Spain

Gouma, Perena
Department of Materials Science and Engineering, State University of New York, Stony Brook, USA

Grobert, Nicole
University of Oxford, Oxford, United Kingdom

Gyékenyesi, John
NASA Glenn Research Center, Cleveland, Ohio, USA

Hampshire, Stuart
Materials Ireland Research Institute, Limerick University, Limerick, Ireland

Herrmann, Mathias
Fraunhofer Institut, Technical Universtity of Dresden, Dresden, Germany

Horvath Ákos
Atomic Energy Research Institute, Hungarian Academy of Sciences, Budapest, Hungary

Hultman, Lars
Thin Film Physics department of Linköping University, Linköpimg, Sweden

Ingram, Abigail
Natural History Museum, London, United Kingdom

Ionescu, Rádu
Department of Electronic Engineering, Universitat Rovira i Virgili , Tarragona, Spain

Jablonski, Alex
Institute of Chemical Physics, Polish Academy of Sciences, Warsawa, Poland

Karl-Heinz Heinig
Institut für Ionenstrahlphysik & Materialforschung, Forschungszentrum Dresden-Rossendorf, Germany

Kasztovszky Zsolt
Department of Nuclear Research, Institute of Isotopes, Budapest, Hungary

Katalin Kamarás
Research Institute for solid State Physics and Optics, Budapest, Hungary

Kern, Klaus
Max Planck Institute for Solid State Physics, Stuttgart, Germany

Kiricsi Imre
Department of Applied and Environmental Chemistry, University of Szeged, Szeged, Hungary

Kiricsi Imre
Applied Chemistry Department, József Attila University, Szeged, Hungary

Kulcsár Sándor
Accusealed Ltd., Budapest, Hungary

Kuznetsov, Vladimir
Boreskov Institute of Catalysis, Novosibirsk, Russia

Lafait, Jacques
Institute de Nanosciences de Paris, Paris, France

Lambin, Philippe
Facultés Universitaires Notre-Dame de la Paix, Namur, Belgium

Langer, Robert
Picogiga International, Grenoble, France

Liedtke, Volker
Austrian Research Centers, Seibersdorf, Austria

Malherbe, Johan
University of Pretoria, Pretoria, South-Africa

Marosné Berkes Mária
Department of Mechanical Engineering, University of Miskolc, Miskolc, Hungary

Matjaz Perc
University of Maribor, Maribor, Slovenia

Maximenko, Sergey
Institute for Nuclear Problems, Belarus State University, Minsk, Belarus

Okotrub, Aleksandr
Nikolaev Institute of Inorganic Chemistry, Novosibirsk, Russia

Padture, Nitin
Department of Materials Science and Engineering, Ohio State University, Ohio, USA

Parker, Andrew
Natural History Museum, London, United Kingdom

Pischow, Kaj
Savcor Ltd., Mikkeli, Finland

Poisson, Marie-Antoinette
Alcatel-Thales III-Vlab, Marcoussis, France

Shen, Zhijan
Arrhenius Laboratory, Stockholm University, Stockholm, Sweden

Shikimaka, Olga
Institute of Applied Physics, Moldavian Acadymy of Sciences, Kisinyov, Moldova

Skorupa, Wolfgang
Forschungszentrum Dresden-Rossendorf, Dresden, Germany

Stoemenos, John
Aristotle University of Thessaloniki, Thessaloniki, Greece

Surján Péter
Roland Eötvös University, Budapest, Hungary

Tekin, Adnan
High Technical Ceramics and Composites Research Center, Istanbul, Turkey

Vigneron, Jean Paul
Facultés Universitaires Notre-Dame de la Paix, Namur, Belgium

Voelskow, Mathias
Forschungszentrum Dresden-Rossendorf, Dresden, Germany

Zalar, Anton
Josef Stephan Institute, Ljubljana, Slovenia

Zayim Ozkan, Esra
Physical Institute, Istanbul Technical University, Istanbul, Turkey

Zhuravlev, Konstantin
Institute of Semiconductor Physics, Novosibirsk, Russia

Visitors

Attolini, Giovanni
CNR-IMEM Institute, Parma, Italy

Bilichuk, Sergei
Academy of Sciences of Ukraine, Ukraine

Ceniga, Ladislav
Microstructure Engineering of Steels, Institute of Materials Research, Kosice, Slovakia

Chae, Chang-Hoon
Department of Oral and Maxillofacial Surgery, Kangdong, Sacred Heart Hospital, Hallym University, Seoul, Korea.

Chernozatonskii, Leonid A.
Institute of Biochemical Physics, Russian Academy of Sciences, Moscow, Russia

Darabont Sándor
Babes-Bolyai University, Cluj, Romania

Dmitruk, N. L.
Physics Institute, Kyiv, Ukraine

Fedkovic, Yuri
Academy of Sciences of Ukraine, Ukraine

Figielski, Tadeus
Polish Academy of Sciences, Warsaw, Poland

Fleischer, Maximillian
Siemens Corporate Technology, Munich, Germany

Gkogos, Georgios
Technological Institute of Crete, Crete, Greece

Groza, Joana
Chemical Engineering and Material Science Department, University of California, Davis, USA

Gruzza, Bernard
Blaise Pascal University, Clermont-Ferrand, France

Hegedűsová, Lucia
Department of Structural Ceramics, Institute of Materials Research, Kosice, Slovakia

Horley, Petro
Academy of Sciences of Ukraine, Ukraine

Hubik, Pavel
Institute of Physics, Czech Acad. Sci., Prague, Czech Republic

Hübner, Christof
Fraunhofer Institute for Chemical Technology ICT, Pfinztal, Germany

Jae-Hoe, Jeon
Materials Science Institute of Korea, Korea

Jang, William
Industrial Technology Research Institute (ITRI), Taiwan

Kechlibarov, T
National Academy of Bulgaria

Khosravi, Esmaeil
Amirkabir University, Tehran, Iran

Kim, Seung Eon
Materials Science Institute of Korea, Korea

Kishi, Teruo
Institute for Materials Science, Tsukuba, Japan

Kolev, Spas
University of Melbourne, Melbourne, Australia

Koós Antal
University of Oxford, Oxford, United Kingdom

Kósa, Gábor
ETH Ltd., Zurich, Switzerland

Krueger, Andreas
SUSS MicroTec Lithography GmbH, Germany

Kumar, A.
Institute of Physics, Indian Institute of Science, Bangalore, India

Lashkarev, Georgii
Academy of Sciences of Ukraine, Ukraine

Lazarov, Vlado
University of Oxford, Oxford, UK

Lences, Zoltan
Slovak Academy of Sciences, Bratislava, Slovakia

Ling, Welkin
Industrial Technology Research Institute, Taipei Economic and Culture Office, Taipei

Lobotka, Peter
Department of Superlattice, Institute of Electrical Engineering, Bratislava, Slovakia

Maggs, Terry
SUSS MicroTec Lithography GmbH, Germany

Mamykin, S.
Physics Institute, Kyiv, Ukraine

Michely, Thomas
University of Köln, Köln, Germany

Park, Jun -Woo
Department of Oral and Maxillofacial Surgery, Kangdong, Sacred Heart Hospital, Hallym University, Seoul, Korea.

Pavlova, T
National Academy of Bulgaria

Rehm, Wolfgang
Technische Hochschule, Munich, Germany

Rizeakos, Georgios
Technological Institute of Crete, Crete, Greece

Sangunni, K. S.
Institute of Physics, Indian Institute of Science, Bangalore, India

Sajgalik, Pavol
Slovak Academy of Sciences, Bratislava, Slovakia

Schneider, Matthias
SUSS MicroTec Lithography GmbH, Germany

Sen-Horn Yen
Sun Yat- Sen University, Kaoshiunk, Taiwan

Stolz, Wolfgang
University of Marburg, Marburg, Germany

Sylvestre, Alain
Grenoble Génie, Electrique Research Center, CNRS, France

Takai, Mikio
Osaka University, Osaka, Japan

Tien Dean, Norman
Case Western Reserve University, Cleveland, Ohio, USA

Yakovlev, Yuri
Ioffe Institute, Sankt-Peterburg, Russia

Vávra, Ivo
Department of Superlattice, Institute of Electrical Engineering, Bratislava, Slovakia

Veprek, Stan
Technical University, Munich, Germany

Volf, Kerstin
University of Marburg, Marburg, Germany

Wosinski, Tadeus
Polish Academy of Sciences, Warsaw, Poland

Patents & Technology Transfers

Submitted applications for patent protection:

In year 2008 two applications were submitted for patent protection. Both of them were started as national application. The details are the following:

P0800128
Priority date: *25th February, 2008*
Title: "Installation for Elimination of Oils and Oil Products from Rain Water"
Applicants: Purator Hungaria Ltd. (40%), Accusealed Ltd. (40%), MFA (20%)
Inventors: Péter Bolgár, Dr. Jenő Imre Fekete, Csaba Horváth, Dr. Zsolt Endre Horváth, Dr. Sádor Kulcsár, and József Talpai.

P0800190
Priority date: *10th March, 2008*
Title: "Measuring Arrangement and Method for Detecting Fluid Hydrocarbon Derivative Come into Water Surface"
Applicants: MFA (75%), Weszta-T Ltd. (25%)
Inventors: Miklós Serényi (50%), János Makai (15%), István Bársony (10%), and Sándor Kulinyi (25%)

Technology transfer:

The MFA has been contracted with Purator Hungaria Ltd. and Accusealed Ltd. for the exploitation of the invented technology described in the above mentioned patent application: P0800128.

The MFA has been contracted with the METALELEKTRO Ltd., as well as with two departments of the Budapest University of Technology and Economics (Department of Broadband Infocommunications and Electromagnetic Theory and Department of Vehicle Manufacturing and Repairing) for the exploitation of the developed novel technologies of the "LOGIMARKER" project.

The license agreement has been renewed between the MFA and the Tactologic Ltd. for the continuation of the exploration patent pending inventions: P0600488: "*Method for Producing Micromechanical Elements can be Integrated into CMOS Technology, Carrying Monolith Si and Monolith SiO Produced by Porous Si Micromanufacturing Process*".

MFA Publications in 2008

1. Alonso M I, Garriga M, Bernardi A, Goñi A R, Lopeandia A F, Garcia G, Rodríguez-Viejo J, Lábár J L: Ellipsometric study of crystallization of amorphous Ge thin films embedded in SiO_2, Thin Solid Films 516 (12): 4277-4281 (2008)
2. Ansari F, Horvath R, Aref A, Ramsden J J: Bacterial adsorption onto thin Fe_3O_4 magnetic nanofilms, In: Technical Proceedings of the 2008 NSTI Nanotechnology Conference and Trade Show, 2008, pp 91-94
3. Arató P, Balázsi C: Carbon Nanotubes in Silicon Nitride, In: Handbooks of Nanoceramics and Their Based Nanodevices (Ed. Tseng T Y, Nalva H S), American Scientific Publishers, Stevensom Ranch, 2008, pp 20-
4. Aref A, Horvath R, Ansari F, Ramsden J J: Attachment and spreading of human embryonal carcinoma stem cells on nanosurfaces monitored by optical waveguides, In: Proceedings of the 2008 NSTI Nanotechnology Conference and Trade Show, 2008, pp 573-576
5. Bakonyi I, Peter L, Horvath Z E, Padar J, Pogany L, Molnar G: Evolution of structure with spacer layer thickness in electrodeposited Co/Cu multilayers, Journal of the Electrochemical Society 155 (11): D688-D692 (2008)
6. Balázsi C, Bishop A, Yang J, Sedlácková K, Wéber F, Gouma P I: Biopolymer-Hydroxyapatite Nanocomposite from Eggshell for Prospective Surgical Applications, Materials Science Forum 589: 61-65 (2008)
7. Balázsi C, Ionescu R, Sedlácková K: Hexagonal WO_3 Films with Carbon Nanotubes for Sensing Applications, Materials Science Forum 589: 67-72 (2008)
8. Balázsi C, Koszor O, Fényi B, Balázsi K: Engineered Electrical and Mechanical Properties of Carbon Nanotube Added Si_3N_4 Nanocomposites, In: Carbon Nanotubes: New Research (Ed. Ottenhouse A P), 2008, pp 200-224
9. Balázsi C, Sedláčková K, Czigány Z: Structural characterization of Si_3N_4-carbon nanotube interfaces by transmission electron microscopy, Composites Science and Technology 68: 1596-1599 (2008)
10. Balázsi C, Sedlácková K, Llobet E, Ionescu R: Novel hexagonal WO_3 nanopowder with metal decorated carbon nanotubes as NO_2 gas sensor, Sensors and Actuators B 133: 151-155 (2008)
11. Balázsi C, Sedlácková K, Pfeifer J, Tóth A L: Synthesis and Examination of hexagonal tungsten oxide nanocrystals for electrochromic and sensing applications, In: NATO Science series, 2008, pp 77-89
12. Balázsi C, Wang L, Zayim E O, Szilágyi I M, Sedlacková K, Pfeifer J, Tóth A L, Gouma P I: Nanosize hexagonal tungsten oxide for gas sensing applications, Journal of the European Ceramic Society 28 (5): 913-917 (2008)
13. Balázsi C: Carbon nanotube-ceramic matrices: Silicon Nitride Composites, In: Introduction to Nanotechnology (Ed. Dusza J, Dragieva I), Heron Press Ltd, Sofia, 2008, pp 103-117
14. Balázsi C: Ceramic Nanocomposites for High Temperature, Sensor and Bio-Applications, In: Nanocomposites: Preparation, Properties and Performance (Ed. Mancini L H, Esposito C L), Nova Science, 2008, pp 201-225

15. Bálint Z, Boyer P, Kertész K, Biró L P: Observations on the spectral reflectances of certain high Andean Penaincisalia and Thecloxurina, with the description of a new species (Lepidoptera : Lycaenidae : Eumaeini), Journal of Natural History 42 (25-26): 1793-1804 (2008)

16. Bálint Z, Wojtusiak J, Kertész K, Biró L P: Description of Penaincisalia biophot with emphasis on the optical properties of the wing dorsal surfaces, Genus 19 (3): 343-353 (2008)

17. Banyasz I, Berneschi S, Cacciari I, Fried M, Lohner T, Nunzi-Conti G, Paszti F, Pelli S, Petrik P, Righini G C, Watterich A, Zolnai Z: Nitrogen-ion-implanted planar optical waveguides in Er-doped tellurite glass: fabrication and characterization In: Proceedings of the Society of Photo-Optical Instrumentation Engineers: (SPIE), Conference on Optical Components and Materials V (Ed. Digonnet M J F, Jiang S, Glesener J W, Dries J C), San Jose, CA, Vol. 6890, 2008, pp 68901A-68901A-9

18. Barna A, Gurbán S, Kótis S, Tóth A L, Menyhard M: Ion mixing at 20 keV: A comparison of the effects of Ga^+, Ar^+ and CF_4^+ ion irradiation, Ultramicroscopy 109 (1): 129-132 (2008)

19. Barradas N P, Arstila K, Battistig G, Bianconi M, Dytlewski N, Jeynes C, Kótai E, Lulli G, Mayer M, Rauhala E, Szilágyi E, Thompson M: Summary of "IAEA intercomparison of IBA software, Nuclear Instruments and Methods in Physics Research B 266 (8): 1338-1342 (2008)

20. Bársony I, Ducso C, Furjes P: Thermometric Gas Sensing In: Solid State Gas Sensing (Ed. Comini E), Springer Science + Business Media, 2008, pp DOI: 10.1007/978-0-387-09665-0_7-

21. Basa P, Alagoz A S, Lohner T, Kulakci M, Turan R, Nagy K, Horváth Z J: Electrical and ellipsometry study of sputtered SiO_2 structures with embedded Ge nanocrystals, Applied Surface Science 254: 3626-3629 (2008)

22. Basa P, Horváth Z J, Jászi T, Pap A E, Molnár G, Kovalev A I, Wainstein D L, Turmezei P: Si_3N_4 based non-volatile memory structures with embedded Si nanocrystals, In: 7th Int. Conf. Advanced Semiconductor Devices and Microsystems (Ed. Hascik S, Osvald J), 2008, pp 63-66

23. Basa P, Molnár G, Dobos L, Pécz B, Tóth L, Tóth A L, Koós A A, Dózsa L, Nemcsics A, Horváth Z J: Formation of Ge nanocrystals in SiO_2 by electron beam evaporation, Journal of Nanoscience and Nanotechnology 8: 818-822 (2008)

24. Basa P, Petrik P, Fried M, Dâna A, Aydinli A, Foss S, Finstad T G: Spectroscopic ellipsometric study of Ge nanocrystals embedded in SiO_2 using parametric models, physica status solidi C (5): 1332-1336 (2008)

25. Beck A, Horváth A, Stefler G, Katona R, Geszti O, Tolnai G, Liotta L F, Guczi L: Formation and structure of Au/TiO_2 and Au/CeO_2 nanostructures in mesoporous SBA-15, Catalysis Today 139 (3): 180-187 (2008)

26. Biró D, Barna P B, Meneve J, Székely L, Devenyi A: Self-lubricating MoS_2-doped nanolayered TiAlCrN tribological coatings prepared with composition-modulated interfaces, Finnish Journal of Tribology 27 (1): 34-44 (2008)

27. Biro D, Barna P B, Székely L, Geszti O, Hattori T, Devenyi A: Preparation of multilayered nanocrystalline thin films with composition-modulated interfaces, Nuclear Instruments and Methods in Physics Research A 590(1-3): 99-106 (2008)

28. Biró L P, Kertész K, Vértesy Z, Bálint Z: Photonic nanoarchitectures occurring in butterfly scales as selective gas/vapor sensors In: The Nature of Light: Light in Nature II, Proc. of SPIE (Ed. Creath K), 2008, pp 705706-1-705706-8
29. Blum I, Portavoce A, Mangelinck D, Daineche R, Hoummada K, Lábár J L, Carron V, Perrin C: Lattice and grain-boundary diffusion of As in Ni_2Si, Journal of Applied Physics 104: 114312 (2008)
30. Budna K P, Mayrhofer P H, Neidhardt J, Hegedűs E, Kovács I, Tóth L, Pécz B, Mitterer C: Effect of nitrogen-incorporation on structure, properties and performance of magnetron sputtered CrB_2, Surface and Coatings Technology 202: 3088-3093 (2008)
31. Cottier K, Horvath R: Imageless microscopy of surface patterns using optical waveguides, Applied Physics B 91 (2): 319-327 (2008)
32. Deák R, Néda Z, Barna P B: A novel kinetic Monte Carlo method for epitaxial growth, Journal of Optoelectronics and Advanced Materials 10 (9): 2445-2450 (2008)
33. Deák R, Néda Z, Barna P B: A Simple Kinetic Monte Carlo Approach for Epitaxial Submonolayer Growth, Communications in Computational Physics 3 (4): 822-833 (2008)
34. di Forte Poisson M A, Magis M, Tordjman M, di Persio J, Langer R, Toth L, Pecz B, Guziewicz M, Thorpe J, Aubry R, Morvan E, Sarazin N, Gaquière C, Meneghesso G, Hoel V, Jacquet J C, Delage S: GaAlN/GaN HEMT heterostructures grown on SiCopSiC composite substrates for HEMT application, Journal of Crystal Growth 310 (23): 5232-5236 (2008)
35. Dobos L, Pécz B, Tóth L, Horváth Z J, Horváth Z E, Beaumont B, Bougrioua Z: Structural and electrical properties of Au and Ti/Au contacts to n-type GaN, Vacuum 82: 794-798 (2008)
36. Dobos L, Pécz B, Tóth L, Horváth Z J, Horváth Z E, Horváth E, Tóth A L, Beaumont B, Bougrioua Z: Al and Ti/Al contacts to n-GaN, In: 12th Joint Vacuum Conference, Balatonalmádi, 2008, p 30
37. Feczkó T, Muskotál A, Gál L, Szépvölgyi J, Sebestyén A, Vonderviszt F: Synthesis of Ni-Zn ferrite nanoparticles in radiofrequency thermal plasma reactor and thier use for purification of histidine-tagged proteins, Journal of Nanoparticle Research 10: 227-232 (2008)
38. Fried M, Khanh NQ, Petrik P: Defect profiling by ellipsometry using ion implantation through wedge masks, physica status solidi (c) 5(5): 1227-1230 (2008)
39. Fried M: Ellipsometry for inhomogeneous structure caused by ion implantation, In: Proceedings of the 1st European School on Ellipsometry From Fundamentals to Applications in Nanoscience and Nanotechnology –A20, Ostuni (BR), Italy, 2008, p A20
40. Fried M: Ellipsometry of ZnO layers for photovoltaic applications, In: Proceedings of the 1st European School on Ellipsometry From Fundamentals to Applications in Nanoscience and Nanotechnology –A22, Ostuni (BR), Italy, 2008, p A22
41. Frigeri C, Nasi L, Serényi M, Csik A, Erdélyi Z, Beke D L: AFM and TEM study of hydrogenated sputtered Si/Ge multilayers, Superlattices and Microstructures, DOI: 10.1016/j.spmi.2008.10.02 (2008)
42. Frigeri C, Serenyi M, Csik A, Erdelyi Z, Beke D L, Nasi L: Structural modifications induced in hydrogenated amorphous Si/Ge multilayers by heat treatments, Journal of Materials Science-Materials in Electronics 19: S289-S293 (2008)

43. Furlan A, Gueorguiev G K, Czigány Z, Högberg H, Braun S, Stafstrom S, Hultman L: Synthesis of phosphorus-carbide thin films by magnetron sputtering, physica status solidi - Rapid Research Letters 2(4): 191-193 (2008)
44. Fürjes P, Rajta I, Battistig G, Bársony I, Dücsö C: Integrated Micro-Membranes by high energy He^+ or H^+ Implantation and Electrochemical Etching, In: Proceedings of Eurosensors XXII, Dresden, 2008
45. Galkin N G, Dózsa L, Turchin T V, Goroshko D L, Pécz B, Tóth L, Dobos L, Khanh N Q, Cherednichenko A I: Properties of $CrSi_2$ nanocrystallites grown in silicon matrix, Journal of Physics-Condensed Matter 19 (50): 506204 (2007)
46. Gergely G, Gácsi Z, Bánhidi O, Kovács J, Rónaföldi A: The effect of rotating magnetic field on the solidification of A356 alloy modified by strontium, Materials Science Forum 589: 305-310 (2008)
47. Gergely G, Gácsi Z: A Si morfológiájának jellemzése a módosított Al-Si ötvözetekben, BKL Kohászat 141 (5) (2008)
48. Gergely G, Gurban S, Menyhard M, Jablonski A, Zommer L: The inelastic mean free path of electrons. Research in Budapest, Warsaw, Wroclaw and Clermont-Ferrand. Brief history and new results, Acta Physica Polonica A 114: S-49-S-58 (2008)
49. Gergely G, Gurbán S, Menyhard M, Jablonski A: Determination of Surface-Excitation Parameters for Elastic Peak Electron Spectroscopy (EPES) Using the Database of Goto, Journal of Surface Analysis 15: 159-165 (2008)
50. Gubicza J, Chinh N Q, Lábár J L, Hegedűs Z, Szommer P, Tichy G, Langdon T G: Delayed microstructural recovery in silver processed by equal-channel angular pressing, Journal of Materials Science 43 (16): 5672-5676 (2008)
51. Gubicza J, Chinh N Q, Lábár J L, Hegedűs Z, Xu C, Langdon T G: Microstructure and yield strength of severely deformed silver, Scripta Materiala 58(9): 775-778 (2008)
52. Gubicza J, Fogarassy Z, Krállics G, Lábár J L, Törköly T: Microstructure and mechanical behavior of ultrafine-grained titanium, Materials Science Forum 589: 99-104 (2008)
53. Gubicza J, Lábár J L, Agócs E, Fátay D, Lendvai J: Effect of nano-quasicrystals on viscosity of a Zr-based bulk metallic glass, Scripta Materialia 58 (4): 291-294 (2008)
54. Guczi L, Paszti Z, Pető G: Metal nanoclusters: electronic aspects and physico-chemical characterization, In: Metal nanoclusters in catalysis and marerials science: the iussue of size control (Ed. Corain B, Schmid G, Toshima N), Elsevier, 2008, pp 99-
55. Gyulai J, Battistig G, Lohner T, Hajnal Z: Wedge etching by anodic oxidation and determination of shallow boron profile by ion beam analysis, Nuclear Instruments and Methods in Physics Research B 266: 1434-1438 (2008)
56. Hámori A, Serényi M, Dér A, Ferencz K, Kökényesi S: All-optical switching possibilities for optical packet switching, In: Proceedings of the European Microwave Association, 2008, pp 221-225
57. Hanus J, Drabik M, Hlidek P, Biederman H, Radnóczi G, Slavinska D: Some remarks on Ag/C:H nanocomposite films, Vacuum 832: 454-456 (2008)
58. Hegedűs E, Kovács I, Pécz B, Tóth L, Budna K P, Mitterer C: Transmission electron microscopy of nanocomposite Cr-B-N thin films, Vacuum 82 (2): 209-213 (2008)

59. Hóbor S, Révész A, Szabó P J, Zhilyaev A P, Kovács-Kis V, Lábár J L, Kovács Z: High pressure torsion of amorphous $Cu_{60}Zr_{30}Ti_{10}$ alloy, Journal of Applied Physics 104 (3): 033525 (2008)
60. Horopantis E E, Presentzis G, Beck A, Guczi L, Pető G, Papdimitriou L: Correlation between Structural and Electrical Properties of Heavily Lithiated Boron Oxide Electrolites, Journal of Non-crystalline Solids 354: 374-379 (2008)
61. Horváth E, Zsíros G, Tóth A L, Sajó I, Arató P, Pfeifer J: Microstructural characterization of the oxide scale on nitride bonded SiC-ceramics, Ceramics International 34(1): 151-155 (2008)
62. Horvath R, Cottier K, Pedersen H C, Ramsden J J: Multidepth screening of living cells using optical waveguides, Biosensors and Bioelectronics 24 (4): 799-804 (2008)
63. Horvath R, McColl J, Yakubov G E, Ramsden J J: Structural hysteresis and hierarchy in adsorbed glycoproteins, Journal of Chemical Physics 129 (7): 071102 (2008)
64. Horvath Z E, Koos A A, Kertesz K, Molnar G, Vertesy G, Bein M C, Frigyes T, Meszaros Z, Gyulai J, Biro L P: The role of defects in chemical sensing properties of carbon nanotube films, Applied Physics A 93 (2): 495-504 (2008)
65. Horváth Z J, Basa P, Jászi T, Pap A E, Dobos L, Pécz B, Tóth L, Szöllősi P, Nagy K: Electrical and memory properties of Si_3N_4 MIS structures with embedded Si nanocrystals, Journal of Nanoscience and Nanotechnology 8: 812-817 (2008)
66. Horváth Z J, Basa P, Jászi T, Pap A E, Kovalev A L, Wainstein D L, Dózsa L: MNOS memory structures with embedded silicon nanocrystals In: 16th International Symposium on "Nanostructures: Physics and Technology (Ed. Solovyova E, Savostyanova E), 2008, pp 126-127
67. Horváth Z J, Hardy V: Simulation of memory behaviour of non-volatile structures, Nanoscience and Nanotechnology 8: 834-840 (2008)
68. Horváth Z J, Rakovics V, Pődör B: Electrical behaviour of Au/InGaAsSb and Au/GaSb junctions In: 7th Int. Conf. on Advanced Semiconductor Devices and Microsystems (Ed. Hascik S, Osvald J), 2008, pp 119-122
69. Horváth Z J: Evaluation of Schottky junction parameters from current-voltage characteristics exhibiting large excess currents, Applied Surface Science 255: 743-745 (2008)
70. Höglund C, Birch J, Beckers M, Alling B, Czigány Z, Mücklich A, Hultman L: Structural characterization of Si_3N_4-carbon nanotube interfaces by transmission electron microscopy, European Journal of Inorganic Chemistry 8: 1193-1195 (2008)
71. Juhász G, Horváth Z, Major C, Petrik P, Polgár O, Fried M: Non-collimated beam ellipsometry, physica status solidi (c) 5 (5): 1081-1084 (2008)
72. Kertész K, Molnár G, Vértesy Z, Koós A A, Horváth Z E, Márk G I, Tapasztó L, Bálint Z, Tamáska I, Deparis O, Vigneron J P, Biró L P: Photonic band gap materials in butterfly scales: A possible source of "blueprints", Materials Science and Engineering B 149: 259-265 (2008)
73. Kis A, Vásárhelyi G: Developing system to detect and analyze spatio-temporal tactile events, In: Proceedings of CNNA 2008, Santiago de Compostela, 2008, p 10
74. Koszor O, Tapasztó L, Markó M, Balazsi C: Characterizing the global dispersion of carbon nanotubes in ceramic matrix nanocomposites, Applied Physics Letters 93 (20): 201910 (2008)

75. Koszor O, Wéber F, Arató P, Lindemann A, Biró L P, Horváth Z E, Kónya Z, Kiricsi I, Balázsi C: Processing, mechanical and thermophysical properties of silicon nitride based composites with carbon nanotubes and graphene, Processing and Application of Ceramics 1 (1-2): 35-41 (2008)

76. Koszor O, Wéber F, Vértesy Z, Horváth Z E, Kónya Z, Biró L P, Kiricsi I, Arató P, Balázsi C: Preparation of Si_3N_4 Composites with Single Wall Carbon Nanotube and Exfoliated Graphite, Materials Science Forum 589: 409-414 (2008)

77. Kotis L, Menyhard M, Tóth L, Zalar A, Panjan P: Determination of relative sputtering yield of Cr/Si, Vacuum 82(2): 178-181 (2008)

78. Kovách G, Karacs A, Radnóczi G, Csorbai H, Guczi L, Veres M, Koós M, Papadimitriou L, Sólyom A, Pető G: Modified π-states in ion-irradiated carbon, Applied Surface Science 254 (9): 2790-2796 (2008)

79. Kovács A, Hirotsu Y: Structural and magnetic properties of L10-FeCoPt nanoparticles prepared by rf-sputtering, Applied Physics A 93: 543-547 (2008)

80. Kovács A, Merkel D G, Tanczikó F, Stankov S, Hirotsu Y, Bottyán L: He ion irradiation induced disordering in L10-FePd thin films: Ion fluence dependence, Scripta Materialia 58: 635-638 (2008)

81. Kovács G J, Bertóti I, Radnóczi G: X-ray photoelectron spectroscopic study of magnetron sputtered carbon–nickel composite films, Thin Solid Films 516 (21): 7942-7946 (2008)

82. Kovács G J, Veres M, Koós M, Radnóczi G: Raman spectroscopic study of magnetron sputtered carbon–nickel and carbon nitride–nickel composite films: The effect of nickel on the atomic structure of the C/CN_x matrix, Thin Solid Films 516 (21): 7910-7915 (2008)

83. Kovalev A I, Wainstein D L, Tetelbaum D I, Mikhailov A N, Golan Y, Lifshitz Y, Berman A, Basa P, Horvath Z J: Electron spectroscopy investigations of semiconductor nanocrystals formed by various technologies, International Journal of Nanoparticles 1: 14-31 (2008)

84. Kozma P, Nagy N, Kurunczi S, Petrik P, Hámori A, Muskotál A, Vonderviszt F, Fried M, Bársony I: Ellipsometric characterization of flagellin films for biosensor applications, physica status solidi (c) 5: 1427-1430 (2008)

85. Lábár J L, Barna P B, Geszti O, Grasin R, Lestyán G, Misják F, Radnóczi G, Sáfrán G, Székely L: A new method for electron diffraction based analysis of phase fractions and texture in thin films of metallic nano-crystals In: EMC 2008 (Ed. Luysberg M, Tillmann K, Weirich T), Springer-Verlag Berlin, 2008, pp 203-204

86. Lábár J L: Electron diffraction based analysis of phase fractions and texture in nanocrystalline thin films, Part I: Principles, Microscopy and Microanalysis 14 (4): 287-295 (2008)

87. Levichev S, Basa P, Horváth Z J, Chahboun A, Rolo A G, Barradas N P, Alves E, Gomes M J M: Memory effect on CdSe nanocrystals embedded in SiO_2 matrix, Solid State Communications 148: 105-108 (2008)

88. Levichev S, Chahboun A, Basa P, Rolo A G, Barradas N P, Alves E, Horváth Z J, Conde O, Gomes M J M: Charging effects in CdSe nanocrystals embedded in SiO_2 matrix produced by rf magnetron sputtering, Microelectronics Engineering 85: 2374-2377 (2008)

89. Lohner T, Angelov C, Mikli V: Comparative ellipsometric and ion beam analytical studies on ion beam crystallized silicon implanted with Zn and Pb ions, Thin Solid Films 516 (22): 8009-8012 (2008)

90. Lohner T, Pongracz A, Khanh N Q, Krafcsik O H, Josepovits K, Deak P: Comparative investigation of the Si/SiO_2 interface layer containing SiC crystallites using spectroscopic ellipsometry, ion beam analysis and XPS, physica status solidi (c) 5(5): 1337-1340 (2008)

91. Lohner T, Serényi M, Basa D K, Khánh N Q, Nemcsics A, Petrik P, Turmezei P: Composition and Thickness of RF Sputtered Amorphous Silicon Alloy Films, Acta Politechnica Hungarica 5 (2): 23-30 (2008)

92. Lohner T, Zolnai Z, Petrik P, Battistig G, López J G, Morilla Y, Koós A A, Osváth Z, Fried M: Complex dielectric function of ion implantation amorphized SiC determined by spectroscopic ellipsometry, physica status solidi (c) 5(5): 1374-1377 (2008)

93. Lukács I E, Riesz F: Sub-pixel detection of a grid's node positions for optical diagnostics, Thin Solid Films 516: 8082-8086 (2008)

94. Major C, Juhász G, Horváth Z, Polgar O, Fried M: Wide angle beam ellipsometry for extremely large samples, physica status solidi, (c) 5 (5): 1077-1080 (2008)

95. Márk G I, Biró L P, Lambin P H, Chernozatonskii L: Wave packet dynamical simulation of electron transport through a line defect on the graphene surface, Physica E 40: 2635-2638 (2008)

96. Merkel D G, Tancziko F, Sajti S, Major M, Nemeth A, Bottyan L, Horvath Z E, Waizinger J, Stankov S, Kovacs A: Modification of local order in FePd films by low energy He^+ irradiation, Journal of Applied Physics 104: 013901 (2008)

97. Misják F, Barna P B, Radnóczi G: Formation of ordered solid solution during phase separation in Cu-Ag alloy films In: EMC 2008, vol II (Ed. Richter S, Schwedt A), 2008, pp 389-390

98. Misják F, Barna P B, Tóth A L, Ujvári T, Bertóti I, Radnóczi G: Structure and mechanical properties of Cu-Ag nanocomposite films, Thin Solid Films 516(12): 3931-3934 (2008)

99. Misják F, Horváth Z E, Barna P B, Radnóczi G: Development of texture and morphology in Cu-Ag thin nanocomposite films on Si, Journal of Physics Conference Series 100: 082008 (2008)

100. Moser M, Mayrhofer P H, Székely L, Sáfrán G, Barna P B: Influence of bipolar pulsed DC magnetron sputtering on elemental composition and micro-structure of Ti-Al-Y-N thin films, Surface and Coatings Technology 203 (1-2): 148-155 (2008)

101. Nagy N, Deák A, Hámori A, Hórvölgyi Z, Fried M, Petrik P, Bársony I: Comparative investigation of Stöber silica Langmuir-Blodgett films as optical model structures, physica status solidi (a) 205: 936-940 (2008)

102. Nemcsics A, Horváth E, Nagy S, Molnár L M, Mojzes I, Horváth Z J: Some remarks to the nanowires grown on III-V substrate In: 7th Int. Conf. on Advanced Semiconductor Devices and Microsystems (ASDAM 2008) (Ed. S. Hascik, J. Osvald), Smolenice, Slovakia, 2008, pp 215-218

103. Nemes-Incze P, Osváth Z, Kamarás K, Biró L P: Anomalies in thickness measurements of graphene and few layer graphite crystals by tapping mode atomic force microscopy, Carbon 46: 1435-1442 (2008)

104. Németh A, Lábadi Z, Rakovics V, Bársony I, Krafcsik I: Solar Cell Technology Innovation Center at MTA MFA, Hiradástechnika 63: 34-38 (2008)

105. Németh A, Major C, Fried M, Lábadi Z, Bársony I: Spectroscopic ellipsometry study of transparent conductive ZnO layers for CIGS solar cell applications, Thin Solid Films 516: 7016-7020 (2008)

106. Ódor G, Menyhárd N: Crossovers from Parity Conserving to Directed Percolation Universality, Physical Review E 78: 041112 (2008)

107. Ódor G: Self-organizing, two-temperature Ising model describing human segregation, International Journal of Modern Physics C 19: 393-398 (2008)

108. Ódor G: Universality in nonequilibrium lattice systems: Theoretical foundations, World Scientific, Singapore, 2008, p. 1-295

109. Orlov L K, Horvath Z J, Orlov M L, Lonchakov A T, Ivina N L, Dobos L: Anomalous electrical properties of $Si/Si_{1-x}Ge_x$ heterostructures with an electron transport channel in Si layers, Physics of the Solid State 50: 330-340 (2008)

110. Ossi P M, Bailini A, Geszti O, Radnóczi G: Morphology and growth mechanism of WO_x films prepared by laser ablation of W in different atmospheres, Europhysics Letters 83: 68005 (2008)

111. Osváth Z, Nemes-Incze P, Tapasztó L, Horváth Z E, Biró L P: Thermal oxidation of few-layer graphite plates: an SPM study, physica status solidi (a) 205: 1419-1423 (2008)

112. Pap A E, Dücső C, Kamarás K, Battistig G, Bársony I: Heavy Water in Gate Stack Processing, Materilas Science Forum 573-574: 119-131 (2008)

113. Pap A E, Petrik P, Pécz B, Battistig G, Bársony I, Szekrényes Z, Kamarás K, Schay Z, Nyényi Z: Si surface preparation and passivation by vapor phase of heavy water, In: 16th IEEE International Conference on Advanced Thermal Processing of Semiconductors – RTP2008, Las Vegas, USA, 2008, pp 219-228

114. Pécz B, Tóth L, Dobos L, Bove P, Langer R, Lahrèche H, di Forte Poisson M A: Transmission electron microscopy of GaN layers grown on composite substrates, In: HETECH 2008 (Ed. Meneghesso G), Venice, 2008, pp 149-150

115. Pecz B, Tóth L, Dobos L, Lahrèche H, Langer R: Composite substrates for GaN growth, Springer Proceedings In: Physics 120, Proc. Of the 15th Conf. on Microscopy of Semiconducting Materials (Ed. Cullis AG, Midgley PA), Cambridge, 2007, pp 53-56

116. Perc M, Szolnoki A, Szabó G: Restricted connections among distinguished players support cooperation, Physical Review E 78: 066101 (2008)

117. Perc M, Szolnoki A: Social diversity and promotion of cooperation in the spatial prisoner's dilemma game, Physical Review E 77: 011904 (2008)

118. Perrin C, Mangelinck D, Nemouchi F, Lábár J L, Lavoie C, Bergman C, Gas P: Nickel silicides and germanides: Phases formation, kinetics and thermal expansion, Materials Science and Engineering B 154-155: 163-167 (2008)

119. Petrik P, Khánh N Q, Li J, Chen J, Collins W, Fried M, Radnóczi G Z, Lohner T, Gyulai J: Ion implantation induced disorder in single-crystal and sputter-deposited polycrystalline CdTe characterized by ellipsometry and backscattering spectrometry, physica status solidi (c) 5 (5): 1358-1361 (2008)

120. Petrik P, Lohner T, Polgár O, Fried M: Ellipsometry on ion implantation induced damage In: 16th International Conference on Advanced Thermal Processing of Semiconductors – RTP2008, Las Vegas, USA, 2008, pp 93-101

121. Petrik P: Ellipsometric models for vertically inhomogeneous composite structures, physica status solidi (a) 205 (4): 732-738 (2008)

122. Piazzoni C, Blomqvist M, Podest A, Bardizza G, Bonati M, Piseri P, Milani P, Davies C, Hatto P, Sedláčková K, Radnóczi G: Nanocomposite TiN films with embedded MoS_2 inorganic fullerenes produced by combining supersonic cluster beam deposition with cathodic arc reactive evaporation, Applied Physics A 90 (1): 101-104 (2008)

123. Polgár O, Fried M, Khanh N Q, Petrik P, Bársony I: Determination of ion track and shapes with damage simulations on the base of ellipsometric and backscattering spectrometric measurements, physica status solidi (c) 5 (5): 1354-1357 (2008)

124. Popa M, Preda S, Fruth V, Sedlácková K, Balázsi C, Crespo D, Calderón-Moreno J M: $BiFeO_3$ films on steel substrate by the citrate method, Thin Solid Films, DOI:10.1016/j.tsf.2008.10.030 (2008)

125. Pődör B, Reményi G: Parabolic negative magnetoresistance in two-dimensional electron gas in InGaAs/InP In: Proc. 31 st Int. Spring Seminar on Electronics Technology ISSE 2008 (Ed.), Budapest, 2008, pp 197-202

126. Pődör B: Hole mobility in InP and GaSb In: Proc. 31 st Int. Spring Seminar on Electronics Technology ISSE 2008 (Ed.), Budapest, 2008, pp 203-206

127. Pramatarova L, Pecheva E, Montgomery P, Dimova-Malinovska D, Petrov T, Toth A L, Dimitrova M: Bioactiviy of polycrystalline silicon layers, Journal of Nanoscience and Nanotechnology 8 (2): 924-930 (2008)

128. Rajta I, Szilasi S, Fürjes P, Fekete Z, Dücső C: Si Micro-turbine by Proton Beam Writing and Porous Silicon Micromachining In: Proceedings of 12th International Conference on Nuclear Microprobe Technology and Applications (Ed.), Debrecen, 2008, pp XX-

129. Rakovics V, Réti I: Infravörös diódák alkalmazása az élelmiszerek spektroszkópiai vizsgálatára In: Műszaki Kémiai Napok '08 (Ed. Nagy E), Veszprém, 2008, pp 64-68

130. Riesz F, Lukács I E, Szabó J, Makai J P, Réti I, Szentpáli B, Eördögh I, Pődör B, Laczik Z J: Makyoh topography: a simple and powerful method for the flatness characterisation of semiconductor wafers, Híradástechnika 61 (1): 28-33 (2008)

131. Riesz F, Pap A E, Ádám M, Lukács I E: Makyoh-topography study of the swirl defect in Si wafers, Thin Solid Films 516 (22): 8087-8091 (2008)

132. Ryć L, Dobrzański L, Dubecký F, Kaczmarczyk J, Riesz F, Słysz W, Surma B: Application of MSM InP detectors to the measurement of pulsed X-ray radiation, Radiation Effects and Defects in Solids 163 (4-6): 559-567 (2008)

133. Sánchez-Garcia JA, Vázquez L, Gago R, Redondo-Cubero A, Albella J M, Czigány Z: Tuning the surface morphology in self-organised ion beam nanopattering of Si(001) via metal incorporation: from holes to dots, Nanotechnology 19 (35): 355306 (2008)

134. Sárkány A, Geszti O, Sáfrán G: Preparation of Pd shell–Au core/SiO_2 catalyst and catalytic activity for acetylene hydrogenation, Applied Catalysis A 350 (2): 157-163 (2008)

135. Sárkány A, Hargittai P, Geszti O: Thermal and radiolysis assisted formation of Au–Pd heteroaggregates, Colloids and Surfaces A 322 (1-3): 124-129 (2008)

136. Sárközi Z, Kertész K, Koós A A, Osváth Z, Tapasztó L, Horváth Z E, Nemes-Incze P, Jenei I Z, Vértesy Z, Daróczi N S, Darabont A L, Pana O, Biró L P: Synthesis of carbon nanotubes from liquid hydrocarbons using a spray-pyrolysis method, Journal of Optoelectronics and Advanced Materials 10 (9): 2307-2310 (2008)

137. Sebestyén A, Muskotál A, Végh B M, Vonderviszt F: The hypervariable D3 domain of Salmonella flagellin is an autonomous folding unit, Protein Peptide Letters 15: 54-57 (2008)

138. Sedlácková K, Grasin R, Radnóczi G: Carbon – Metal (Ni, Ti) nanocomposite films as protective coatings In: New Research on Nanocomposites (Ed. Krause LM), Nova Science Publ, 2008, pp 223-246

139. Sedláčková K, Ujvári T, Grasin R, Lobotka P, Bertóti I, Radnóczi G: C–Ti nanocomposite thin films: Structure, mechanical and electrical properties, Vacuum 82: 214-216 (2007)

140. Seeman K, Leiste H, Kovács A: Damping and ferromagnetic resonance linewidth broadening in nanocrystalline soft ferromagnetic Fe-Co-Hf-N films, Journal of Magnetism and Magnetic Materials 320: 1952-1957 (2008)

141. Serenyi M, Lohner T, Petrik P, Zolnai Z, Horvath Z E, Khanh N Q: Characterization of sputtered and annealed niobium oxide films using spectroscopic ellipsometry, Rutherford backscattering spectrometry and X-ray diffraction, Thin Solid Films 516 (22): 8096-8100 (2008)

142. Shandalov M, Makai J P, Balazs J, Horvath Z J, Gutman N, Sa'ar A, Golan Y: Optical properties of size quantized PbSe films chemically deposited on GaAs, European Physical Journal-Applied Physics 41: 75-80 (2008)

143. Skakalova V, Kaiser A B, Osváth Z, Vértesy G, Biró L P, Roth S: Ion irradiation effects on conduction in single-wall carbon nanotube networks, Applied Physics A 90: 597-602 (2008)

144. Süle P, Kotis L, Toth L, Menyhard M, Egelhoff Jr W F: .,Asymmetric intermixing in Co/Ti bilayer, Nuclear Instruments and Methods in Physics Research B 266: 904-910 (2008)

145. Süle P: Anisotropy driven ultrafast nanocluster burrowing, Journal of Chemical Physics 129: 084707 (2008)

146. Süle P: Self-organized transient facilitated atomic transport in Pt/Al(111), Journal of Chemical Physics 128: 134708 (2008)

147. Szabó G, Szolnoki A, Borsos I: Self-organizing patterns maintained by competing associations in a six-species predator-prey model, Physical Review E 77: 041919 (2008)

148. Szabó G, Szolnoki A: Phase transitions induced by variation of invasion rates in spatial cyclic predator-prey model with four or six species, Physical Review E 77: 011906 (2008)

149. Szabo G: Spreading mechanisms of cooperation for the evolutionary prisoner's dilemma games, Banach Center Publications 80: 197-215 (2008)

150. Szentpáli B, Réti I, Molnár F B, Farkasvölgyi J, Kazi K, Mirk Z, Sonkoly A, Horváth Z: Isotropic Broadband E-Field Probe, Active and Passive Electronic Components, DOI:10.1155/2008/816969 (2008)

151. Szilagyi I M, Madarasz J, Pokol G, Kiraly P, Tarkanyi G, Saukko S, Mizsei J, Toth A L, Szabo A, Varga-Josepovits K: Stability and controlled composition of hexagonal WO_3, Chemistry of Materials 20 (12): 4116-4125 (2008)

152. Szilágyi I M, Pfeifer J, Balázsi C, Tóth A L, Varga-Josepovits K, Madarász J, Pokol G: Thermal stability of hexagonal tungsten trioxide in air, Journal of Thermal Analysis and Calorimetry 94 (2): 499-505 (2008)

153. Szolnoki A, Perc M, Danku Z: Making new connections towards cooperation in the prisoner's dilemma game, Europhysics Letters 84: 50007 (2008)

154. Szolnoki A, Perc M, Danku Z: Towards effective payoffs in the prisoner's dilemma game on scale-free networks, Physica A 387: 2075 (2008)

155. Szolnoki A, Perc M, Szabó G: Diversity of reproduction supports cooperation in the prisoner's dilemma game on complex networks, European Physical Journal B 61: 505 (2008)

156. Szolnoki A, Perc M: Coevolution of teaching activity promotes cooperation, New Journal of Physics 10: 043036 (2008)

157. Szolnoki A, Perc M: Promoting cooperation in social dilemmas via simple coevolutionary rules, European Physical Journal B, DOI:10.1140/epjb/e2008-00470-8 (2008)

158. Tapasztó L, Dobrik G, Lambin P, Biró L P: Tailoring the atomic structure of graphene nanoribbons by scanning tunnelling microscope lithography, Nature Nanotechnology 3: 397-401 (2008)

159. Tapasztó L, Dobrik G, Nemes-Incze P, Vertesy G, Lambin P, Biró L P: Tuning the electronic structure of graphene by ion irradiation, Physical Review B 78: 233407 (2008)

160. Tapasztó L, Nemes-Incze P, Osváth Z, Bein MC, Darabont Al, Biró LP: Complex superstructure patterns near defect sites of carbon nanotubes and graphite, Physica E 40: 2263-2267 (2008)

161. Tóth L, Dobos L, Pécz B, di Forte Poisson M A, Langer R: GaN layers grown by MOCVD on composite SiC substrate, In: Microscopy of Semiconducting Materials 2007 (Ed. Cullis AG, Midgley PA), Springer, Cambridge, UK, 2007, pp 57-60

162. Tunyogi A, Tancziko F, Osváth Z, Pászti F: Structural characterization of Fe/Ag bilayers by RBS and AFM, Nuclear Instruments and Methods in Physics Research B 266 (22): 4916-4920 (2008)

163. Vásárhelyi G, Kis A, Adam M, Ducso C, Barsony I: Tactile Development System for Dynamic 3D Contact Force Mapping, In: Proceedings of IEEE Sensors 2008, Lecce, 2008, p 10

164. Vásárhelyi G, Kis A, Ádám M, Dücső C, Bársony I: Tactile sensing arrays – design and processing, Híradástechnika 63: 22-27 (2008)

165. Vass-Várnai A, Fürjes P, Rencz M: Possibilities of Humidity Sensing with Thermal Transient Testing on Porous Structures, In: Proceeding of Therminic 2008 Conference, Rome, 2008, pp 200-203

166. Vértesy G, Pardavi-Horvath M: Hysteretic properties of a two dimensional array of small magnetic particles: a test-bed for the Preisach model, In: International Conference on Soft Computing (Ed.), Uherske Hradiste, 2008, pp 171-177

167. Vértesy G, Tomáš I, Kobayashi S, Kamada Y: Investigation of thermally aged samples by Magnetic Adaptive Testing, Journal of Electromagnetism 59: 82-86 (2008)

168. Vértesy G, Tomáš I, Takahashi S, Kobayashi S, Kamada Y, and Kikuchi H: Inspection of steel degradation by Magnetic Adaptive Testing, NDT & E International 41: 252-257 (2008)

169. Vértesy G: Inspection of steel degradation by Magnetic Adaptive Testing, In: Fifth International Conference on Flow Dynamics, Global Center of Excellence (GCOE), Sendai, Japan, 2008, pp OS10-7-

170. Vértesy Z, Kertész K, Bálint Z, Márk G I, Tapasztó L, Biró L P: Photonic crystal type nanoarchitectures in butterfly wing scales In: Proceedings: EMC 2008, Vol. 3: Life Science (Ed. Aretz A, Hermanns-Sachweh B, Mayer J), Springer-Verlag Berlin Heidelberg 2008, Aachen, 2008, pp 101-102

171. Vigneron J P, Kertész K, Vértesy Z, Rassart M, Lousse V, Bálint Z, Biró L P: Correlated diffraction and fluorescence in the backscattering iridescence of the male butterfly Troides magellanus (Papilionidae), Physical Review E 78 (2): 021903 (2008)

172. Volk J, Hakansson A, Miyazaki H T, Nagata T, Shimizu J, Chikyow T: Fully engineered homoepitaxial zinc oxide nanopillar array for near-surface light wave manipulation, Applied Physics Letters 92: 183114 (2008)

173. Vonderviszt F, Namba K: Structure, function and assembly of flagellar axial proteins. In: Fibrous Proteins (Ed. Scheibel T), 2008, pp 58-76

174. Vouroutzis T T, Zorba C A, Dimitriadis K M, Paraskevopoulos L, Dózsa L, Molnár G: Growth of β-$FeSi_2$ particles on silicon by reactive deposition epitaxy, Journal of Alloys and Compounds 448: 202-205 (2008)

175. Vukov J, Szabó G, Szolnoki A: Evolutionary prisoner's dilemma game on Newmann-Watts networks, Physical Review E 77: 026109 (2008)

176. Yastrubchak O, Domagala J Z, Sadowski J, Kulik M, Zuk J, Szymczak R, Toth A L, Wosinski T: Influence of Ion Implantation on Magnetic, Structural and Optical Properties of (Ga,Mn)As Epitaxial Films, acta physica polonica (a) 114 (5): 1445-1450 (2008)

177. Yong T Y, Tou T Y, Yow H K, Sáfrán G: Pulsed Nd:YAG laser deposition of indium tin oxide thin films in different gases and organic light emitting device applications, Thin Solid Films 516(2): 4267-4271 (2008)

178. Zommer L, Jablonski A, Gergely G, Gurban S: Monte Carlo backscattering yield (BY) calculations applying continuous slowing down approximation (CSDA) and experimental data, Vacuum 82: 201-204 (2008)

179. Zommer L, Jablonski A, Kotis L, Menyhard M: Monte Carlo calculation of backscattering factor for Ni-C multilayer system, Journal of Physics D 41: 155312 (2008)

180. Zourob M, Skivesen N, Horvath R, Morf S, Goddard N: Integrated deep-probe optical waveguides for label-free bacteria detection, In: Principles of Bacterial Detection: Biosensors, Recognition Receptors and Microsystems (Ed. Zourob M, Elwary S, Turner A), 2008, pp 137-166